
Biophysical techniques to study cell and matrix properties in the context of single cell migration

Von der Fakultät für Physik und Geowissenschaften
der Universität Leipzig
genehmigte

DISSERTATION

zur Erlangung des akademischen Grades

doctor rerum naturalium

Dr. rer. nat.

vorgelegt

von Dipl.-Phys. Tony Fischer

geboren am 18.08.1985 in Oschatz

Gutachter: Prof. Dr. Hans-Günther Döbereiner
Prof. Dr. Claudia Tanja Mierke

Tag der Verleihung 18. November 2019

Bibliographische Beschreibung:

Fischer, Tony

„Biophysical techniques to study cell and matrix properties in the context of single cell migration“

Universität Leipzig, Dissertation

128 S., 233 Lit., 70 Abb., 14 Tab.

Referat (abstract):

Die Einzelzellmigration in künstlichen Kollagenetzwerken als ein *in vitro* Modellsystem im Kontext von Krebs wurde studiert. Mechanische Eigenschaften von Zellen und der verwendeten Kollagenetzwerke wurden mithilfe der Atomic Force Microscopy (AFM) und weiterentwickelten Analysemethoden bestimmt. Die Porengröße der verwendeten Kollagenetzwerke wurde mit einer neuentwickelten Auswertemethode analysiert. Eine neuartige, minimal-invasive Methode zur Bestimmung der Verformung der Mikroumgebung von Zellen während der Migration verursacht durch Kräftegenerierung der Zelle wird beschrieben. Die Analyse des Invasions-Assays wurde automatisiert und eine nutzerfreundliche Software entwickelt, mit der große Datenmengen ausgewertet werden können. Diese Methoden wurden verwendet, um mechanische Eigenschaften und Migration der humanen Brustkrebszelllinien MDA-MB-231 und MCF-7 zu studieren. Die Rolle der focal adhesion kinase (FAK) wurde mithilfe von embryonalen Maus-Fibroblasten studiert. Sowohl eine FAK knock-out Zelllinie FAK^{-/-} und Kontrolle FAK^{+/+}, als auch eine kinase-dead Mutante FAK^{R454/R454} und Kontrolle FAK^{WT/WT} wurden hinsichtlich ihrer Invasion und Verformung der Mikroumgebung analysiert.

Single cell migration in artificial collagen gels as an *in vitro* model system in the context of cancer are studied. Cell and matrix mechanical properties are determined using atomic force microscopy and an advanced analysis method. Matrix pore-size is studied using a novel approach and analysis method. A novel, minimally invasive approach to determine the amount of displacement of the cell microenvironment due to force generation of single cells during migration in artificial 3D collagen gels is introduced. An automated analysis and user friendly software to analyze high-throughput cell invasion is introduced. These methods are used to study cell migration and mechanical properties of the breast cancer cell lines MDA-MB-231 and MCF-7 and the influence of cell nuclear elasticity is investigated. Using mouse embryonic fibroblasts, the role of focal adhesion kinase (FAK) during cell migration is studied using FAK deficient knock-out cell lines FAK^{-/-} and control FAK^{+/+} as well as kinase-dead mutants FAK^{R454/R454} and control FAK^{WT/WT}.

Abstract

Biophysical techniques to study cell and matrix properties in the context of single cell migration

der Fakultät für Physik und Geowissenschaften der Universität Leipzig eingereicht von

Dipl.-Phys. Tony Fischer, geb. Kurth

angefertigt an

Peter Debye Institute for Soft Matter Physics / Biological Physics

September 2019

Cancer is an ever-changing disease, emerging from various reasons and progresses unpredictably (Lipinski et al. 2016; Hosseini et al. 2019). This malignant progression, called metastasis, involves the migration and invasion of single cancer cells into the tumor surrounding and ultimately the patients tissue and body (Chaffer et al. 2011; Seyfried et al. 2013). The vast amount of possible mutations in cancer cells result in complex properties and interactions (Claudia Tanja Mierke 2018a; Claudia Tanja Mierke 2018b).

Cell migration is influenced by many aspects, such as cellular mechanical properties and traction forces (Khatau, Bloom, et al. 2012; F. Huber et al. 2013; Fruleux et al. 2016). The cytoskeleton and nucleus are major contributors to cell mechanical properties (F. Huber et al. 2013) and influence cell migration (Okeyo et al. 2009). However, the microenvironment, the so called extracellular matrix (ECM), a cell resides in and migrates through has a major impact on cellular properties and processes (Sapudom et al. 2015; Fischer, Wilharm, et al. 2017). Thus, the investigation of single cell migration demands sophisticated biophysical methods to study metastasis.

In this work, single cell migration in artificial collagen gels as a *in vitro* model system in the context of cancer was studied. Existing biophysical methods, such as atomic force microscopy (AFM), were advanced and further developed. The so called invasion assay, a method to quantify cell migration into artificial 3D collagen networks, was automated

and a user friendly software for high throughput analysis is presented. Furthermore, completely novel methods were developed. First, a novel, minimally invasive approach to quantify the amount of deformation of the microenvironment was developed. Second, a highly advanced pore-size analysis to precisely measure the space in collagen networks available for cells to migrate through was developed. These methods comprise a toolset for single cell migration studies.

The breast cancer cell line MDA-MB-231 was shown to be more invasive and invaded deeper than the breast cancer cell line MCF-7. The more invasive cancer cell line MDA-MB-231 has been shown to be softer than MCF-7. A pharmacological study revealed the major impact of nuclear deformability on cytoskeletal and nuclear mechanics and cell invasion. MDA-MB-231 cells deformed their microenvironment, reconstituted 1.5 g/l collagen I matrices, more than the less invasive MCF-7 cells. Additionally, the role of focal adhesion kinase (FAK), a protein connecting the cytoskeleton to the ECM, on cell migration and fiber displacement was studied. FAK deficient mouse embryonic fibroblasts $FAK^{-/-}$ were less invasive and deformed their microenvironment less than the control cell line $FAK^{+/+}$. The kinase-dead mutant $FAK^{R454/R454}$ showed a higher invasiveness but similar invasion depth to the control cell line $FAK^{WT/WT}$. Additionally, no significant difference in fiber displacement was observed for $FAK^{WT/WT}$ and $FAK^{R454/R454}$ cells.

Acknowledgements

Throughout the writing of this dissertation I have received a great deal of support and assistance. I would first like to thank my supervisor, Prof. Dr. Claudia Tanja Mierke, whose expertise was invaluable in the formulating of the research topic and methodology in particular. I want to thank you for your excellent cooperation and for all of the opportunities I was given to conduct my research and further my dissertation. I would also like to thank my committee, Prof. Dr. Ralf Seidel and Prof. Dr. Tilo Pompe. I would particularly like to single out Prof. Dr. Tilo Pompe for excellent cooperation and co-authorship. I would like to acknowledge my colleagues from my research group Biological Physics for their wonderful collaboration. You supported me greatly and were always willing to help me. I would also like to express my deep gratitude to Prof. Dr. Josef Käs for granting access to his laboratories and devices. I would also like to thank my colleague Alexander Hayn for all the valuable discussions regarding analysis principles and methodology. In addition, I would like to thank my wife for her wise counsel and relentless support. You are always there for me. Finally, there are my family and friends, who were of great support in deliberating over our problems and findings, as well as providing happy distraction to rest my mind outside of my research.

Contents

Abstract	i
Acknowledgements	iii
1 Introduction	1
2 Background	5
2.1 Cancer — An ever-changing Disease	5
2.1.1 Carcinogenesis and Neoplasm	6
2.1.2 Hallmarks of Cancer	7
2.1.3 Metastasis — The malignant Progression of Cancer	7
2.1.4 Metastatic Cascade	9
2.2 The Cell — Where it begins	10
2.2.1 Actomyosin Complex	12
2.2.1.1 Actin Monomer	12
2.2.1.2 Polymerization	12
2.2.1.3 Structures	14
2.2.1.4 Actin Cortex	15
2.2.1.5 Filopodia	16
2.2.1.6 Lamellipodium	16
2.2.1.7 Invadopodium	17
2.2.1.8 Stress Fibers	17
2.2.1.9 Actin in Cancer and Metastasis	17
2.2.1.10 Myosin and Actin	18
2.2.2 Focal Adhesions	19
2.2.3 Microtubules	20
2.2.4 Intermediate Filaments	21
2.2.5 Cellular Stiffness	22

2.2.6	Nuclear Deformability	23
2.3	The Extracellular Matrix — Where it happens	24
2.3.1	Components and Structure	25
2.3.2	Collagen as a Model System	26
2.3.2.1	Collagen I Fibril Formation	27
2.3.2.2	The Rat/Bovine-Collagen-Mix Model System	28
2.4	Single Cell Migration — Why it spreads	29
3	Materials and Methods	31
3.1	Cell Culture	31
3.1.1	Cancer Cells	31
3.1.2	Mouse fibroblasts	32
3.1.3	Pharmacological treatment	34
3.2	Collagen matrices	34
3.3	Cell Elasticity	36
3.3.1	Atomic Force Microscopy	36
3.3.2	Preparation	37
3.3.3	Data Aquisition	38
3.3.4	Data Analysis	38
3.4	Matrix Stiffness	40
3.4.1	Preparation	40
3.4.2	Data Aquisition	41
3.4.3	Data Analysis	41
3.5	Invasion Assay	42
3.5.1	Preparation	42
3.5.2	Data aquisition	44
3.5.3	Data Analysis	44
3.6	Matrix Topology	48
3.6.1	Preparation	49
3.6.2	Data Acquisition	50
3.6.3	Data Analysis	51
3.6.3.1	Binarization	51
3.6.3.2	Pore-Size	53
3.6.3.3	Fiber Thickness	54

3.7	Fiber Displacement	55
3.7.1	Preparation	56
3.7.2	Data Acquisition	56
3.7.3	Data analysis	57
3.7.3.1	Fiber Displacement	59
3.7.3.2	Cell Segmentation	60
3.7.3.3	Shell Analysis	61
3.8	A toolset to understand Single Cell Migration and what influences it . .	62
4	Results	65
4.1	Cell Elasticity	65
4.1.1	Example Force-Distance Curves	66
4.1.2	Single Cell Elasticity	67
4.2	Matrix Stiffness	69
4.3	Invasion	71
4.4	Matrix Topology	75
4.5	Influence of Cell Nucleus on Cell Migration	79
4.5.1	Cellular Elasticity	79
4.5.2	Invasion	81
4.6	Fiber Displacement	89
4.7	Effect of FAK on Cell Invasion and Fiber Displacement	93
4.7.1	FAK Knock-Out	93
4.7.2	Kinase-dead FAK Mutant	96
5	Discussion	103
	References	107

Dedicated to my wife and daughter.

Chapter 1

Introduction

An animal cell is not a fixed entity, but rather an active, biochemical and biophysical machine (Claudia Tanja Mierke 2018a). They are able to progressively alter their shape and function (F. Huber et al. 2013; Alberts 2015), sense and probe their environment with protrusions (Claudia Tanja Mierke 2018a; Claudia Tanja Mierke 2018b). These protrusions are ultimately involved in cell migration (Alberts 2015; Claudia Tanja Mierke 2018b) and force generation through stress fibers (F. Huber et al. 2013).

Elastic properties of the cell and more important the mechanical properties of different cell compartments are an integral part in characterizing the organization and migration of cells (Kollmannsberger et al. 2011; Claudia Tanja Mierke 2018a). Cellular mechanics are an emergent consequence of the cytoskeletal network (F. Huber et al. 2013). Thus, the cytoskeleton influences these mechanical properties and cell migration (Okeyo et al. 2009).

However, cell migration is not only influenced by properties of the cell itself, but also highly affected by topological and elastic properties of the 3D microenvironment the cell resides in (Petrie and Yamada 2015; Fischer, Wilharm, et al. 2017; Claudia Tanja Mierke 2018a; Claudia Tanja Mierke 2018b).

Cancer is an ever-changing, cruel disease, caused and evolving from various reasons and progresses unpredictably (Lipinski et al. 2016; Hosseini et al. 2019). The nastiness lies in the malignant progression of cancer (Chaffer et al. 2011; Seyfried et al. 2013). There, single cancer cells escape the primary tumor, migrate through the patients body and ultimately cause a secondary tumor and start over (Chaffer et al. 2011; Seyfried et al. 2013). The broad amount of possible mutations in cancer cells makes it necessary

to utilize biophysical methods to describe metastasis (Claudia Tanja Mierke 2018a; Claudia Tanja Mierke 2018b).

During metastasis, a cancer cell needs to travel through the body containing a mixture of cells and non-cellular components forming a well organized network of secreted extracellular molecules called extracellular matrix (ECM) (Frantz et al. 2010; Mecham 2011; Theocharis, Spyros S. Skandalis, et al. 2016). Collagens constitute up to 30 % of the proteins mass in humans and are the most abundant protein in the ECM (Frantz et al. 2010). Artificial collagen I matrices polymerized from commercially available collagen I monomers of different origin and concentration have developed as a model system to study cell migration (Sapudom et al. 2015; Fischer, Wilharm, et al. 2017; Fischer, Hayn, et al. 2019). These reconstituted collagen gels are highly reproducible and their mechanical and topological properties can be tuned to specific applications (Sapudom et al. 2015; Fischer, Wilharm, et al. 2017; Fischer, Hayn, et al. 2019).

Single cell migration in 3D microenvironments such as artificial collagen gels is a highly complex process. It is not easily separable into single aspects and rather needs to be studied with different methods covering multiple biophysical properties such as mechanical and topological properties as well as active processes such as cell migration.

Mechanical properties of cells can be determined using different techniques such as atomic force microscopy (AFM) (Fischer, Wilharm, et al. 2017) or optical stretcher device (Kunschmann, Puder, Fischer, Steffen, et al. 2019). Different cellular components such as the cell nucleus have different mechanical properties and influence cell migration (Khatau, Bloom, et al. 2012; Fruleux et al. 2016). The AFM enables the distinction between cellular components such as the cytoskeleton and nucleus due to the small, subcellular sized probe.

During migration, a cell exerts forces upon its microenvironment (F. Huber et al. 2013). Recent studies determined the fiber displacement of reconstituted collagen matrices using fluorescent bead as fiducial markers (Steinwachs et al. 2016). However, it has been shown that cellular motility is drastically reduced when cells phagocytosed those beads (Claudia T. Mierke 2013).

Not only cells have different biophysical properties, but also the microenvironment they reside in (Frantz et al. 2010; Mecham 2011; Theocharis, Spyros S. Skandalis, et al. 2016). In recent years, the so called pore-size, constituting the physical space available for cells to migrate, has emerged as the major parameter to describe collagen matrix topology. Recent studies suggest a random 2D bubble analysis based on a statistical

algorithm (Molteni et al. 2013a) or faster non-random approaches (Münster et al. 2013) that are still error prone (Molteni et al. 2013b). However, the highly complex structure of artificial collagen networks needs sophisticated methods to reliably determine the pore-size. This complexity also makes it difficult to characterize these collagen models in terms of mechanical properties. The AFM is a well established method to determine the bulk elastic modulus of artificial collagen gels (Sapudom et al. 2015; Fischer, Wilharm, et al. 2017).

Finally, as cellular and microenvironmental properties influence cell migration, this highly dynamic process needs to be characterized as well (Alberts 2015; Fischer, Wilharm, et al. 2017; Claudia Tanja Mierke 2018a; Claudia Tanja Mierke 2018b). Thus, the so called invasion assay has emerged as a method to quantify multiple aspects of cell invasion into artificial collagen networks (Fischer, Wilharm, et al. 2017; Claudia T. Mierke et al. 2017; Kunschmann, Puder, Fischer, Steffen, et al. 2019). However, a precise and automated analysis to enable high throughput experiments is not an easy task.

In this thesis, a toolset of biophysical methods to study the above mentioned aspects of single cell migration in the context of cancer cell migration is introduced. The used assays include existing methods that have been improved in terms of conducting the experiment and especially the analysis, as well as completely new approaches to quantify pore-size and fiber displacements. These methods comprise a toolset to describe single cell migration and influences to the latter. The applicability is shown for cancer cells as well as the influence of nuclear elasticity on cell migration and cellular mechanical properties. Additionally, the role of focal adhesion kinase (FAK) on cell migration and fiber displacement is studied using these novel techniques.

First, the scientific background to the principles studied in this work are established. In section 2.1 on page 5, the cancer disease is introduced and discussed. The emergence of cancer is described in section 2.1.1 on page 6. Section 2.1.2 on page 7 describes crucial properties of cancer and cancer cells. The malignant progression of the cancer disease is described in section 2.1.3 on page 7 and section 2.1.4 on page 9, respectively.

Second, a biological view on the eukaryotic cell is given in section 2.2 on page 10. Major components and processes that are involved in and affect cell migration are explained in section 2.2.1 to section 2.2.6 on pages 12–23. The structure and composition of the extracellular matrix (ECM) is described in section 2.3.1 on page 25. Section 2.3.2 on page 26 introduces the collagen I model system. Finally, the interaction and effect of different components and biophysical properties during single cell migration are

discussed in section 2.4 on page 29.

Chapter 3 on page 31 describes the used materials and methods, such as cell lines, cell culture and collagen gels. Additionally, the preparation, data acquisition and analysis of the used and developed methods are introduced and explained in detail. The context of these methods is illustrated in section 3.8 on page 62.

The results of cancer cell elasticity are shown in section 4.1 on page 65, cancer cell invasion results are shown in section 4.3 on page 71. Section 4.2 on page 69 shows outcomes of matrix stiffness experiments, section 4.4 on page 75 shows results of the pore-size analysis. The influence of nuclear elasticity on cancer cell migration is shown in section 4.5 on page 79. Section 4.6 on page 89 reveals the fiber displacements of the used cancer cell lines. The influence of focal adhesion kinase (FAK) on single cell migration and fiber displacements are shown in section 4.7 on page 93.

Chapter 2

Background

Contents

2.1	Cancer — An ever-changing Disease	5
2.2	The Cell — Where it begins	10
2.3	The Extracellular Matrix — Where it happens	24
2.4	Single Cell Migration — Why it spreads	29

2.1 Cancer — An ever-changing Disease

Cancer is an ever-changing disease, arises for numerous reasons and progresses unpredictably (Lipinski et al. 2016; Hosseini et al. 2019). Even worse, cancer has the potential to spread in the patients body and start over (Chaffer et al. 2011; Seyfried et al. 2013).

In this chapter we discuss how cancer emerges and how it progresses maliciously. We explain distinct properties of cancer cells — the hallmarks of cancer (Hanahan and Robert A Weinberg 2000; Hanahan and Robert A. Weinberg 2011) — and the process of metastasis with the metastatic cascade (Claudia Tanja Mierke 2018a; Claudia Tanja Mierke 2018b).

2.1.1 Carcinogenesis and Neoplasm

Carcinogenesis is generally the process of cancer formation and can be divided in three phases: *initiation*, *promotion* and *progression* (Siddiqui et al. 2015). See figure 2.1 for an illustration. A specific carcinogenic process exists, such as virus induced carcinogenesis (Chen et al. 2014). The transformation of normal cells to *cancer cells* involves proto-oncogenes (Weinstein et al. 2006). An activation of proto-oncogenes and an inactivation of tumor suppressor genes accompany the initiation of a *neoplasm* that can lead to an abnormal and excessive tissue growth (Lodish 2016). Cancer cells show a stimulation of cell division, while simultaneously they exhibit impaired cell differentiation and reduction in cell death (Weinstein et al. 2006). These distinct cancer cell features represent three of the hallmarks of cancer (Hanahan and Robert A. Weinberg 2011), see section 2.1.2 on the next page.

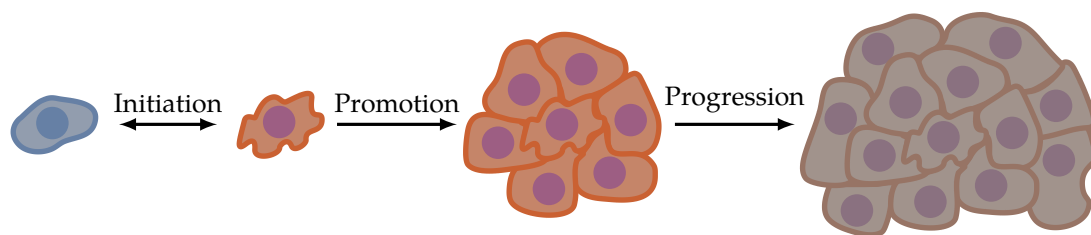


Figure 2.1: Illustration of the initiation of a neoplasm. Initiation involves spontaneous mutations that are reversible by DNA repair. During promotion, preneoplastic cells accumulate. The final step is progression where cancer cells proliferate and tumor growth occurs. Image adapted from (Siddiqui et al. 2015).

Due to the reduced blood flow and decreased oxygen levels during tumor growth, the tumor interior changes from normoxia to hypoxia (McKeown 2014). Alterations in the oxygen concentration can drive the transformation to cancer cells (Claudia Tanja Mierke 2018a). Moreover, a gradient in oxygen concentration causes a change of cellular energy metabolisms (Eales et al. 2016). As a consequence, a distinction of two cancer cell subpopulations is possible (Claudia Tanja Mierke 2018a). One population utilizes the glycolysis cycle or Warburg-dependent metabolism secreting lactate (Cairns et al. 2011; Eales et al. 2016; Claudia Tanja Mierke 2018a). The other adopts energy generation using the citric acid cycle based on lactate (Kennedy et al. 2009; San-Millán et al. 2017; Claudia Tanja Mierke 2018a). Both cancer cell populations act in symbiosis (Claudia Tanja Mierke 2018a).

Additionally, not only cancer cells show alterations in primary tumors, but also the tumor environment (Claudia Tanja Mierke 2018a). For example, extracellular acidity represents a major selection pressure (Kato et al. 2013; V. Huber et al. 2017; Persi et al. 2018). Another prominent characteristic of tumor growth is neoangiogenesis (Claudia Tanja Mierke 2018a) that is the growth of new blood vessels which is essential for tumor nutrient supply and waste product removal (Lodish 2016; Claudia Tanja Mierke 2018a).

2.1.2 Hallmarks of Cancer

The *hallmarks of cancer* are a set of principles to describe the complexity of cancer (Claudia Tanja Mierke 2018a). The six classical hallmarks include: (1) sustaining proliferative signaling, (2) evading growth suppressors, (3) activating invasion and metastasis, (4) enabling replicative immortality, (5) inducing angiogenesis, (6) resisting cell death (Hanahan and Robert A Weinberg 2000). Hanahan and Robert A. Weinberg later proposed two new hallmarks: (1) the utilization of abnormal metabolic pathways, (2) the repression of the immune system (Hanahan and Robert A. Weinberg 2011). An illustration of the hallmarks of cancer and their relation to tumor progression can be seen in figure 2.2 on the following page.

2.1.3 Metastasis — The malignant Progression of Cancer

Most cancer-related deaths involve metastasis (Chaffer et al. 2011). Metastasis is a process and includes numerous consecutive steps and may include other sidesteps (Claudia Tanja Mierke 2018a). Each neoplasm has the potential to metastasize (Lambert et al. 2017; Claudia Tanja Mierke 2018a). Whether neoplastic cells of the primary tumor are able to metastasize depends on the properties of the parent healthy cell (Claudia Tanja Mierke 2018a). The type and aggressiveness of cancer cells and the microenvironment influences the metastatic potential (Lambert et al. 2017; Claudia Tanja Mierke 2018a). Altered cellular mechanical properties of primary cancer cells (Kumar et al. 2009; Fischer, Wilharm, et al. 2017) and surrounding tissue (Fischer, Wilharm, et al. 2017; Lambert et al. 2017) promote metastasis.

Malignant progression begins with the release of cancer cells from the primary tumor into the surrounding microenvironment and is called *metastasis* (Lodish 2016; Claudia Tanja Mierke 2018a). Healthy cells usually stay in distinct places in the organism facilitated

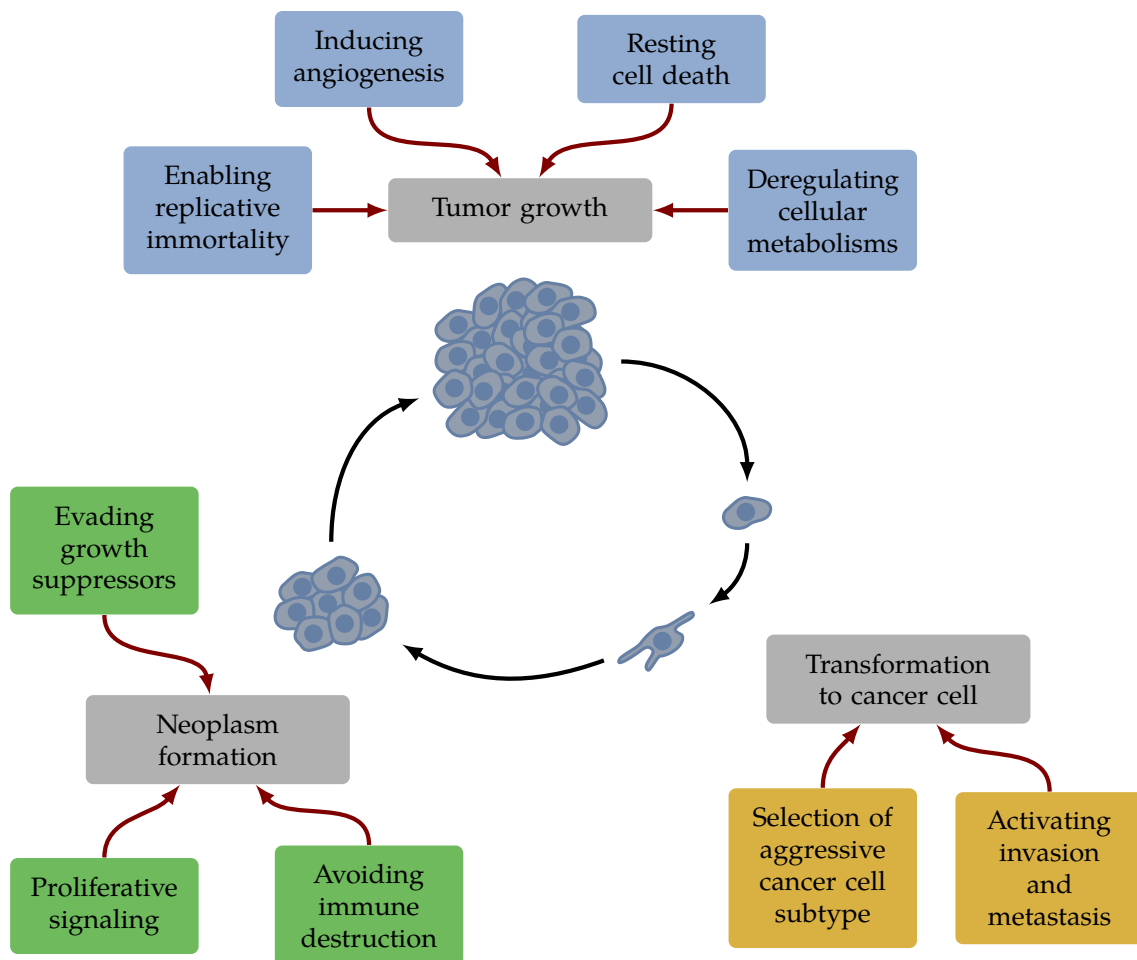


Figure 2.2: The hallmarks of cancer. Each of the three main hallmarks depicted in grey include several processes depicted in colors. Adapted from (Claudia Tanja Mierke 2018a).

by cell-cell adhesion and physical barriers (Lodish 2016). In conclusion, the migration of single cancer cells out of the primary tumor is a major component of the metastatic process (Claudia Tanja Mierke 2018a). This *cancer cell migration* is an intermittent process involving multiple steps: (1) actin polymerization-dependent pseudopod protrusions at the leading edge; (2) integrin-mediated adhesion to the extracellular matrix; (3) contact-dependent matrix degradation; (4) actomyosin-facilitated contraction of the cell body generating tension; and finally (5) translocation of the whole cell body (Alberts 2015; Lodish 2016). See section 2.4 on page 29 for more information.

Metastatic cancer cells employ a protrusive, blebbing or intermediate *lobopodial* migration mode (Claudia Tanja Mierke 2018a). Lamellipodial protrusions in 2D and

invadopodia in 3D environments enable cancer cells to generate forces (Ridley 2011). Filopodial protrusions serve environmental and force sensing purposes, invadosomes facilitate tissue barrier breach and invasion (Ridley 2011; Rottner and T. E. Stradal 2011; Paterson et al. 2017). Invadopodia are a prominent characteristic of cancer cells as they enable penetration of physical barriers such as basal membrane (Lodish 2016). The ability of a cell to invade connective tissue and migrate through tissue barriers is an essential prerequisite for metastasis (Claudia Tanja Mierke 2018a). How potent a migrating and invading cancer cell overcomes the different hindrances in connective tissue depends greatly on cell mechanical properties and force generation (Claudia Tanja Mierke 2018a). Therefore, biophysical and material properties determine the preferred migration mode of an individual type of cancer (Claudia Tanja Mierke 2018a).

The following parameters influence the migration of cancer cells: (1) cell adhesion and de-adhesion processes, such as focal adhesion turnover and strength (2) cytoskeletal remodeling dynamics and cellular stiffness (3) extracellular matrix remodeling and enzymatic degradation (4) generation of protrusive and contractile forces (Claudia Tanja Mierke, Rösel, et al. 2008; Kumar et al. 2009; Claudia Tanja Mierke 2018a). Cancer cell migration is not determined by specific values of the aforementioned parameters, but by a distinct balance of all four (Claudia Tanja Mierke 2013b; Sapudom et al. 2015; Fischer, Wilharm, et al. 2017; Claudia T. Mierke et al. 2017; Kunschmann, Puder, Fischer, Steffen, et al. 2019).

2.1.4 Metastatic Cascade

In the beginning of the cancer disease, after carcinogenesis a neoplasm has formed (Claudia Tanja Mierke 2018a). This primary tumor grows and adapts to the microenvironment (Claudia Tanja Mierke 2018a), see section 2.1.1 on page 6. For an illustration of the metastatic cascade, see figure 2.3 on the next page.

At some point, single cancer cells break out of the primary tumor mass and breach the basal membrane (Lodish 2016; Claudia Tanja Mierke 2018a). *Dissimination* is the process of such cancer cells spreading out (Klein 2008) and is an important step in metastasis (Pantel et al. 2004). Single cancer cells migrate through and invade the tumor microenvironment and surrounding tissue that has been locally transformed by the primary tumor itself (Claudia Tanja Mierke 2018a). Frequently, the migrating cancer cell encounters a blood or lymph vessel (Claudia Tanja Mierke 2018a). *Intravasation* is

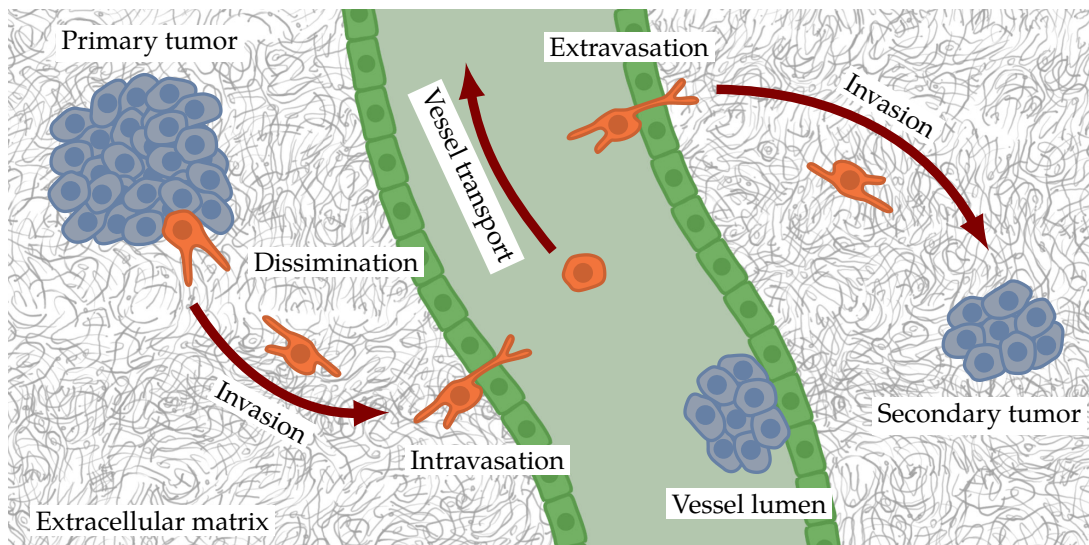


Figure 2.3: The metastatic cascade is a multi-step process. Shown are the major states and processes with red arrows. Blood or lymph vessel is depicted in green, extracellular matrix (ECM) in grey, tumor and migrating cells in blue and orange. Adapted from (Claudia Tanja Mierke 2018a).

the processes of a cancer cell breaking through and migrating into a blood or lymph vessel (Claudia Tanja Mierke 2018a). Subsequently, the vessels transport these cancer cells through the blood or lymph system (Lodish 2016; Claudia Tanja Mierke 2018a). Nevertheless, to produce metastases, a cancer cell has to adhere to the inner vessel wall first (Lodish 2016). A vessel lumen is a secondary tumor that formed directly at the inner vessel wall (Claudia Tanja Mierke 2018a). The single cancer cell possibly breaks through the vessel wall again, also called *extravasation* (Lodish 2016; Claudia Tanja Mierke 2018a). After a second migration and invasion phase, a secondary tumor forms in the surrounding tissue outside the previous vessel (Claudia Tanja Mierke 2018a). In order to produce metastases at distant sites, the cancer cell has to adapt to a potentially different microenvironment (Lodish 2016).

2.2 The Cell — Where it begins

Animals on earth consist of eukaryotic cells and connective tissue (Alberts 2015). These eukaryotic cells — further referenced to as cells — are biological entities filled

with biopolymers serving a large variety of functions with different biophysical and biochemical properties (F. Huber et al. 2013; Alberts 2015; Berg et al. 2015).

The most prominent parts of a cell are the nucleus containing DNA, the *cytoskeleton* containing microfilaments, microtubules and intermediate filaments and responsible for cell shape and motility, and the cell membrane enclosing all cellular components (Alberts 2015). See figure 2.4 for an illustration of the basic components of a eukaryotic cell.

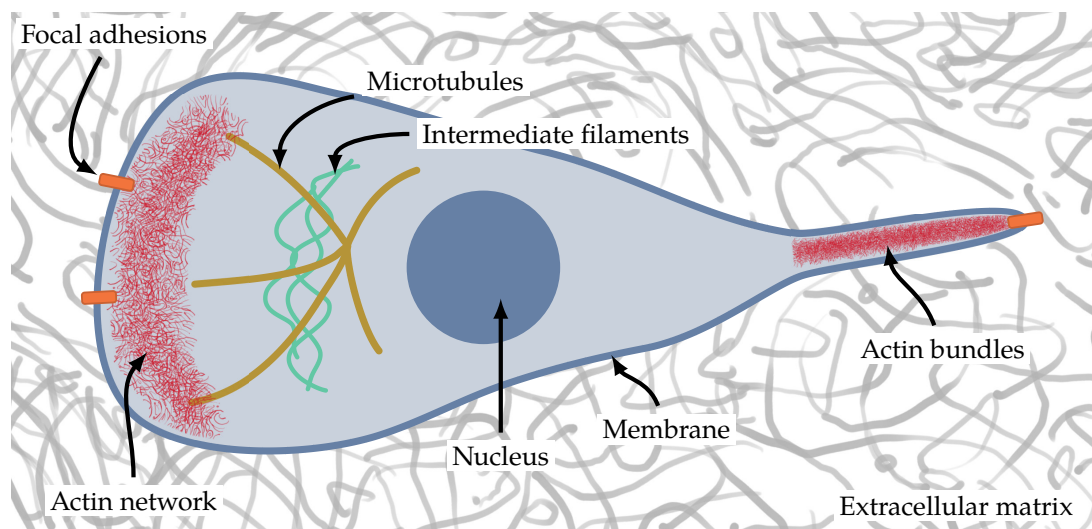


Figure 2.4: Simplified illustration of the main components of a cell. ECM in grey, cell body, membrane and nucleus in blue, actin in red, microtubules and intermediate filaments in yellow and green. Adapted from (Alberts 2015).

The nucleus contains genetic information to synthesize basically all cellular and extracellular molecules (Alberts 2015; Lodish 2016). The cytoskeleton contains mainly actin filaments, microtubules and intermediate filaments, providing structure, stiffness as well as elasticity and cellular motility (F. Huber et al. 2013; Alberts 2015; Lodish 2016). The cell membrane envelops all internal cellular components but also provides connections from internal to external structures and transports ions and signaling proteins (Alberts 2015; Lodish 2016; Claudia Tanja Mierke 2018a; Claudia Tanja Mierke 2018b).

A cell is a highly dynamic machine undergoing constant changes and adaptations under physiological conditions and proportions (Alberts 2015; Lodish 2016). Nevertheless, all these complex processes and structures are susceptible to malignant changes eventually leading to carcinogenesis and cancer (Claudia Tanja Mierke 2018a; Claudia Tanja Mierke 2018b), as described in section 2.1 on page 5.

In the following section, we will discuss the structure and function of cells and their components. Beginning with the different existing actin structures and the actomyosin complex as the workhorse of cellular motility and force generation, we describe how cells bring these forces to action during cell migration. We finally explain the contribution of the cytoskeleton and nucleus to cellular stiffness.

2.2.1 Actomyosin Complex

Actin is the most abundant polymer in eukaryotic cells (Dominguez and K. C. Holmes 2011). It plays a crucial role in cellular structures like lamellipodia, filopodia and invadopodia (Alblazi et al. 2015). Interaction with myosin II motor proteins (Kasza et al. 2011) building the *actomyosin complex* mediates cell contractility and force generation (Claudia Tanja Mierke 2018a; Claudia Tanja Mierke 2018b). The actin network is highly dynamic (Brugués et al. 2010) and constitutes a scaffold for the cell membrane (Guolla et al. 2012), which is directly connected to the actin cytoskeleton that thus regulates the shape of a cell (Diz-Muñoz et al. 2010).

2.2.1.1 Actin Monomer

The actin monomer exists in three main iso-forms: α -, β - and γ -actin (Herman 1993). Actin comprises 375 amino acids (Alberts 2015). Each globular monomer, also called G-actin, consists of an adenine ring, a ribose sugar and inorganic phosphate (Otterbein et al. 2001; Lodish 2016).

The molecular weight of actin is 42 kDa (Mornet et al. 1984). Each actin monomer has two main parts with two subdomains called α and β domain or outer and inner domain and is divided by a cleft containing adenosine diphosphate (*ADP*) or adenosine triphosphate (*ATP*) (Otterbein et al. 2001; Lodish 2016). This structure results in two clefts, the upper cleft binds covalent cations such as Mg^{2+} and the lower cleft binds many actin-binding proteins that provide longitudinal contacts between the actin subunits (Dominguez 2004; Fujii et al. 2010).

2.2.1.2 Polymerization

Monomeric globular actin (G-actin) *polymerizes* to filamentous actin (F-actin) structures (G. M. Cooper 2000). Nucleotide hydrolysis, ions and actin binding proteins

regulate actin polymerization (Carrier et al. 1994; Pollard 2016). Hydrolysis of an ATP nucleotide involves energy release, making it effectively an energy carrier in different metabolic processes (Alberts 2015). A number of phases describe actin polymerization: (1) nucleation, where three monomers aggregate; (2) elongation phase, where the filament grows at both ends with the +end growing 10 times faster, the monomers bind ATP which hydrolyze to ADP at assembly; (3) equilibrium state, regulated by free monomer concentration (G. M. Cooper 2000). See figure 2.5 for an illustration.

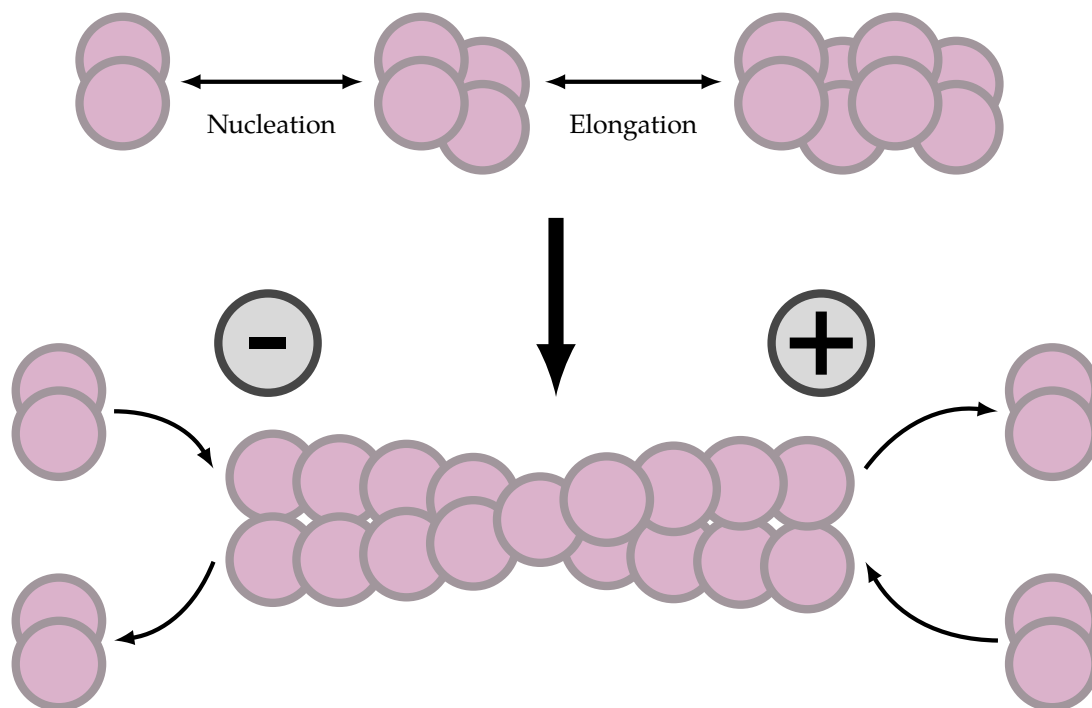


Figure 2.5: Actin monomers depicted in light red need to aggregate in order to start polymerization. After nucleation and elongation, the actin filament enters a state of growth, shrinkage or steady state. Adapted from (Alberts 2015).

The actin monomers polymerize into a left-hand twisted doubly-helix with a rotation of 166° around the helical axis (Berg et al. 2015). Each twist repeats every 37 nm (Alberts 2015) and a polymerized filament has a diameter of approximately 8 nm (Alberts 2015; Berg et al. 2015). 13 molecules in a distance of 2.76 nm repeat every six turns in an axial distance of 35.9 nm (Dominguez and K. C. Holmes 2011). As the helix twisting is close to 180° , the actin polymer appears as two wider turning right-handed chains (Dominguez and K. C. Holmes 2011). As a result of polar G-actin, the actin filaments express a specific polarity with two different ends (Alberts 2015). This polarity is crucial for

polymer assembly and myosin movement along a filament (Alberts 2015). The ATP bound state of actin has a higher stability than the ADP bound state, leading to distinct ends of an actin filament: the *+end* and *-end* (Alberts 2015).

Actin polymerization depends on the concentration of present G-actin monomers with critical polymerization concentrations of $0.1 \mu\text{M}$ at the *+end* and $0.8 \mu\text{M}$ at the *-end* (Lodish 2016). If the G-actin concentration is too low, the filament shrinks at both ends while growing if the concentration is too high (Alberts 2015). This discrepancy leads to a concentration range at which the actin filament grows at the *+end* while it shrinks at the *-end* (Alberts 2015). ATP bound monomers bind to the fast-growing *+end* while ADP bound monomers dislodge from the *-end*, effectively balancing out polymerization rates at both ends, called *steady state* (Wanger et al. 1985). In this steady state of polymerization at one and depolymerization at the other end, actin monomers bound in the filament hike through it from the *+end* to the minus end, called actin treadmilling (Wanger et al. 1985).

2.2.1.3 Structures

Single actin filaments build a variety of structures through actin binding proteins (ABP) (Alberts 2015; Claudia Tanja Mierke 2018a), as seen in figure 2.6. There are two main actin structures: bundles and networks (Alberts 2015; Claudia Tanja Mierke 2018a), as seen in figure 2.4 on page 11. Fimbrin packs actin filaments tightly building parallel bundles (Bartles 2000). α -actinin binds filaments to loosely connected networks forming contractile networks (Alberts 2015; Claudia Tanja Mierke 2018a). The increased distance between the filaments enables the interaction with motor proteins like myosin II (Alberts 2015; Claudia Tanja Mierke 2018a).

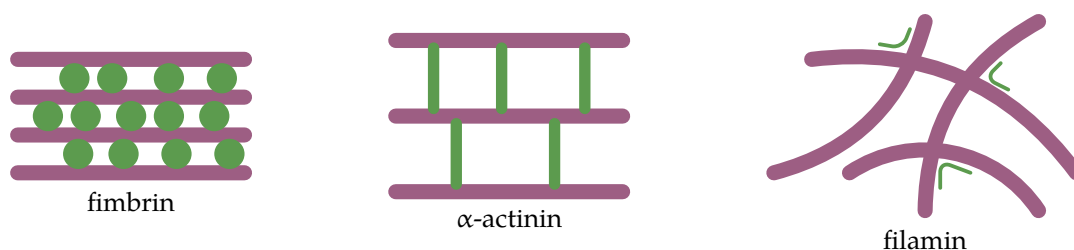


Figure 2.6: Some actin structures with actin in purple and ABP in green. Adapted from (Alberts 2015).

The basis of actin structure assembly are *actin binding proteins (ABP)* (Claudia Tanja Mierke 2018a). Actin bundling proteins like fimbrin and α -actinin shape actin bundles (Bartles 2000). They build densely packed parallel bundles of actin filaments (Bartles 2000). Large ABPs like filamin (also called ABP-280) connect actin networks (Gorlin et al. 1990). Filamin is a flexible V-shaped dimer with actin binding sites at both ends forming looser orthogonal networks providing structural support at the cell membrane (Claudia Tanja Mierke 2018a).

Actin crosslinking proteins have two or more actin binding sites making them essentially dimerized (Alberts 2015; Claudia Tanja Mierke 2018a). Their position controls filament arrangement and the resulting structure during filament polymerization (Alberts 2015; Claudia Tanja Mierke 2018a). ATP hydrolysis maintains the polarity of the actin structure (Pollard and J. A. Cooper 2009).

Actin structures are a key element in the formation of stress fibers (elastic contractile bundles), lamellipodia (sheet-like protrusions), filopodia (spike-like protrusions), microvilli (finger-like surface protrusions) and invadopodia (small invasive cell feet) (Claudia Tanja Mierke 2018a).

2.2.1.4 Actin Cortex

The *actin cortex* is a thin, crosslinked actin network below the cell membrane regulating cell morphology and mechanical properties (Alberts 2015). It provides a mechanical coupling of actin cytoskeleton to the cell membrane (Claudia Tanja Mierke 2018a) and the cortex stiffness influences cell migration (Alberts 2015; Claudia Tanja Mierke 2018a). The cortex is contractile (Claudia Tanja Mierke 2018a) through non-muscle myosin II motor proteins (Narumiya et al. 2009). Filamin bundles actin filaments into parallel bundles providing mechanical resistance and signal transduction near the membrane (Popowicz et al. 2006), as described in section 2.2.1.3 on the preceding page. Similarly, α -actinin cross-links filaments into loose networks providing contractility through myosin II (Alberts 2015; Claudia Tanja Mierke 2018a). Filamin is a mechanosensory protein that regulates transcription, membrane trafficking, ion channel function and cell adhesion (Popowicz et al. 2006; Alberts 2015). The actin cortex providing a physical coupling of the cytoskeleton to the membrane play a major role in signal transduction (Heinemann et al. 2013; Fritzsche, Thorogate, et al. 2014; Saka et al. 2014). It has a thickness of roughly 100 nm to 500 nm (Clark et al. 2013; Fritzsche, Erlenkämper, et

al. 2016). Actin kinetics affect the cortical network structure and the dynamic remodeling defines mechanical properties (Colin-York et al. 2016).

2.2.1.5 Filopodia

A *filopodium* is a thin, long membrane protrusion containing actin, promoting cell migration (Mattila et al. 2008; Nürnberg et al. 2011). Fascin bundles parallel actin filaments (Josephine C Adams 2004a; Josephine C. Adams 2004b; Hashimoto, Kim, et al. 2011). Fascin contributes to the reinforcement of filaments, stabilization of filopodia and invasive structures and cellular motility (Hashimoto, Skacel, et al. 2005; Hashimoto, M. Parsons, et al. 2007; C. Li et al. 2010; Schoumacher et al. 2010). At the tip of filopodia, Ena/VASP proteins induce actin polymerization and thus promote actin bundling (Scott et al. 2005; Breitsprecher, Kieseewetter, Linkner, Urbanke, et al. 2008; Breitsprecher, Kieseewetter, Linkner, Vinzenz, et al. 2011) and focal adhesion formation (Pula et al. 2008).

2.2.1.6 Lamellipodium

Lamellipodia contain an actin network built by an Arp2/3 complex mediated branching (Alberts 2015), which is essential for lamellipodia formation (Suraneni et al. 2012; Wu et al. 2012; Koestler et al. 2013). The polymerization of actin regulates the formation of lamellipodia (Dimchev et al. 2017) Stochastic insertion of actin monomers at the leading edge generates forces (Small et al. 2002). Actin filaments polymerize between the cell membrane and the actin cytoskeleton (Y. L. Wang 1985; Iwasa et al. 2007; Lai et al. 2008; Alberts 2015). The biochemical signaling chain involves the Rac GTPase activating the Scar/Wave complex that finally regulates the Arp2/3 complex (Campellone et al. 2010; Ridley 2011; Steffen, Koestler, et al. 2014). At the leading edge, increased expression levels of the Arp2/3 activator Wave and associated Wave complex (Innocenti et al. 2004; Steffen, Rottner, et al. 2004), FMNL2 and 3 formins (Block et al. 2012; Kage et al. 2017) and Ena/VASP family members (Rottner, Behrendt, et al. 1999; Svitkina et al. 2003) exist. While 2D lamellipodia are flat networks spread along the cell culture surface, 3D lamellipodia have more complex forms and are also called membrane ruffles (F. Huber et al. 2013; Claudia Tanja Mierke 2018a).

2.2.1.7 Invadopodium

Invadopodia are a distinct characteristic of invasive cancer cells (Weaver 2006; Alberts 2015). They contain bundled and branched actin networks (Schoumacher et al. 2010) and remodel the ECM (Claudia Tanja Mierke 2018a). Actin-bundling proteins like fascin (A. Li et al. 2010; Schoumacher et al. 2010), α -actinin, formins and Ena/VASP proteins regulate invadopodia formation (Murphy et al. 2011). Their function comprises membrane extrusion into the ECM and release of endocytic cargo like matrix metalloproteinases (Murphy et al. 2011).

2.2.1.8 Stress Fibers

Stress fibers contain 10 to 30 parallel actin filament bundles with mixed polarity, connected by crosslinking proteins (Cramer et al. 1997). They interact with myosin II and are crosslinked by α -actinin, as described in section 2.2.1.3 on page 14 (Claudia Tanja Mierke 2018a). Distinct types of actin stress fibers constitute essential contractile structures (Tojkander et al. 2012) in fibroblasts and distinct cancer cell lines (Claudia Tanja Mierke 2018a). Stress fibers are thicker and more stable in non-motile cells while thinner and less pronounced in motile cells (Pellegrin et al. 2007).

Stress fibers anchor the cytoskeleton to focal adhesions (Edlund et al. 2001; Claudia Tanja Mierke 2018a) and thus connect the cytoskeleton to the extracellular matrix (Wolfenson et al. 2009) through α -actinin-1 connections (Edlund et al. 2001).

2.2.1.9 Actin in Cancer and Metastasis

The actin cytoskeleton ensures normal cellular functions (Claudia Tanja Mierke 2018a). Diseases such as cancer involve changes in the cytoskeleton facilitating distinct cancer properties (Hanahan and Robert A. Weinberg 2011; Claudia Tanja Mierke 2018a), see section 2.1.2 on page 7. Aggressive cancer cells promote membrane protrusions facilitated by actin bundles for migration and invasion (Claudia Tanja Mierke 2018a). In order to adapt to changing micro-environments during invasion (Hanahan and Robert A. Weinberg 2011; Roussos et al. 2011), the cytoskeleton serves as a foundation for signal transduction and force generation (F. Huber et al. 2013; Alberts 2015).

The associated deregulation of cancer cell motility facilitates metastasis (Bravo-Cordero et al. 2014; Martin et al. 2014; Fischer, Wilharm, et al. 2017). Alterations in cellular

motility involve ABPs influencing actin dynamics (Weaver 2008; Albiges-Rizo et al. 2009; Gau et al. 2015; Madsen et al. 2015). In line with this, cellular mechanical stiffness correlates with cancer cell migration and the metastatic potential (Claudia Tanja Mierke, Zitterbart, et al. 2008; Narumiya et al. 2009; Claudia Tanja Mierke, Frey, et al. 2011; F. Huber et al. 2013; Claudia Tanja Mierke 2013a)

2.2.1.10 Myosin and Actin

Myosins are actin-associated motor proteins utilizing ATP hydrolysis for energy generation (Lodish 2016). They are an important component of the cytoskeleton and formation of contractile structures (Claudia Tanja Mierke 2018a). Myosins are a superfamily of large and diverse proteins with different classes (Hartman et al. 2012) with myosin II being the most important for actin based cell migration (Claudia Tanja Mierke 2018a).

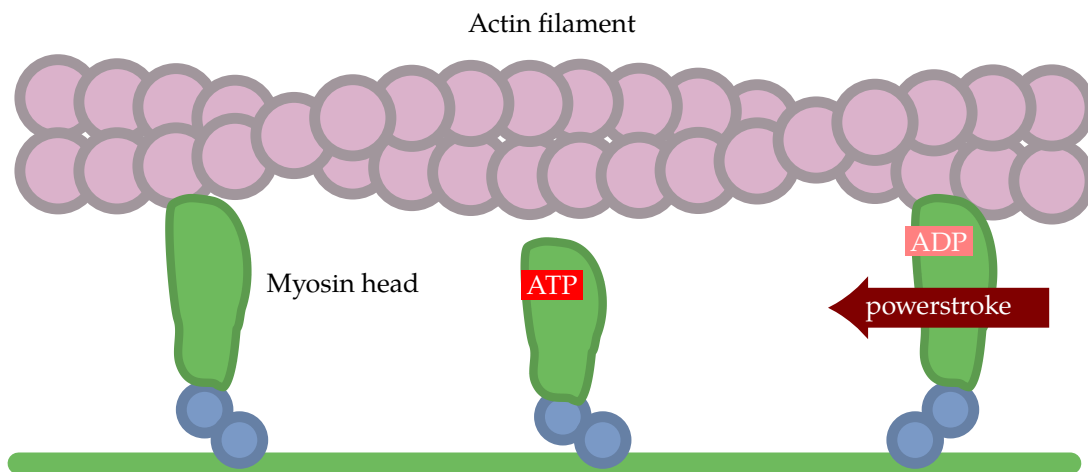


Figure 2.7: Illustration of myosin movement along an actin filament. Shown are the main structures involved and the basic three-step motion mechanism, where the myosin head detaches, changes conformation and attaches back again performing a power stroke, indicated by a red arrow. Adapted from (Alberts 2015).

Myosin II consists of two heavy protein chains in a coiled-coil structure with two globular head light chains at the N-terminus (Alberts 2015). In muscle cells, the coiled-coil tail of the myosin molecule binds to other myosin molecules and forms filaments with the heads pointing outwards from the polymer (Alberts 2015; Lodish 2016). This so called thick filaments are able to slide along actin filament +ends under ATP hydrolysis (Alberts 2015). In non-muscle cells like fibroblasts or cancer cells, myosin II forms small bundles with actin which are much less organized than in muscle

cells (Alberts 2015). These actin-myosin II bundles constitute contractile stress fibers that connect the cytoskeleton to the extracellular matrix through focal adhesions (Alberts 2015; Claudia Tanja Mierke 2018a), see section 2.2.1.8 on page 17. Here, the bundles convert ATP hydrolysis into mechanical work where the neck domain of the myosin II molecule acts as a lever arm performing a stepwise movement (Alberts 2015), as seen in figure 2.7 on the preceding page.

2.2.2 Focal Adhesions

Focal adhesions anchor stress fibers to the extracellular matrix (Wolfenson et al. 2009). In fact, this couples the entire cytoskeleton to the extracellular matrix via actomyosin bundles (Pellegrin et al. 2007; Naumanen et al. 2008). Focal adhesions influence the cell shape especially when the cells reside in 3D environments (Harunaga et al. 2011). The assembly of focal adhesions relies on integrin trafficking (Stehbens et al. 2012; Jacquemet et al. 2013). Microtubules regulate focal adhesion turnover (Stehbens et al. 2012; Yue et al. 2014).

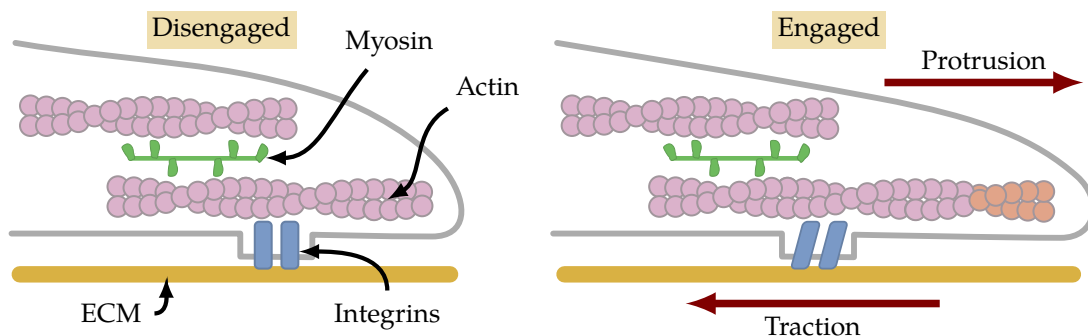


Figure 2.8: Illustration of a focal adhesion during cell migration. Integrins depicted in blue attach intracellularly to actin and extracellularly to collagen. When the cell generates forces through actin polymerization or myosin motor activity, focal adhesions transmit traction forces. Adapted from (Alberts 2015).

The connection of the cell-surface to the extracellular matrix initiates a signaling cascade mediated by focal adhesions (Critchley 2000; Zimmerman et al. 2004; J. T. Parsons et al. 2010) and the integrin adhesion complex (Winograd-Katz et al. 2014; Horton et al. 2015). *Integrins* are cell-cell and cell-matrix adhesion proteins (Hynes 2002), as seen in figure 2.8. They provide the physical connection between the cytoskeleton and the extracellular matrix in conjunction with other focal adhesion proteins (Geiger et al. 2001).

Those include proteins like vinculin and *focal adhesion kinase (FAK)* which are crucial for cell motility and invasion (Gilmore et al. 1996; Claudia T. Mierke et al. 2017) and cellular stiffness (Claudia Tanja Mierke 2013b; Claudia T. Mierke et al. 2017). FAK is a cytoplasmic non-receptor tyrosine kinase located in focal adhesions (J. T. Parsons 2003). It serves as a scaffolding protein and mediates integrin-dependent tyrosine phosphorylation (Mitra et al. 2005; Claudia T. Mierke et al. 2017). FAK also regulates cell mechanics (Zhou et al. 2015; Claudia T. Mierke et al. 2017) and the assembly and disassembly of focal adhesions (Webb et al. 2004; Ezratty et al. 2005; Claudia T. Mierke et al. 2017).

2.2.3 Microtubules

Microtubules play an important role in intracellular vesicle (Welte 2004) and macromolecule transport (S. M. Liu et al. 1993), cytoskeletal remodeling (Birukova et al. 2004) and cell migration (Watanabe et al. 2005; Claudia Tanja Mierke 2018b). Kinesin and dynein motor proteins facilitate the dynamic role of microtubules (Hirokawa 1998; Goldstein et al. 2000; Claudia Tanja Mierke 2018b).

The basic building block of microtubules are α -tubulin carrying a negative charge and β -tubulin carrying a positive charge (Desai et al. 1997). For an illustration of microtubule assembly, growth and shrinkage, see figure 2.9 on the next page. Many of these tubulin dimers form a proto-filament with alternating α and β subunits (F. Huber et al. 2013; Alberts 2015). Exactly 13 proto-filaments with α - α and β - β contacts with a slight stagger form a sheet that rolled up to a tube under the hydrolysis of *guanosine triphosphate (GTP)*, enabling further polymerization (Desai et al. 1997; Nogales et al. 2006). These rolled up sheets assemble monomeric tubulin subunits to hollow cylinders with a diameter of approximately 25 nm (Schek et al. 2007).

As α and β subunits are always aligned, the tube has a polarity with α tubulins at the minus end and β tubulins at the plus end (Alberts 2015; Lodish 2016; Claudia Tanja Mierke 2018b). Both subunits bind GTP during polymerization, but the GTP bound α subunit is stable while the GTP bound to the β subunit hydrolyzes to *adenosine diphosphate (GDP)* when more dimers add to the plus end of the tube (Alberts 2015; Lodish 2016). This leads to a stable cap of GTP bound tubulin dimers at one end of the tube, called *plus end*, and an unstable GDP bound tubulin end, called *minus end* (Alberts 2015; Lodish 2016). As the minus end is unstable, the microtubule depolymerizes at

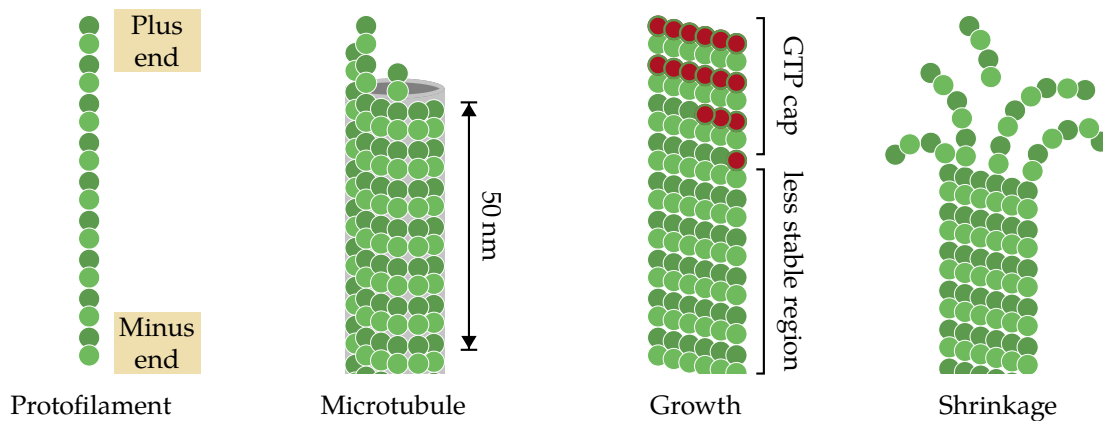


Figure 2.9: Microtubule assembly and growth. Monomers polymerize to a protofilament that assemble to a tube. These tubes grow or shrink as described in section 2.2.3 on the preceding page. Adapted from (Alberts 2015).

this end (Alberts 2015; Lodish 2016). When the hydrolyzation of β subunits catches up to the polymerization rate at the plus end, the stable GTP cap disappears and a rapid depolymerization occurs, called *catastrophe* (Alberts 2015; Lodish 2016). When GTP bound subunits stick back to the collapsed end, the catastrophe stops, called *rescue* (Alberts 2015; Lodish 2016). If the polymerization rates at both ends balance out, the microtubule stays in *pause* (Alberts 2015; Lodish 2016). This random growing and shrinking if the microtubule polymer is called *dynamic instability* (F. Huber et al. 2013; Alberts 2015; Lodish 2016; Claudia Tanja Mierke 2018b).

Microtubules along with actin filaments are key regulators of cell morphogenesis, cell division and motility and vesicle and organelle transport (Etienne-Manneville 2013; Alberts 2015; Mohan et al. 2015). They also play an important role in focal adhesion and force generation (Mohan et al. 2015; Claudia Tanja Mierke 2018b). The molecular interactions between microtubules and actin influence the exertion of cell protrusions and cell adhesion, regulated by the small GTPases Rho, Rac1 and Cdc42 (Alberts 2015; Claudia Tanja Mierke 2018b).

2.2.4 Intermediate Filaments

Intermediate filaments are a class of proteins that build viscoelastic gels (Claudia Tanja Mierke 2018a). Their non-linear elasticity is necessary for normal cell function in soft tissues (Claudia Tanja Mierke 2018a). Intermediate filaments regulate numerous

biological functions such as microtubule organization, nuclear structure regulation and the connection of the nuclear lamina to chromatin and thus are involved in gene regulation, the cell cycle and signal transduction (Claudia Tanja Mierke 2018a). They play a major role in cellular mechanical properties, mechano-transduction and cell migration and cancer invasion (Claudia Tanja Mierke 2018a).

Intermediate filaments are a large family of proteins with a diameter of roughly 10 nm (Fuchs et al. 1994). They possess a tripartite structure with a central alpha-helical rod domain flanked by two non-alpha-helical domains (Lee et al. 2012). Other than actin or microtubules, intermediate filament monomers directly assemble from dimers associating directly with other dimers in an anti-parallel manner building a tetramer (Claudia Tanja Mierke 2018a). These tetramers polymerize laterally into unit length filaments (ULF) with roughly 60 nm length and subsequently longitudinal into longer filaments (Strelkov et al. 2003). Polymerization and depolymerization is solely regulated by phosphorylation and dephosphorylation (Izawa et al. 2006).

2.2.5 Cellular Stiffness

Mechanical properties characterize the structural organization of cells (Kollmannsberger et al. 2011; Claudia Tanja Mierke 2018a). Cellular mechanics are an emergent consequence of the cytoskeletal network (F. Huber et al. 2013) and thus the cytoskeleton influences these mechanical properties and cell migration (Okeyo et al. 2009). Cells are entities filled with biopolymers building stiff networks that are permeable to allow molecule transport (F. Huber et al. 2013). As such, cells represent mechanical and chemical machines that generate forces (Janmey et al. 2009). In turn, cells are also affected by mechanical and structural properties and these forces (Janmey et al. 2009). The dynamic internal organization of cells is reflected by viscoelastic properties as cells show linear viscoelastic behaviour under external stress (F. Huber et al. 2013). For example, cancer cells possess pronouncedly altered mechanical properties (Fischer, Wilharm, et al. 2017). These properties can be studied at the whole-cell level or at subcellular level (Lanzicher et al. 2015; Fischer, Wilharm, et al. 2017; Claudia Tanja Mierke 2018a; X. Wang et al. 2018).

2.2.6 Nuclear Deformability

The *cell nucleus* as the largest cell compartment emerges as a major influence during cell migration in 3D (Khatau, Bloom, et al. 2012; Fruleux et al. 2016). The position of the nucleus inside the cell body is critical for cell polarization (Gundersen et al. 2013). The nucleus resists deformation and therefore counteracts squeezing through narrow extracellular confinements (Claudia Tanja Mierke 2018b). Cancer cells show irregular nuclear shapes and altered stiffness (Claudia Tanja Mierke 2018b).

The nucleus connects to the cytoskeleton and therefore it is also physically linked to the extracellular matrix (Starr 2007; Tapley et al. 2013). This means there exists a mechano-transduction of forces at focal adhesions, transmitted through the cytoskeleton and subsequently to the nucleus (Khatau, Hale, et al. 2009; Alam et al. 2014). As the nucleus deforms under external stress, the internal structures are also redistributed (Claudia Tanja Mierke 2018b). These changes additionally cause alterations in gene expression (Claudia Tanja Mierke 2018b). As a consequence, the nucleus itself reacts to mechanical stimuli (Guilluy et al. 2014).

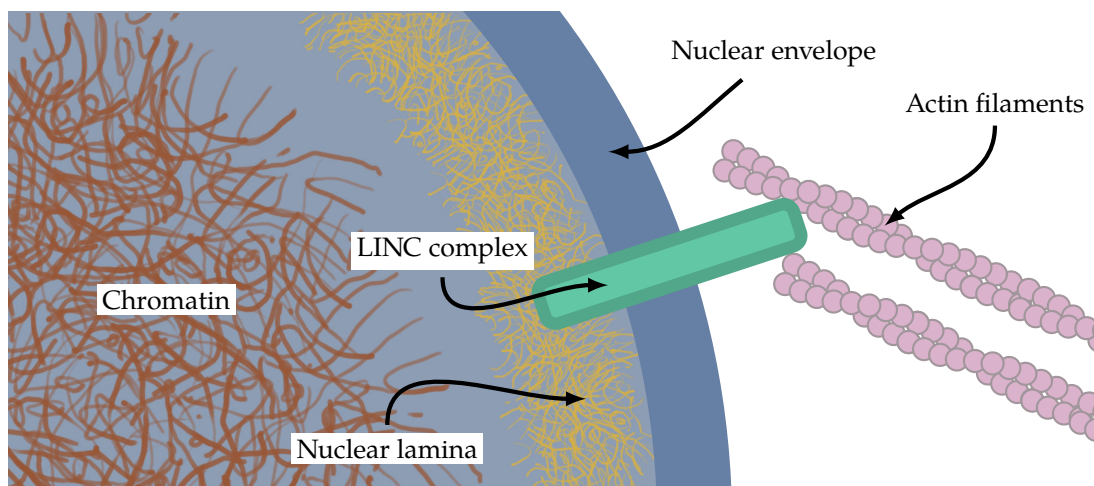


Figure 2.10: Illustration of the structures that influence nuclear mechanical properties. Nuclear envelope depicted in blue, chromatin in brown, nuclear lamina in yellow. The LINC complex connecting the nuclear lamina with actin filaments depicted in green and red. Adapted from (Claudia Tanja Mierke 2018b).

The nuclear envelope has an inner and outer membrane separating it physically from the surrounding cytoplasm (Hetzer 2010). The inner surface is called nuclear lamina and consists of lamins that build a thin meshworks of intermediate filaments contributing to nuclear stiffness (Davidson et al. 2014; Gruenbaum et al. 2015). An

illustration is shown in figure 2.10 on the preceding page. The remodeling of the nuclear lamina is the most important mechanism to alter the nuclear stiffness (Lammerding et al. 2006; Swift et al. 2014). The second most important contributor to nuclear stiffness is chromatin (McGinty et al. 2015). Chromosomes respond elastically to deformation (Schreiner et al. 2015). Another major contributor to nuclear stiffness is the linkage complex of nucleoskeleton and cytoskeleton (LINC) that physically connects the nuclear envelope to the cytoskeleton (Rothballer et al. 2013; Tapley et al. 2013; Chang et al. 2015). The so called perinuclear actin cap consists of actin stress fibers surrounding the nucleus (Khatau, Hale, et al. 2009). All the above mentioned structures contribute to a nuclear stiffness usually an order of magnitude higher than other cell compartments (Friedl, Wolf, and Lammerding 2011) and enables the nucleus to revert to its original shape after deformation on short time-scales (Neelam et al. 2015).

2.3 The Extracellular Matrix — Where it happens

All tissues and organs in animals contain a mixture of cells and non-cellular components forming a well organized network of secreted extracellular molecules called *extracellular matrix (ECM)* (Frantz et al. 2010; Mecham 2011; Theocharis, Spyros S. Skandalis, et al. 2016). The distinct types of ECM and connective tissue in animals serve different functions and consist of a large number of proteins and other molecules (Frantz et al. 2010; Mecham 2011; Theocharis, Spyros S. Skandalis, et al. 2016). They provide structure and stability, regulate cell support, act as storage for nutrients (Frantz et al. 2010; Mecham 2011; Theocharis, Spyros S. Skandalis, et al. 2016) and are important for wound healing processes (Schultz et al. 2009). ECM properties determine the microenvironment in which cells survive, differentiate and migrate and influence chemical and mechanical signalling (Brábek et al. 2010; Sapudom et al. 2015; Fischer, Wilharm, et al. 2017; Claudia Tanja Mierke, Sauer, et al. 2017).

2.3.1 Components and Structure

The ECM is a 3D network of extracellular macromolecules such as collagens, glycoproteins and enzymes supporting cells (Bonnans et al. 2014; Theocharis, Spyros S. Skandalis, et al. 2016). Although the composition varies, cell-cell and cell-matrix adhesion and communication and differentiation are common functions of the ECM (Abedin et al. 2010). Between cells lies the *interstitial matrix* that contains polysaccharides and fibrous proteins serving as a compression buffer against external stress (Alberts 2004). Basement membranes are sheet-like precipitates of ECM in epithelial tissues (Alberts 2015). The ECM constitutes a physical scaffold for cells and regulates cellular processes including growth, migration, homeostasis and morphogenesis (Frantz et al. 2010).

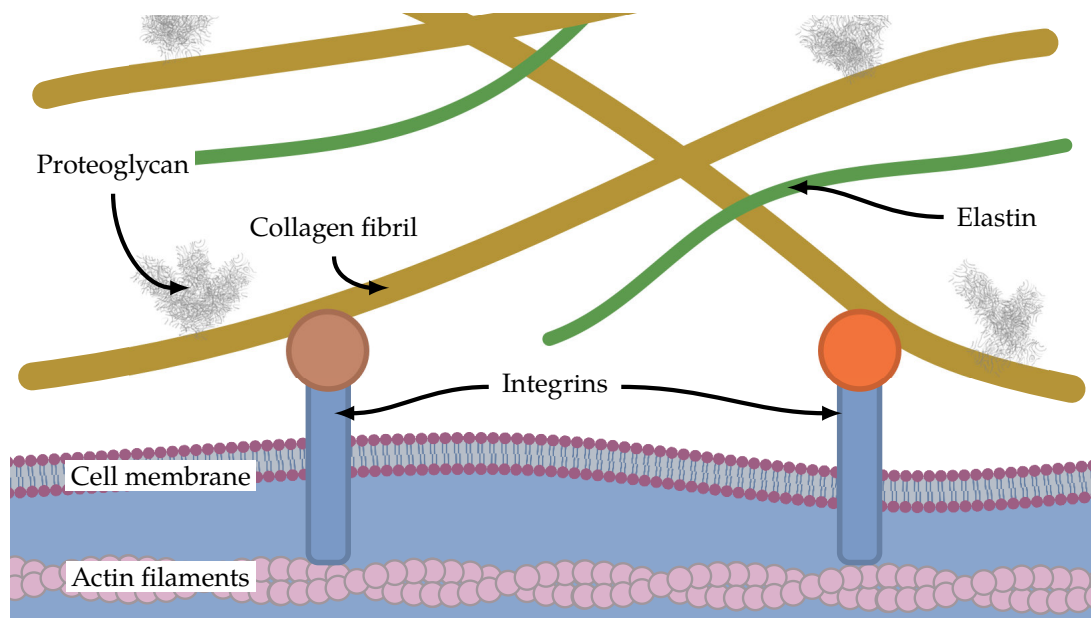


Figure 2.11: Main components of the extracellular matrix. In the top area, ECM components are shown, in the bottom area the cell and integrins connecting the cell to the ECM are depicted. Adapted from (Frantz et al. 2010; Mecham 2011; Theocharis, Spyros S. Skandalis, et al. 2016).

The ECM consists of two main protein classes: proteoglycans and fibrous proteins (Järveläinen et al. 2009; Schaefer et al. 2010). An illustration of the main ECM components in the context of cell adhesion is shown in figure 2.11. *Proteoglycans* are glycosaminoglycans (GAGs) bound to ECM proteins with a net negative charge attracting positively charged sodium ions and thus water molecules through osmosis, keeping the ECM and enclosed cells hydrated (Theocharis, Spyridon S. Skandalis, et al.

2010). Proteoglycans are the most important structural and functional macromolecule in tissues (Theocharis, Spyridon S. Skandalis, et al. 2010). *Hyaluronan or hyaluronic acid* is a linear GAG but non-proteoglycan polysaccharide responsible for tissue resistance to compression (Mecham 2011).

The main fibrous proteins in ECMs are *collagens* (Rozario et al. 2010). They provide mechanical strength, regulate and mediate cell adhesion and migration, support chemotaxis and direct tissue development (Rozario et al. 2010). Collagens constitute up to 30 % of the proteins mass in humans (Frantz et al. 2010) and 90 % of bone protein content (Teitelbaum 2000). Mainly fibroblasts synthesize and secrete collagen in the ECM (De Wever et al. 2008). Fibroblasts exert tension on the surrounding matrix and thus organize collagen fibrils into sheets and cables and dramatically influence the alignment of collagen fibers (Frantz et al. 2010).

Collagen is a superfamily of 28 different collagen types with collagen type I being the most abundant as a major structural element in tissues such as dermis, bone and tendon (Mecham 2011), see section 2.3.2. Another important fibrous ECM component is the structural protein *elastin* (Fratzl 2008) providing elasticity to tissues like skin, blood vessels, lung and heart (Wagenseil et al. 2007; Wise et al. 2009).

Other important ECM molecules are cell adhesion proteins such as fibronectin (Smith et al. 2007). Fibronectin consists of two subunits with roughly 250 kDa size covalently binding integrins (Hynes 2002). The integrin binding of fibronectin is an extracellular mechano-regulator (Smith et al. 2007) and important for cell migration (Rozario et al. 2010). Laminin is found in basal laminae forming web-like networks resisting tensile forces (Iorio et al. 2015).

2.3.2 Collagen as a Model System

Collagen monomers are either secreted inside the cell via translation in the rough endoplasmic reticulum or outside where tropocollagen is formed by procollagen peptidases (Fratzl 2008). Research on collagen networks requires laboratory grade collagen I monomers polymerized under specific conditions for reproducibility (Sapudom et al. 2015; Fischer, Wilharm, et al. 2017; Fischer, Hayn, et al. 2019). Thus, commercially available collagen I monomers comprise the standard model system regarding any experiments utilizing polymerized collagen networks.

2.3.2.1 Collagen I Fibril Formation

Monomers of fibrillar collagens aggregate into fibrils which can further assemble into fibers, bundles and networks (Mecham 2011). Collagen I consists of three α -chains building a heterotrimer with two $\alpha 1$ chains and a slightly different $\alpha 2$ chain (Fratzl 2008; Mecham 2011). They are encoded by the COL1A1 and COL1A2 genes and differ in the (Gly-X-Y)_n triplet structure with n being the number of chains and X and Y being amino acids (Fratzl 2008; Mecham 2011). Each α -chain consists of 338 to 343 uninterrupted amino acid triplets and forms a left-handed polyproline-type-II helix and three helices intertwine to form a right-handed super helix (Mecham 2011). Hydrogen bonds between Gly on one chain and Pro in the X-position of a neighbor chain stabilize the triple helical structure (Mecham 2011). Each monomer has a length of roughly 300 nm and a thickness of up to 1.5 nm (Kadler et al. 1996; Fratzl 2008).

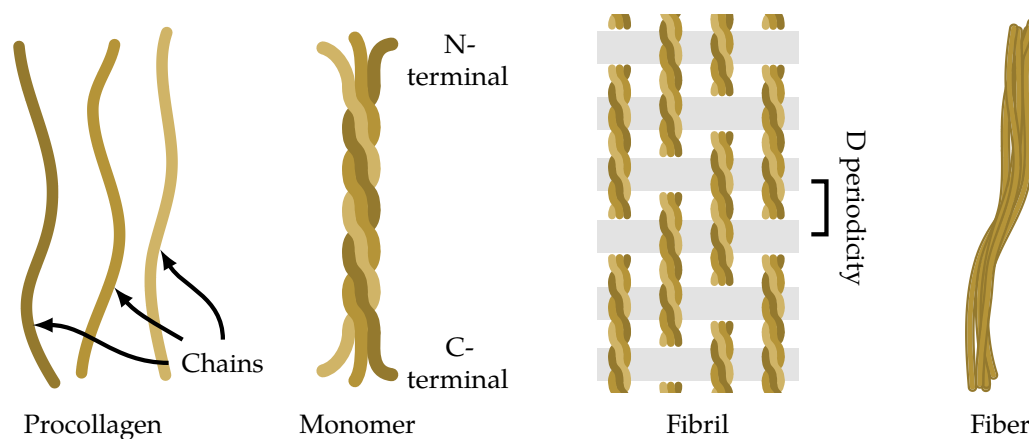


Figure 2.12: Collagen I polymerization and fiber formation. The heterotrimer consists of three α -chains building procollagen, called collagen monomer. These monomers covalently bind to fibrils that build fibers as described in section 2.3.2.1. Adapted from (Kadler et al. 1996; Fratzl 2008).

Collagen I monomers aggregate via covalent bonds between the C-terminal telopeptide and the helical domain into fibrils (Kadler et al. 1996; Fratzl 2008) and networks with different structural and mechanical properties (Mecham 2011). This results in a repeated banding pattern with a periodicity of 64 nm to 67 nm, called D periodicity (Kadler et al. 1996; Fratzl 2008). An illustration of collagen aggregation and fiber formation is shown in figure 2.12.

The aggregation of monomers and lateral growth of fibrils depends on the concentration of monomers that influence fibril formation and fibril diameter (Gelman et al. 1979;

Kadler et al. 1996; Sapudom et al. 2015). Collagen polymerization is also a temperature dependent process (Gelman et al. 1979). An increasing temperature during fibrillation causes a decrease in fibril diameter and length (M.-Y. Liu et al. 2005; Sapudom et al. 2015). The fiber structure is also influenced by pH value (Christiansen et al. 2000; Sapudom et al. 2015).

2.3.2.2 The Rat/Bovine-Collagen-Mix Model System

Collagen I monomers are commercially available with monomers extracted from animals such as rat tail or bovine skin being the most represented (Antoine et al. 2014; Fischer, Wilharm, et al. 2017; Claudia T. Mierke et al. 2017; Fischer, Hayn, et al. 2019). The monomer extraction method influences the hydrogel properties: for example pepsin digestion damages or destroys telopeptides, which play a key role in fiber nucleation (Wolf et al. 2009; Kreger et al. 2010; Parenteau-Bareil et al. 2011). Thus, the extraction method alters the molecular structure during collagen fibril formation and subsequently the assembly kinetics (Gelman et al. 1979; Kreger et al. 2010). Bovine collagen monomers are extracted via pepsin-digestion from bovine skin building long fibers with large pores, while rat tail collagen is nonpepsin-treated (Antoine et al. 2014). Removal of cross-link mediating telopeptides leads to a reduction in fiber nucleation sites (Wolf et al. 2009), rendering telopeptide essential for fibril formation (Kadler et al. 1996). Furthermore, a loss of telopeptides has pronounced effects on fibril growth, including loss of diameter uniformity, loss of unidirectional packing and changes in the fibril assembly pathway (Kadler et al. 1996; Kreger et al. 2010). Telopeptides also play a role in gel lattice contraction (Woodley et al. 1991) and influence the structural and physical properties of collagen hydrogels (Lang et al. 2015; R. Holmes et al. 2017). Recent studies approved these findings and that a collagen matrix comprised of a mix of collagen I monomers extracted from rat tail and bovine skin have much more physiological elastic properties than pure rat tail collagen matrices (Antoine et al. 2014; Lang et al. 2015).

2.4 Single Cell Migration — Why it spreads

Cells are active biochemical machines able to progressively locomote themselves, called *single cell migration* (Claudia Tanja Mierke 2018a). In order to actually migrate, cells need to generate and exert forces (F. Huber et al. 2013). Less complex cells use flagella or cilia to push themselves forward (Alberts 2015) while more complex cells like fibroblasts employ different sophisticated modes of migration (Alberts 2015; Claudia Tanja Mierke 2018b). Those include blebbing motion, mediated solely by actin absent membrane protrusions (Woolley et al. 2017) and crawling motion, utilizing the dynamic and force-generating cytoskeleton (Fletcher et al. 2004; F. Huber et al. 2013). The available migration modes depend on the surrounding a cell adheres to: on 2D substrates cells adhere only to a single surface, while in 3D environments vastly different structures are present that cells need to adapt to, leading to crucial differences in 3D migration (Caswell et al. 2018). The most common type of migration is a form of crawling motion, where the dynamic actomyosin cytoskeleton and actin polymerization pushes the membrane forward and myosin motor proteins generate forces (Kasza et al. 2011; Alberts 2015; Claudia Tanja Mierke 2018b).

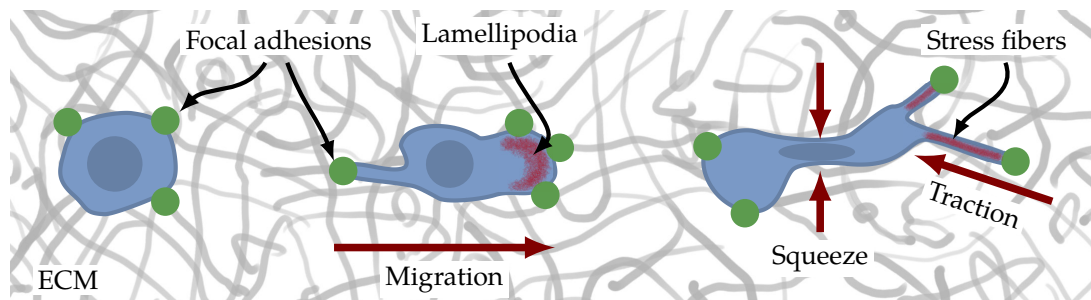


Figure 2.13: Illustration of a single cell migrating in a 3D extracellular matrix. Protrusions enable the cell to sense and penetrate its environment and anchor to it via focal adhesions. Protrusive actin structures such as lamellipodia enable migration. Stress fibers transmit traction forces and enable the cell to squeeze through narrow confinements. Adapted from (Friedl and Wolf 2010; Claudia Tanja Mierke 2018b)

To physically translocate, cells need to transmit the generated forces to their surrounding (Alberts 2015; Claudia Tanja Mierke 2018b). In more detail, the cell needs to establish traction forces (Alberts 2015; Claudia Tanja Mierke 2018b). During blebbing motion,

hydrostatic pressure leads to the formation of lobopodia (Charras et al. 2008; Petrie, Harlin, et al. 2017). Actomyosin driven migration requires focal adhesions to anchor cells to their surrounding (Alberts 2015; Claudia Tanja Mierke 2018b). The different actin protrusions have different functions to sense and traverse the ECM (Alberts 2015; Claudia Tanja Mierke 2018b). An illustration of the basic principles of single cell migration is shown in figure 2.13 on the preceding page.

Signalling proteins such as RAC1 and Cdc42 direct actin nucleating proteins like Arp2/3 leading to branched actin networks that push against the cell membrane (**steffenSra1Nap1Link** **blockFMNL2DrivesActinBased2012a**; T. E. B. Stradal et al. 2004; Bosse et al. 2007; Petrie and Yamada 2015; Kunschmann, Puder, Fischer, Steffen, et al. 2019). Integrin receptors are a crucial component of focal adhesions (Petrie and Yamada 2015; Kunschmann, Puder, Fischer, Perez, et al. 2017) that mature by connecting stress fibers regulated by RhoA and formin (Petrie and Yamada 2015; Claudia Tanja Mierke 2018b). Actomyosin contractility finally generates forces and pulls cells forward (Petrie and Yamada 2015).

Cell migration in 3D environments is also highly affected by the properties of the extracellular matrix such as pore-size and stiffness (Fischer, Wilharm, et al. 2017; Claudia Tanja Mierke 2018b), see section 2.3 on page 24. In order to invade into 3D extracellular matrices, cells need protrusions such as filopodia and lamellipodia to sense and penetrate the ECM network (Claudia Tanja Mierke 2018a; Claudia Tanja Mierke 2018b). Recent studies have shown that different mechanical and structural properties of the ECM crucially influence cell and — more importantly — cancer cell migration (Petrie and Yamada 2015; Fischer, Wilharm, et al. 2017; Claudia Tanja Mierke 2018a; Claudia Tanja Mierke 2018b).

Chapter 3

Materials and Methods

Contents

3.1	Cell Culture	31
3.2	Collagen matrices	34
3.3	Cell Elasticity	36
3.4	Matrix Stiffness	40
3.5	Invasion Assay	42
3.6	Matrix Topology	48
3.7	Fiber Displacement	55
3.8	A toolset to understand Single Cell Migration and what influences it	62

3.1 Cell Culture

3.1.1 Cancer Cells

Human breast cancer cell lines MDA-MB-231 and MCF-7 were purchased from ATCC-LGC-PROMOCHEM (Wesel, Germany). Culture medium consisted of high-glucose 4.5 g/L DMEM (Biochrom, Berlin, Germany) supplemented with 10 % FCS (Biochrom, Berlin, Germany) and 1 % P/S (Biochrom, Berlin, Germany). Standard cell culture was done in 25 cm² cell culture flasks (Greiner, Frickenhausen, Germany).

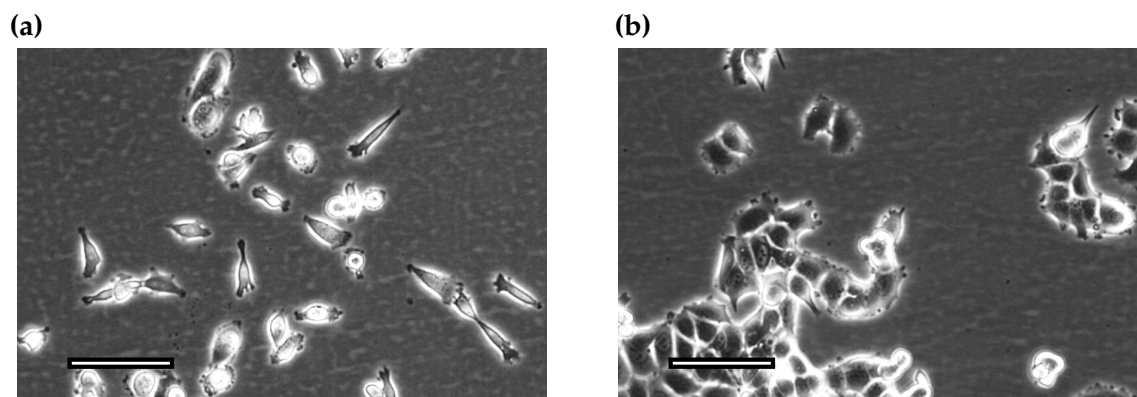


Figure 3.1: Sample phase contrast images of each cancer cell line used in this work. (a) MDA-MB-231 cells, (b) MCF-7 cells. Scale bar is 100 μm .

Cells were passaged for cultivation and harvested for experiments at $\sim 80\%$ confluency with passage numbers of 5 to 35. Passaging was done using 0.125% Trypsin/EDTA solution in PBS applied for 4 min in an incubator at 37°C , 5% CO_2 , 95% humidity. Low passage numbers of 0 to 2 were stored cryogenically in 5% DMSO-medium. These cells were thawed in 75 cm^2 cell culture flasks (Greiner, Frickenhausen, Germany) supplemented with 4.5 g/L DMEM in an incubator at 37°C , 5% CO_2 , 95% humidity and cultured for at least three passages over two weeks.

3.1.2 Mouse fibroblasts

Mouse embryonic wild-type fibroblasts ($\text{FAK}^{+/+}$) as well as FAK deficient fibroblasts ($\text{FAK}^{-/-}$) were purchased from ATCC-LGC-PROMOCHEM (Wesel, Germany). The $\text{FAK}^{\text{WT}/\text{WT}}$ and $\text{FAK}^{\text{R454}/\text{R454}}$ cells were kindly provided by Dr. David D. Schlaepfer. Primary $\text{FAK}^{\text{R454}/\text{R454}}$ (kinase-dead) and $\text{FAK}^{\text{WT}/\text{WT}}$ mouse embryonic fibroblasts (MEFs) were isolated from E8.5 embryos. In short, the R454 FAK knock-in point mutation was generated by homologous recombination as described in (Lim et al. 2010; Claudia T. Mierke et al. 2017). Immortalization of primary MEFs were performed using retrovirus-mediated expression of human telomerase reverse transcriptase (hTERT). $\text{FAK}^{\text{R454}/\text{R454}}$ possess a kinase-dead variant of FAK while $\text{FAK}^{\text{WT}/\text{WT}}$ serves as a wild-type control. FAK was present at focal adhesions in $\text{FAK}^{\text{R454}/\text{R454}}$ cells but was not phosphorylated, leading to no change in cell growth (Lim et al. 2010). Culture medium consisted of high-glucose 4.5 g/L DMEM (Biochrom, Berlin, Germany) supplemented with 10% FCS

(Biochrom, Berlin, Germany) and 1 % P/S (Biochrom, Berlin, Germany). Standard cell culture was done in 25 cm² cell culture flasks (Greiner, Frickenhausen, Germany).

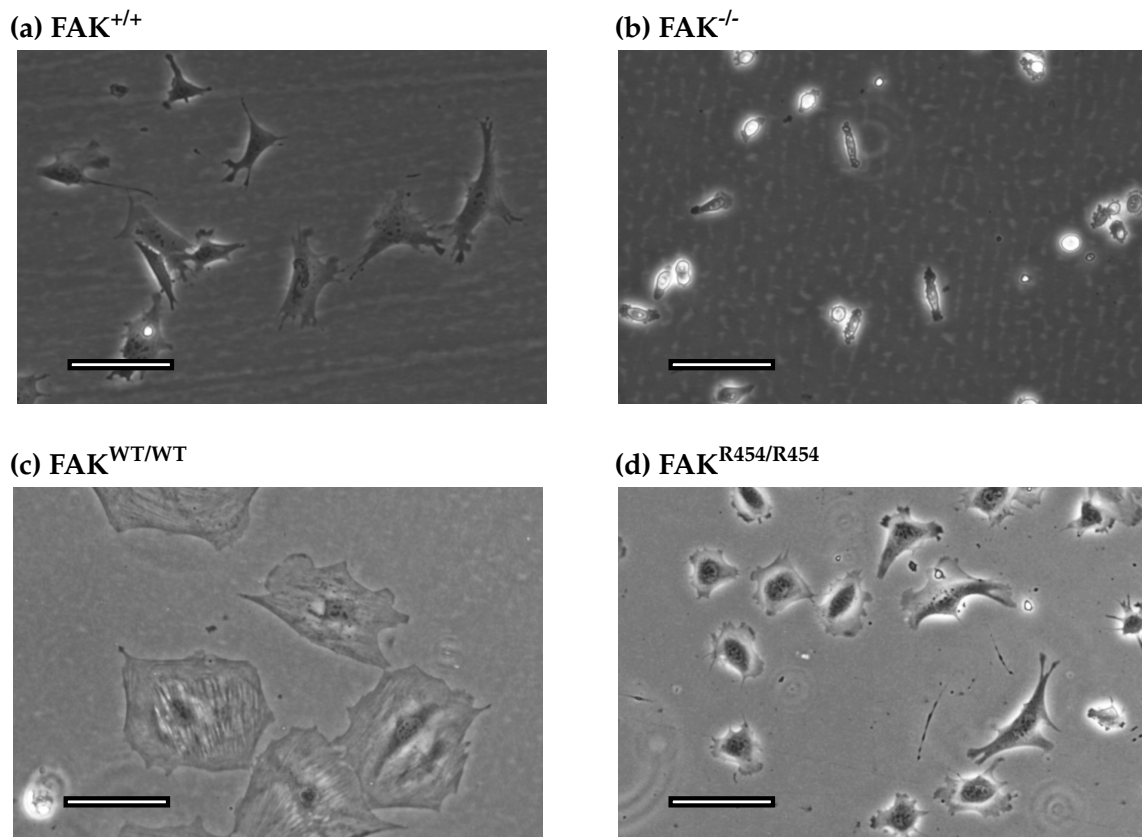


Figure 3.2: Sample phase contrast images of each cancer cell line used in this work. Scale bar is 100 μ m. Shown are (a) FAK^{+/+}, (b) FAK^{-/-}, (c) FAK^{WT/WT}, (d) FAK^{R454/R454} cells.

Cells were passaged for cultivation and harvested for experiments at ~80 % confluency with passage numbers of 5 to 35. Passaging was done using 0.125 % Trypsin/EDTA solution in PBS applied for 10 min in an incubator at 37 °C, 5 % CO₂, 95 % humidity and intermittent soft mechanical shaking to support dislodging. Low passage numbers of 0 to 2 were stored cryogenically in 5 % DMSO-medium. These cells were thawed in 75 cm² cell culture flasks (Greiner, Frickenhausen, Germany) supplemented with 4.5 g/L DMEM in an incubator at 37 °C, 5 % CO₂, 95 % humidity and cultured for at least three passages over two weeks.

3.1.3 Pharmacological treatment

The cell nucleus plays a key role in cellular stiffness, see section 2.2.6 on page 23. To investigate the contribution of nuclear stiffness on cell migration, the cells need to be treated pharmacologically.

The cell nucleus was treated using 900 ng/ml *TrichostatinA* (TSA) for at least 24 h. TSA inhibits the histone deacetylases I and II by preventing acetyl group removal from lysine residues of histone tails and as a consequence causes chromatin de-condensation (Krause et al. 2013). The latter leads to a softening of the cell nucleus (Krause et al. 2013).

In this work, a TSA concentration of 900 ng/ml has been found to be most effective while preserving cell viability.

For control experiments and mechanistic insight into cellular stiffness alterations using TSA, two cytoskeletal influencing drugs were used in this work. First, 25 μ M BLEBBISTATIN was utilized to reduce the affinity of myosin II motor proteins to the filamentous actin network by blocking myosin II in the state where it is detached from filamentous actin (Kovács et al. 2004). Second, 0.2 μ M LATRUNCULIN A was used to inhibit actin polymerization, which in turn effectively eliminates actin filaments (Fischer, Wilharm, et al. 2017; Kunschmann, Puder, Fischer, Steffen, et al. 2019).

For AFM measurements, the cells were seeded into a 4 cm petri dish 48 h before each measurement, as described in section 3.3.1 on page 36. After 24 h of adhesion and proliferation on the petri dish surface, TSA was applied for another 24 h. As a result, at an AFM measurement start, the cells proliferated for 24 h and were pharmacologically treated with TSA for 24 h.

For 3D invasion assays as described in section 3.5 on page 42, the cells were seeded on top of the collagen gels and proliferated for 12 h. Subsequently, fresh cell culture medium with the desired TSA concentration was applied. After this TSA application, the cells were put in an incubator at 37 °C, 5 % CO₂, 95 % humidity for the default invasion time of 72 h. After this time period, the samples were treated as described in section 3.5 on page 42.

3.2 Collagen matrices

To study 3D single cell migration, an ECM model system physiologically similar to real ECM has to be used (Paszek et al. 2005; Lang et al. 2015), as described in section 2.3.2

on page 26. In this work, artificial collagen I matrix scaffolds composed of a mixture of two differently extracted collagen I monomers have been used as a general ECM model system, as published in (Fischer, Wilharm, et al. 2017; Claudia T. Mierke et al. 2017; Fischer, Hayn, et al. 2019). More information can be found in section 2.3.2.2 on page 28. A detailed protocol can be found in.

Commercially available collagen I monomers from rat tail (Serva, Heidelberg, Germany, Cat.No.: 47256) and bovine skin (Biochrom, Berlin, Germany, Cat.No.: L7213) are stored in acidic solution at 4 °C. Both rat and bovine stock solution concentrations were 4 g/l. A phosphate buffered solution consisting of a mixture of sodium dihydrogen phosphate $\text{NaH}_2\text{PO}_4 \cdot \text{H}_2\text{O}$ (Sigma Aldrich, Cat.No: 71507) and disodium hydrogen phosphate Na_2HPO_4 (Sigma Aldrich, Cat.No: 71636) in ultrapure water dH_2O was used to set a specific pH value and ionic strength ensuring specific fibrillation parameters. The solution was prepared with pH 7.4, ionic strength of 0.7 and 200 mM phosphate according to the Henderson–Hasselbalch equation and kept on ice at 4 °C.

Both collagen monomer stock solutions and the pre-mixed buffer solution were kept on ice at 4 °C. The pre-cooled buffer solution and collagen I monomer stock solutions were mixed together and subsequently thoroughly vortexed, but only for a short amount of time to ensure proper cooling. The pipet tips and mixing tubes at 4 °C. Collagen I monomer stock solution and phosphate buffer quantities used in the mixture were calculated considering two parameters: (1) the mass ratio of rat and bovine collagen monomers in this work was kept at 1/3 rat and 2/3 bovine and (2) the desired final collagen monomer concentration, for example 1.5 g/l or 3.0 g/l.

Finally, this buffered collagen monomer solution was put in an incubator at 37 °C, 5 % CO_2 , 95 % humidity to initialize fibrillation, as described in section 2.3.2.1 on page 27. After a fibrillation process of 2 h in the incubator at 37 °C, 5 % CO_2 , 95 % humidity, the fibrillated gels were washed three times with PBS to eliminate residual phosphate ions and collagen monomers. The final collagen gels were kept hydrated in PBS in an incubator at 37 °C, 5 % CO_2 , 95 % humidity.

3.3 Cell Elasticity

3.3.1 Atomic Force Microscopy

Atomic Force Microscopy (AFM) started as a tool to measure forces as small as 10^{-18} N (Binnig et al. 1986), advanced to record surface height maps (Radmacher et al. 1992) and force-distance curves (Cappella et al. 1999), and ultimately found a variety of applications in biophysics, such as cell elasticity measurements (Alessandrini et al. 2005; Fischer, Wilharm, et al. 2017; Claudia T. Mierke et al. 2017).

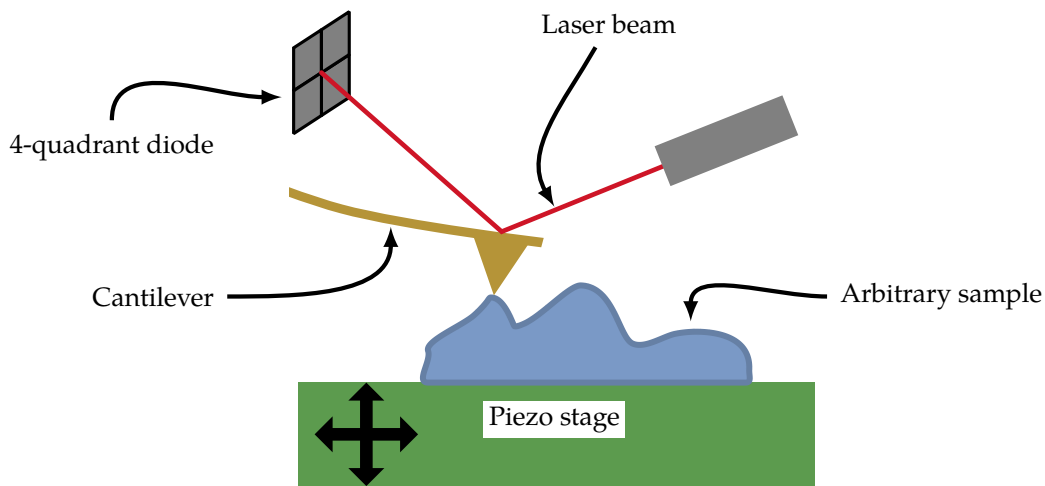


Figure 3.3: The basic working principle of an AFM measurement recording a force-distance curve. The sample in blue resists indentation by the cantilever, which is bent. The laser beam is deflected, generating a voltage difference on the 4-quadrant diode, representing the cantilever bending.

Figure 3.3 illustrates the basic working principle. The deformation of an elastic cantilever is measured using a laser. In more detail, the laser beam is reflected on the surface of the cantilever. When the cantilever is bent, the laser reflection changes direction slightly, which is detected by small voltage changes on a four-quadrant photo diode. Using piezo-motors, the AFM device or the sample itself is moved in height with nanometer precision. This height is correlated with the cantilever deflection, called a *force-distance curve*.

In this work, the AFM was used to record force-distance curves and calculate the Young's Modulus as a measure of elasticity. Therefore, a polystyrene bead radius was glued to the tip of a cantilever and indented into cells or collagen gels. The

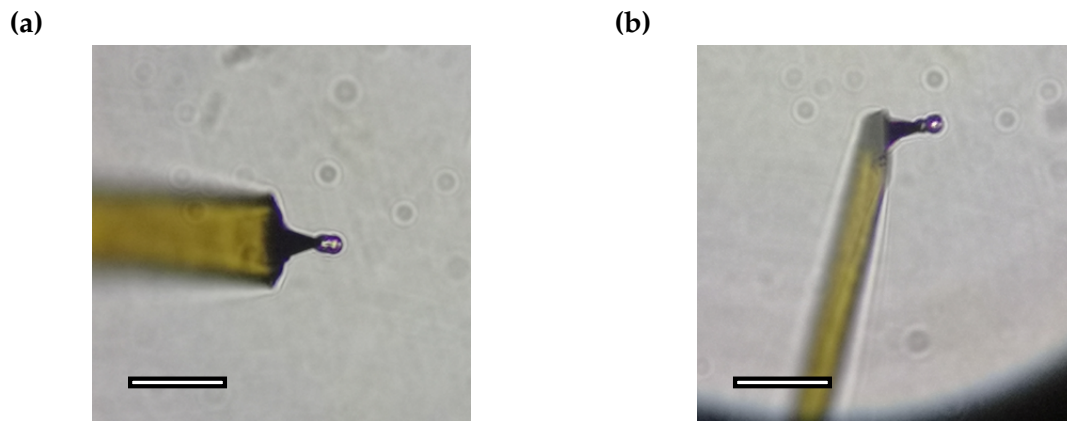


Figure 3.4: Microscopic images of a cantilever with 6 μm polystyrene bead glued to the pyramidal tip. Shown are (a) top view and (b) side view. The preparation was done using a micromanipulator microscope. Images were taken using a cell phone and the ocular port of the microscope. Scale bar is 30 μm .

recorded force-distance curves were fitted using the Hertz model to calculate the elastic modulus (Kuznetsova et al. 2007; Fischer, Wilharm, et al. 2017; Claudia T. Mierke et al. 2017). Depending on the specific application, the cantilever, bead size and maximum indentation force can be varied, as described in the following sections.

3.3.2 Preparation

Cells were prepared according to section 3.1 on page 31. The cell suspension was put in a 4 cm cell culture dish and in an incubator at 37 °C, 5 % CO₂, 95 % humidity for at least 24 h. After this time period, the cells adhered to the plastic substrate and their spreading area increased. Pharmacological drugs were applied prior to each measurement, depending on the optimal application time, see section 3.1.3 on page 34.

A polystyrene bead with a diameter of 6 μm was glued to the very tip of a cantilever with pyramidal tip. This was performed using a custom micromanipulator microscope device. In the first step, epoxy glue was applied to the cantilever tip. Subsequently, a single polystyrene bead was picked up with the cantilever tip. Finally, the cantilever-bead composite was baked in an oven at 80 °C over night to cure the glue. Figure 3.4 shows top and side view photographs of the final AFM cantilever.

3.3.3 Data Acquisition

The cell culture dish with adhered cells was put in a heated stage with humidified CO₂ influx, in order to maintain similar cell culture conditions as in an incubator at 37 °C, 5 % CO₂, 95 % humidity. A NanoWizard ® NanoOptics AFM system (JPK, Berlin, Germany) with an automated x-y stage was used. Utilizing a live camera video, the measurement points were set precisely. These points were then probed automatically.

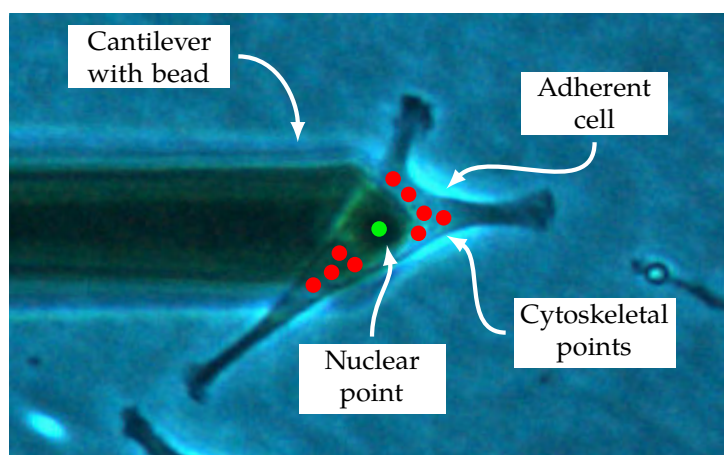


Figure 3.5: Representative phase-contrast image of adherent cell, the cantilever and illustrative measurement points. Cytoskeletal points are marked red and nuclear points are marked green.

To determine cytoskeletal elasticity, 10 to 20 randomized measurement points in peri-nuclear areas of a adherent cell were chosen for probing. An exemplary point selection for the cytoskeleton can be seen in figure 3.5. For each measurement point, a force distance curve with a maximum indentation force of 0.5 nN was recorded.

To determine the nucleus elasticity, a single measurement point centered above the cell nucleus was chosen. An exemplary point selection for the nucleus is presented in figure 3.5. For this single point, 5 repetitive force distance curves with a maximum indentation force of 5 nN were recorded.

3.3.4 Data Analysis

To calculate cell elasticity, the approach part of the force-distance curves were fitted using the Hertz-model for a sphere indented into a half-space:

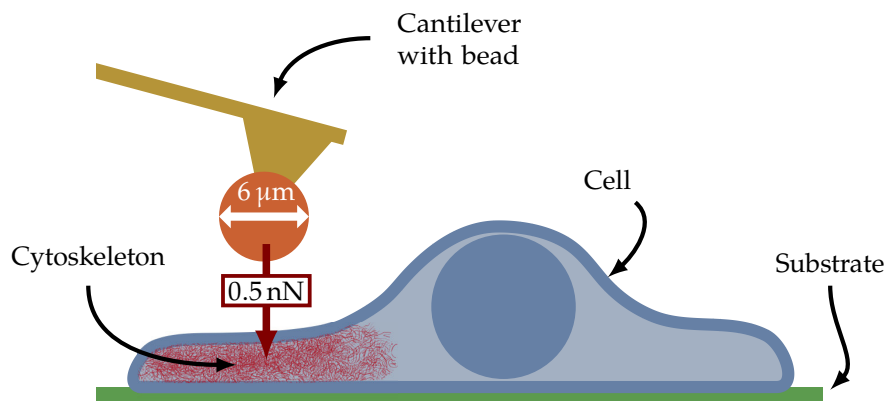


Figure 3.6: Side-view illustration of a measurement to determine cytoskeletal elasticity. The cell adhered to the plastic substrate of the cell culture dish. The cytoskeleton was indented with a maximum indentation force of 0.5 nN at random points along the peri-nuclear area of the cell.

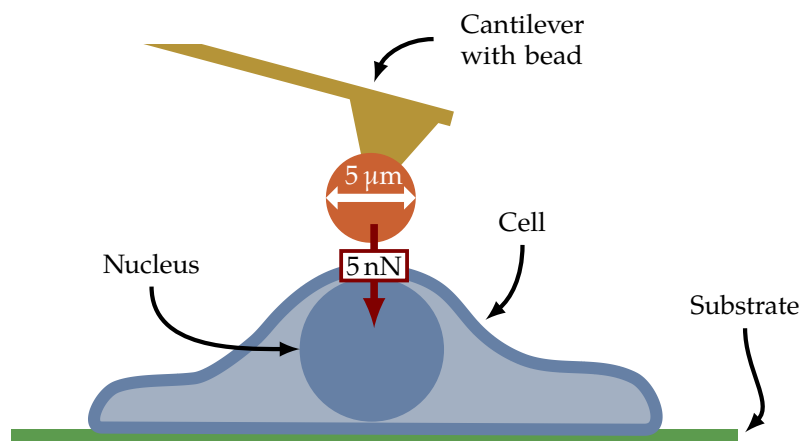


Figure 3.7: Side-view illustration of a measurement to determine nuclear elasticity. The cell adhered to the plastic substrate of the cell culture dish. The nucleus was indented centrally with a maximum indentation force of 5 nN. 5 repetitive force-distance curves were recorded for the same point.

$$F = \frac{3}{4}ER^{\frac{1}{2}}d^{\frac{3}{2}}$$

with indentation force F , elastic modulus E , sphere radius R and displacement d .

The recorded force-distance curves were analyzed using the JPK SPM DATA PROCESSING v6.1.92 application. With this software, the curves were drift-corrected, aligned and fitted using the implemented pre-defined „Hertz-fit“ process with a default poisson ratio of 0.5, tip radius of 3 μm. The resulting data table was saved as a tab-separated-value

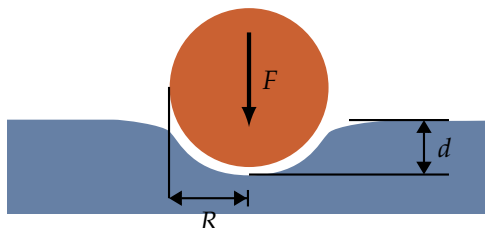


Figure 3.8: Illustration of the Hertz-model with indentation force F , sphere radius R and displacement d . A sphere was indented into a soft material surface. Elastic properties can be derived from indentation and sphere radius.

(TSV) text file which can be easily processed in custom written PYTHON scripts. The curves were filtered by the residual Root Mean Square (RMS) value, which represents a quality of fit parameter. A maximum RMS of 150 pN was used to eliminate poor fits.

3.4 Matrix Stiffness

The working principle of an AFM has been described in section 3.3.1 on page 36.

3.4.1 Preparation

Collagen gels were prepared according to section 3.2 on page 34. 500 μL of the non-polymerized collagen buffer solution were pipetted in a 4 cm cell culture dish as a droplet. These samples were placed in an incubator at 37 $^{\circ}\text{C}$, 5% CO_2 , 95% humidity for 2 h to polymerize the collagen gels, resulting in small dome-shaped collagen gels on the plastic surface of the petri dishes.

A polystyrene bead with a diameter of 45 μm was glued to a tipless cantilever. In the first step, a diluted solution of the 45 μm was distributed on one half of a glass cover slip and dried over night, resulting in single beads distributed on the glass surface. In the second step, a thin layer of epoxy glue was applied to the other half of the cover slip, as seen in figure 3.9a on the next page. Next, a small amount of liquid epoxy glue was applied to the outer most tip of the cantilever and immediately afterwards a bead was picked up with the un-cured glue droplet. An exemplary cantilever with attached bead is shown in figure 3.9b on the facing page. The epoxy was cured in an oven at 80 $^{\circ}\text{C}$ over night.

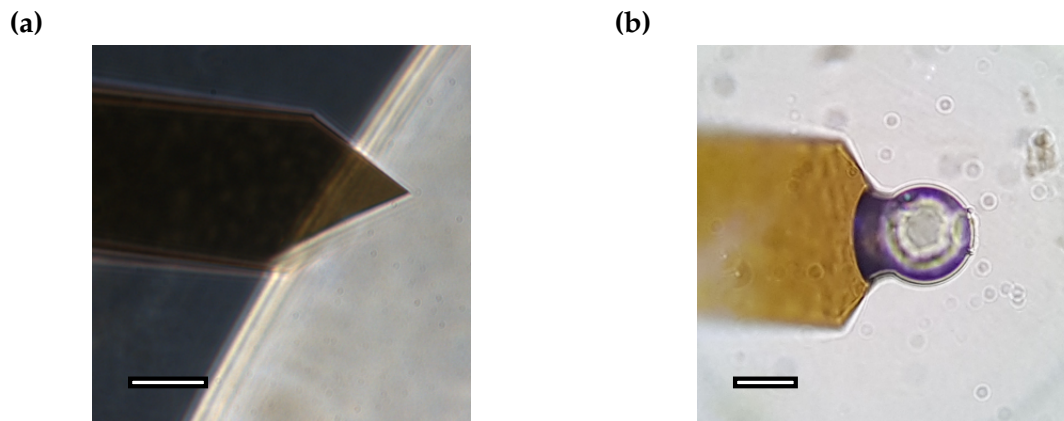


Figure 3.9: Microscopic images of a cantilever with 45 μm polystyrene bead. The preparation was done using an AFM. (a) Untreated cantilever in brown and un-cured glue layer as bright area on the right, (b) front view of cantilever in brown with bead attached to it. Scale bars are 30 μm .

3.4.2 Data Acquisition

The cell culture dish with collagen gels was put in a heated stage at 37 °C. A CellHesion ® 200 AFM (JPK, Berlin, Germany) with a 100 μm z-piezo was used. This allowed for a high retract length necessary to overcome probe adhesion to the sticky collagen surface. Utilizing a live camera video, the measurement points can be set precisely. However, due to a lack of an automated x-y stage, the measurement points had to be set manually using micrometer screws.

To determine matrix stiffness, 50 to 100 randomized measurement points around the center of a collagen gel surface were chosen for probing. For each measurement point, a force distance curve with a maximum indentation force of 5 nN was recorded. An illustration is shown in figure 3.10 on the next page.

3.4.3 Data Analysis

Data analysis was performed as described in section 3.3.4 on page 38. However, the retract curve was fitted rather than the approach curve, as published in (Sapudom et al. 2015).

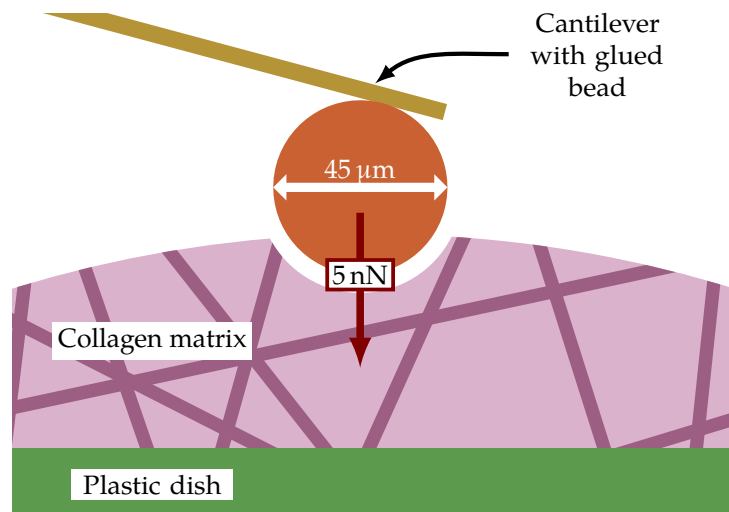


Figure 3.10: Side-view illustration of a measurement to determine collagen matrix stiffness. The collagen surface was indented with a maximum indentation force of 5 nN at random points around the center of the polymerized collagen droplet.

3.5 Invasion Assay

The *invasion assay* represents a sophisticated, well established method to study single cell migration in large quantities (Claudia Tanja Mierke, Frey, et al. 2011; Claudia Tanja Mierke 2013a; Fischer, Wilharm, et al. 2017; Claudia T. Mierke et al. 2017).

As described in section 3.5.1, cells were seeded on top of crafted collagen gels inside a well plate. The cells adhered and ultimately migrated into the gel, depending on the metastatic potential (Fischer, Wilharm, et al. 2017; Claudia T. Mierke et al. 2017). After three days, the assay was fixed and 3D cell nuclei positions were determined, leading to detailed invasion statistics.

3.5.1 Preparation

Collagen gels with specific concentrations such as 1.5 g/l or 3.0 g/l were prepared as described in section 3.2 on page 34. 1.2 ml of the pre-cooled collagen-buffer-solution were pipetted into each well of a 6-well plate (Cat.No: 657160, Greiner, Frickenhausen, Germany), resulting in a collagen gel of about 400 μm to 450 μm height. Pipet tips as well as the well plate were kept at 4 °C.

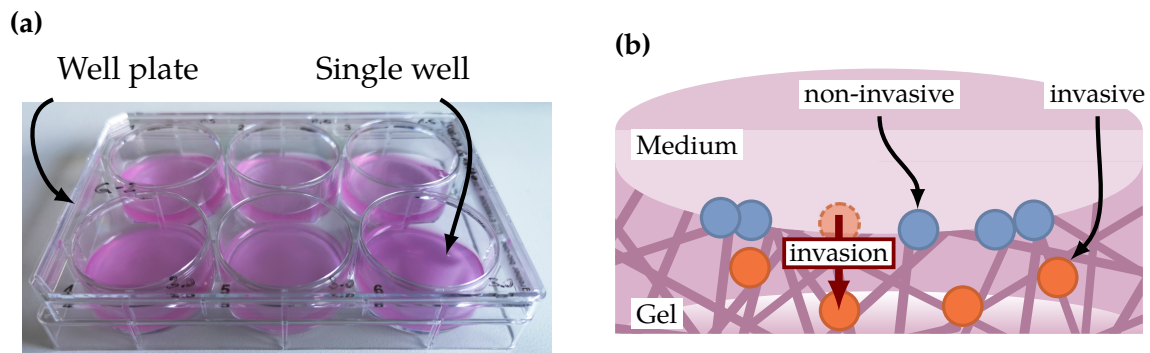


Figure 3.11: Photograph and illustration of working principle of the invasion assay. (a) Photograph of a 6-well plate with polymerized collagen and medium in pink. (b) Side-view of the basic principle of the invasion assay. Cells (blue) adhere to the collagen surface and possibly migrate (orange) into the collagen gel (pink).

In the first step, collagen gels were prepared. The pre-cooled well plate with unfibrillated collagen-buffer solution in each well was placed in an incubator at 37°C , 5% CO_2 , 95% humidity to initialize fibrillation. After 2 h in the incubator at 37°C , 5% CO_2 , 95% humidity, the fibrillated gels were washed three times with PBS to remove residual phosphate ions and collagen monomers. Finally, the washing PBS was rinsed and 2 ml 4.5 g/L DMEM were applied and left over night. Thereby, nutrients can diffuse into the gel to ensure proper cell culture conditions.

The second step was to seed cells on top of the prepared collagen gels. Therefore, cells at ~80% confluency were passaged using 0.125% Trypsin/EDTA as described in section 3.1 on page 31. Using a hemocytometer, the cell concentration was determined. A fraction of the cell suspension was diluted in 2 ml 4.5 g/L DMEM to a resulting absolute number of cells, such as 50 000 cells. The residual medium in the wells of the 6-well plate was replaced with the prepared 2 ml cell suspension containing 50 000 cells. An exemplary 6-well plate with collagen and medium in each well can be seen in figure 3.11.

The well plate with seeded cells was placed in an incubator at 37°C , 5% CO_2 , 95% humidity immediately. Thereby cells sunk to the collagen scaffold surface and adhered to it. Subsequently, the cells grew, migrated and invaded into the 3D collagen matrices, due to their metastatic potential. Figure 3.11 shows an illustration of the 3D migration assay.

After an invasion time of three days, the well plate was removed from the incubator. The whole collagen matrix with cells was fixed using 2.5% glutaraldehyde for 20 min

in an incubator at 37°C, 5 % CO₂, 95 % humidity. After washing 3 times with PBS, cell nuclei were stained using 4 µg/ml Hoechst 33342 over night.

3.5.2 Data acquisition

3D image stacks were recorded using an automated DMI6000B epifluorescence microscope (Leica, Wetzlar, Germany) with a 20 × objective (Leica, Wetzlar, Germany), 0.55 c-mount adapter (Leica, Wetzlar, Germany) and an Orca-R2 CCD camera (Hamamatsu-Photonics, Munich, Germany).

Utilizing a custom written LABVIEW program that was able to control all mechanized microscope components and capture images from the camera. At least 100 image stacks per well at measurement points in a randomized 10 × 10 grid were recorded. Images in each stack had a x-y resolution of 1366 pixel × 1024 pixel and a distance of 4 µm in the z-direction. These stacks were roughly aligned to the gel surface manually prior to automatic recording. Each stack was recorded 200 µm above and 450 µm below the surface, resulting in 163 aligned image layers per stack. These limits ensured that the whole gel depth was recorded and enough space above the surface was left to reveal possible slight surface unevenness and cell clusters at the surface.

3.5.3 Data Analysis

The recorded image data was analyzed utilizing a custom written PYTHON software. CELLCOUNTER3D is a platform independent software library with graphical user interface (GUI) and programming API.

Using the GUI, the user can load a single folder containing an image stack or multiple nested folders containing multiple measurements into an analysis queue. Each one of the items contains several individual image stacks as sub-items, depending on the folder structure. For each item in the queue, the user can set up nested, categorical meta-data that can be extended and modified to specific needs. An example can be seen in figure 3.12 on the facing page. This meta-data includes information such as cell line name, passage number, collagen concentration, experiment dates and much more. When the analysis is started, the analysis queue is processed in the FIFO (First In – First Out) manner. An item is removed from the queue, when all sub-items have been analyzed.

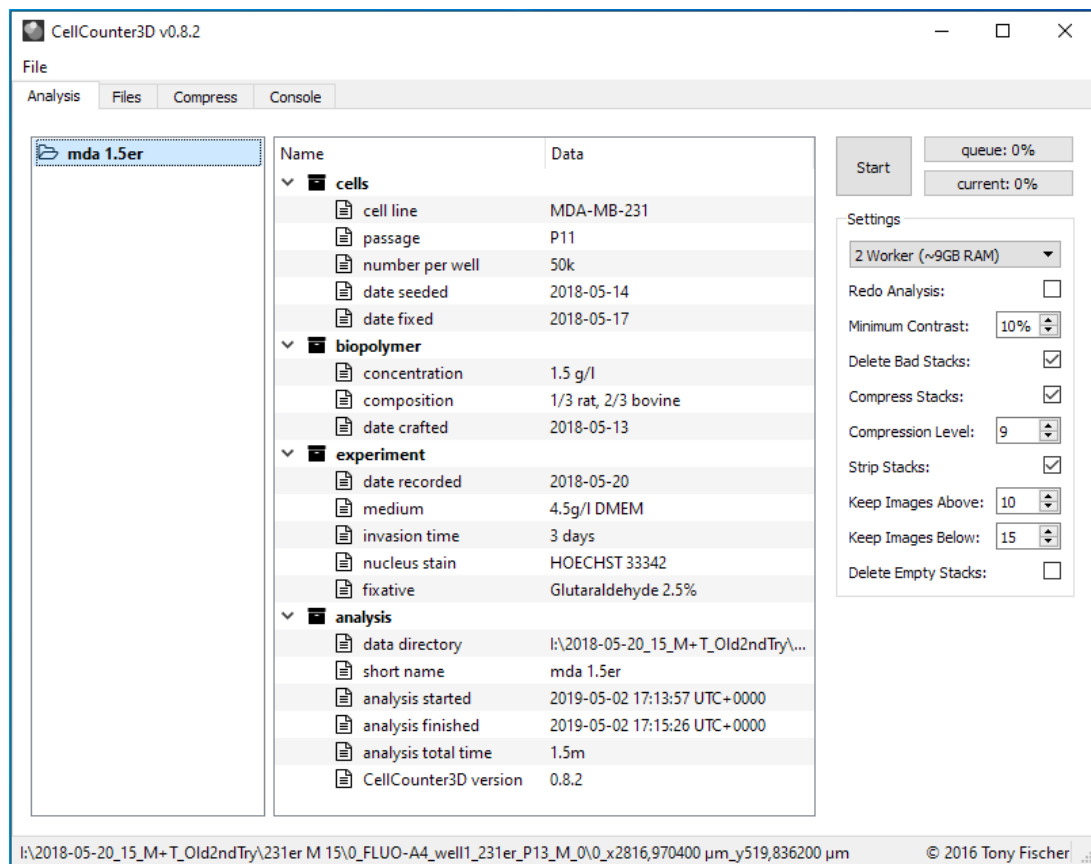


Figure 3.12: CELLcounter3D user interface

In other parts of the GUI, the user can manage meta-data of already analyzed folders. Here, meta-data can be fully edited. Additionally, folders can be compressed after an analysis process.

Depending on the available computer device resources, multiple so called workers can run in parallel, maximizing computational efficiency at the cost of computer RAM and CPU threads. Several other settings are available, such as the deletion of stacks lacking a certain contrast value if image quality is not sufficient, or compression of the raw images to drastically save disk space after analysis.

A full analysis process is depicted in figure 3.13 on the next page. The first step was to apply a three-dimensional Laplacian of Gaussian (LoG) filter on the raw image data, representing a well established blob-detection algorithm. In more detail, the 3D intensity value matrix representing the input image $i(x, y, z)$ was convolved with a 3D

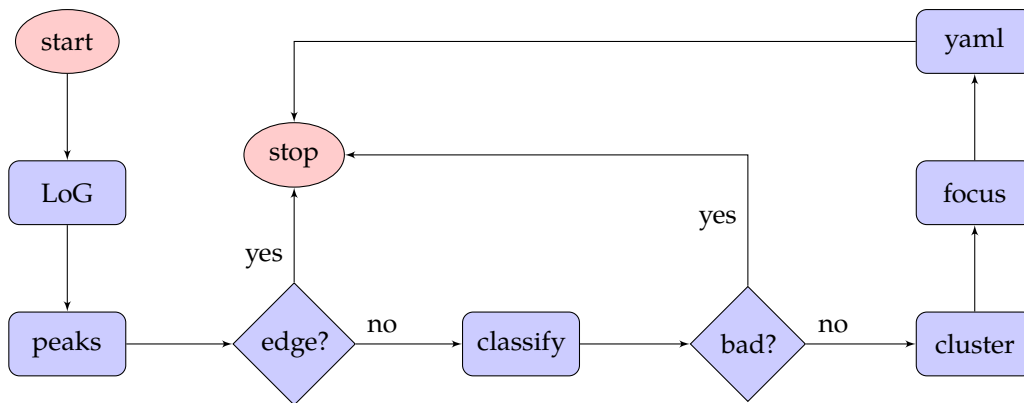


Figure 3.13: Working principle of a full invasion image stack analysis. After a rough feature detection, these features were filtered, classified, and finally cell nuclei positions were saved.

Gaussian kernel

$$g(x, y, z; t) = \frac{1}{2\pi t} \exp\left(-\frac{x^2 + y^2 + z^2}{2t}\right)$$

with scale factor t resulting in a scale space representation $L(x, y, z; t) = g(x, y, z; t) * i(x, y, z)$. Applying the Laplacian operator

$$\nabla^2 L = L_{xx} + L_{yy} + L_{zz}$$

gives a response-matrix with high response values for features, also called blobs, with a radius of $r = \sqrt{3t}$. Setting an estimated cell nuclei size in pixel, we can compute a response matrix with strong responses for bright cell nuclei. Taking the local maxima of the response matrix results in three-dimensional feature positions. Subsequently, positions near the image stack edges were deleted because the cell nuclei near the edges were not recorded entirely. 3D image data around each position was cut out and filtered for size and shape to eliminate false positives such as occasional dirt particles. To consider cell division, nuclei positions in close proximity much less than nuclei size were agglomerated using a MeanShift clustering algorithm. Finally, a standard focus-finder algorithm utilizing Fast-Fourier-Transformation (FFT) was used to refine the z-position of each nuclei.

The user can also program own analyses using the CELL_COUNTER3D API library. It was written in the object oriented programming paradigm and was well documented for easy of use. In basic principle, the user loads a single image stack as an InvasionStack

instance and an empty `NucleiPositions` instance that later contains the detected cell nuclei positions and saves data to disk. An exemplary analysis process is depicted in the following:

```
1 from CellCounter3D import NucleiPositions, InvasionStack
2
3 pos = NucleiPositions() # create empty NucleiPositions
4 stack = InvasionStack("path/to/image/folder") # load stack folder
5 pos.analyze(stack) # start analysis
6 pos.save_data("nuc_pos.yaml") # save data
```

Both GUI and API usage approaches use a standardized output file format for reproducible data analysis, one file for each image stack. The files contain all meta- and analysis-data as plain text structured using the human readable YAML data-serialization language.

Finally, multiple image stack YAML files can be loaded to an `InvasionHistogram` instance automatically computing a global histogram aligned by means of each stack surface, and calculating bootstrapped statistics over all image stacks, such as all 100 image stacks of one well:

```
1 from CellCounter3D import InvasionHistogram
2
3 data = InvasionHistogram("path/to/yaml/data") # load yaml data
4 data.cum_prob.plot(x='Depth [µm]',y='Cumulative probability') # plot some data
5 data.save_data("saved_hist.yaml") # save accumulated data
```

Several statistical numbers and data tables as well as additional data handling methods were included in the `InvasionHistogram` class which can be studied in the source code available on request. Most importantly, `InvasionHistogram.histogram`, `InvasionHistogram.cum_prob` and `InvasionHistogram.stats` contain the global histogram, cumulative probability and bootstrapped statistics, respectively.

Mainly three key numbers were calculated: invasiveness, invasion depth, total number of cells and the cumulative probability. The total number of cells is the number of detected cell nuclei in the experiment. Invasiveness is the ratio of the amount of cells that migrated into the collagen gel below the surface to the number of cells that adhered and

stayed on the surface of the collagen gel. Cells were counted as invasive, if their invasion depth was 8 μm or higher. Likewise, this represents two recorded image planes, as each image plane was 4 μm apart, as described in section 3.5.2 on page 44. This accounts for slight surface irregularities. Taking the distribution of invaded cells, representing 100 % of cells that invaded into the collagen gel, the invasion depth was determined by summing up the number of cells in each image plane with increasing depth, starting with 0 μm invasion depth. If the number of cells for a specific depth exceeds 95 % of the invaded cell population, this depth was considered as the invasion depth. This can be compared to a 95 % confidence interval, where the invasion depth was reached by 95 % of invaded cells and the remaining 5 % representing outliers.

Invasiveness, invasion depth and total number of cells were single, fixed values for each experiment condition and thus an error estimation needs to be carried out. For this, a bootstrapping algorithm was used as follows: for a certain number of bootstrap processes n , a random image stack out of all available image stacks from a specific `InvasionHistogram` was taken out and subsequently invasiveness, invasion depth and total number of cells were calculated. This gives n values for each of the three parameters that were random normal distributed. We can now calculate the mean and standard deviation as usual and state a mean value with error estimation.

The cumulative probability gives a more in depth view on the distribution of invasive single cells. It is a form of invasion distribution of cells along the collagen gel depth that allows to compare different cell populations without scaling problems arising from possibly vastly different cell numbers. Here, the probability at a certain depth to still find cells below this certain depth was calculated. This results in the cumulative probability value in dependence of the collagen gel depth and ranges from 1 to 0.

3.6 Matrix Topology

Cell migration in 3D environments is greatly influenced by the properties of the extracellular matrix such as pore-size and stiffness (Fischer, Wilharm, et al. 2017; Claudia Tanja Mierke 2018b). However, pore-size determination is a complex analysis. Recent studies suggest a random, statistical 2D bubble analysis (Molteni et al. 2013a) or faster non-random approaches (Münster et al. 2013) that are still error prone (Molteni et al. 2013b). In this work, an automated method has been developed that is completely user

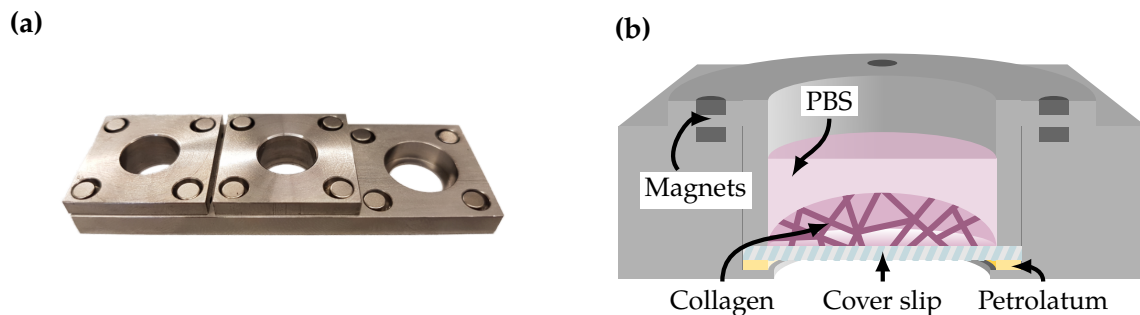


Figure 3.14: Mounting device to hold the glass cover slips with fluorescently stained collagen gels on top. The thin glass cover slip enables superior imaging quality and PBS keeps the gel hydrated. (a) Photograph of metal device with mounting pots and magnets to hold the lid, (b) Side-view illustration. Indicated are the metal device and lid held by magnets, sealed glass cover slip and hydrated collagen gel.

independent and reliable, as published in (Fischer, Hayn, et al. 2019). However, in this thesis, several advancements such as fiber thickness determination are introduced.

3.6.1 Preparation

In the first step, round glass cover slides with 13 mm diameter were functionalized with (3-Aminopropyl) trimethoxysilane (APTMS) (Sigma Aldrich, Cat.No: 281778). Collagen buffer solutions were prepared as described in section 3.2 on page 34. A drop of 100 μl unpolymerized collagen buffer solution was put on top of these functionalized cover slips and subsequently put in an incubator at 37 °C, 5 % CO₂, 95 % humidity to start polymerization for 2 h.

The gels were washed three times with PBS. These samples were fluorescently stained using 20 $\mu\text{g}/\text{ml}$ 5(6)-Carboxytetramethylrhodamine N-succinimidylester (*TAMRA-SE*) (Sigma Aldrich, Cat.No: 21955) over night. After a last washing with PBS three times, the samples were kept hydrated and stored in an incubator at 37 °C, 5 % CO₂, 95 % humidity.

A single glass cover slip with dome-shaped collagen gel was put in a custom built mounting device, as seen in figure 3.14. The mounting device hole has a small rim that was sealed with petrolatum. A single glass cover slip was put into the hole on the sealed lid and arrested with a lid that presses the cover slip onto the rim through magnets. A detailed illustration can be seen in figure 3.14b.

3.6.2 Data Acquisition

The stained gels in the mounting device were imaged using a confocal laser scanning microscope (Leica TCS SP8, Mannheim, Germany) with a 40x NA/1.10 water immersion objective. A laser with 561 nm wavelength was used to excite TAMRA-SE and emission filters were set to 570 nm to 700 nm. Image data was recorded using the Leica® LAS-X software suite and saved in a proprietary file format including all measurement parameters and meta-data such as pixel to μm conversion factors.

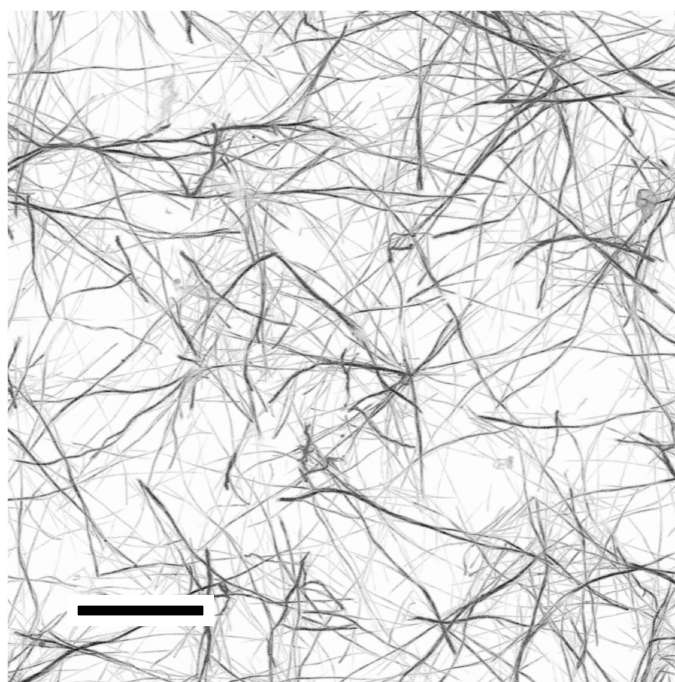


Figure 3.15: Representative CLSM image of fluorescently stained 1.5 g/l collagen gel. Black represents collagen fiber network. Scale bar is 20 μm .

Three-dimensional image cubes with an edge length of 150 μm and x-y resolution of 2048 pixel \times 2048 pixel and a vertical stack size of 600 planes were recorded. The bottom most image plane was set at roughly 50 μm to 100 μm above the glass cover slip to consider possible binding effects near the silanized glass cover slip. Figure 3.15 shows an exemplary confocal laser scanning image of a single plane. Subsequently, a deconvolution was applied automatically using the Huygens Essentials v16.10 software (Scientific Volume Imaging B.V., Hilversum, Netherlands).

3.6.3 Data Analysis

The whole analysis algorithm presented in this chapter has been implemented in a custom built PYTHON module called `BioMatrixTopology`. Raw image data and associated meta-data was loaded using the custom built PYTHON module `LeicaBioFormats`, based on the `BIOFORMATS` library (Linkert et al. 2010). Source code can be provided on request. A simplified illustration of a full analysis process is outlined below:

```
1 import LeicaBioFormats as lbf
2 import BioMatrixTopology as bmt
3
4 # load image data
5 lif_file_collagen = lbf.LifFile('path/to/lif/file')
6 lif_image = lbf.LifImage(lif_file=lif_file_collagen, name='stack1')
7 data = lif_image.read_image()
8
9 bw = bmt.get_binary(data) # segment network
10 pore_sizes = bmt.get_pore_sizes(bw) # pore size
11
12 # fiber thickness
13 fiber_bw = logical_not(bw)
14 fiber_thickness = bmt.get_pore_sizes(fiber_bw)
```

3.6.3.1 Binarization

The first crucial step in collagen scaffold analysis is a proper segmentation of the raw image data obtained from CLSM images into polymer- and fluid-phase. Simple methods such as a fixed threshold of intensity values or automated approaches such as Otsu's method (Otsu 1979) do not adapt to changing image properties and thus were error prone and need user supervision.

Image data was preprocessed using total variation denoising (Chambolle 2004; van der Walt et al. 2014). The recorded 3D image cubes have an edge length of 150 μm , as described in section 3.6.2 on the preceding page, while the bottom most image plane was roughly 50 μm to 100 μm above the glas cover slip. Thus, the exciting laser and the emitted light during confocal laser scanning needs to pass more than 400 μm through a dense polymer scaffold. The higher light scattering and absorption was compensated

by applying the following segmentation on a per-plane basis. For each image plane im_z along the z dimension in the image stack im , a segmentation was calculated as follows:

$$sgm_z(x, y) = \begin{cases} 1, & \text{if } im_z(x, y) > t(x, y) \\ 0, & \text{otherwise} \end{cases} \quad (3.6.1)$$

The cross cross-correlation of im_z with a Gaussian kernel of size $\sigma = k/6$ and k being the equivalent window size around an image pixel (x, y) gives a local adaptive threshold $t(x, y)$. Each image pixel $im_z(x, y)$ was classified according to $t(x, y)$ leading to the image plane segmentation $sgm_z(x, y)$. These per-plane segmentations were vertically stacked together to the 3D segmentation result sgm . Finally, a morphological closing was applied to sgm to refine the binary segmentation, as seen in figure 3.16.

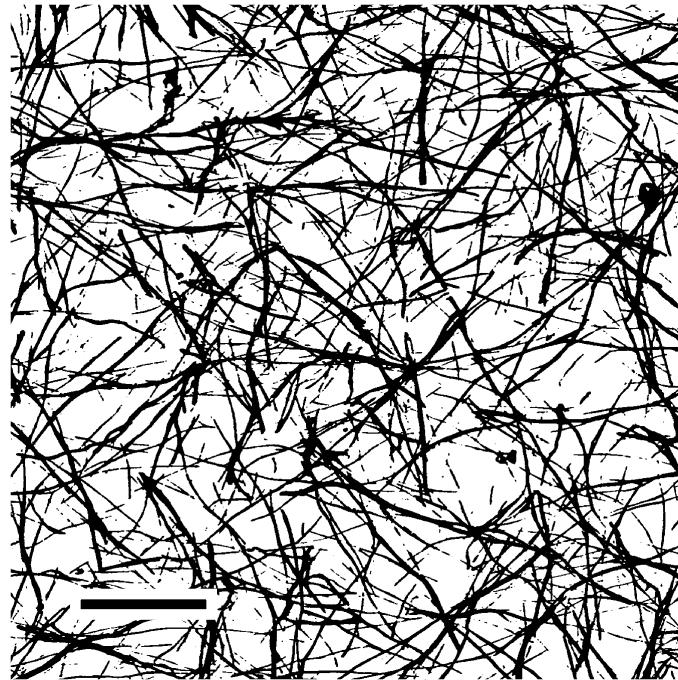


Figure 3.16: Binary segmentation of the representative 1.5 g/l collagen gel seen in figure 3.15 on page 50. Black represents segmented collagen fibrils. Scale bar is 20 μm .

The segmentation sgm was the basis for all following analyses. It contains entries with value 1 if the pixel constitutes a collagen fibril and 0 if not. Parameters for the segmentation process were set automatically according to image properties such as image size and can be further studied in the source code of the library developed in this thesis. The post-deconvolution and multiple post-processing steps allow for a precise,

pixel-wise analysis. The possible resolution was considered to be below the physical diffraction limit.

3.6.3.2 Pore-Size

To determine the collagen scaffold pore-size, an Euclidean Distance Transform (EDT) (Jones et al. 2001) was applied to the non-fibril or fluid phase of the binary segmentation sgm . This process creates a new image matrix edm where for each pixel of the fluid phase the minimal distance to the next fibril phase pixel was calculated. Using a small gaussian kernel, edm was smoothed to diminish small artifacts and subsequently local maxima (x_i, y_i, z_i) were determined. Each value $edm(x_i, y_i, z_i)$ represents a sphere:

$$(x - x_i)^2 + (y - y_i)^2 + (z - z_i)^2 = r_i^2 \quad (3.6.2)$$

with radius r_i and center point (x_i, y_i, z_i) that fits exactly between a specific 3D collagen pore.

This analysis process resulted in a set of pore coordinates and the corresponding pore radii r_i or diameter $d_i = 2r_i$ for a single 3D image cube. Figure 3.18 on page 55 shows an illustration of the segmented collagen fibrils and fitted pore spheres on the left side.

Due to the inhomogeneous structure of reconstituted collagen matrices, a refined pore-size determination algorithm has been proposed (Fischer, Hayn, et al. 2019). Therefore, a second binary sgm_p was calculated that contains 1 for every pixel that the detected pores occupy and 0 otherwise. In more detail, for each pore with center point (x_i, y_i, z_i) and radius r_i , all points (x, y, z) fulfilling equation 3.6.2 were set to 1 in an initially empty zero-matrix.

A second pore-size detection step was applied to the combined residual segmentation:

$$sgm_r = sgm + sgm_p \quad (3.6.3)$$

representing a binary image with values 1 at pixels that either represent collagen fibrils or detected pore volumes. This led to a second set of pore center points $(x_{i,r}, y_{i,r}, z_{i,r})$ and radii $r_{i,r}$ or diameter $d_{i,r} = 2r_{i,r}$. These residual pores can detect smaller spaces in the collagen scaffold not detected by a single pore detection process and leads to a distribution of pore diameters:

$$d_p = d_i \cup d_{i,r} \quad (3.6.4)$$

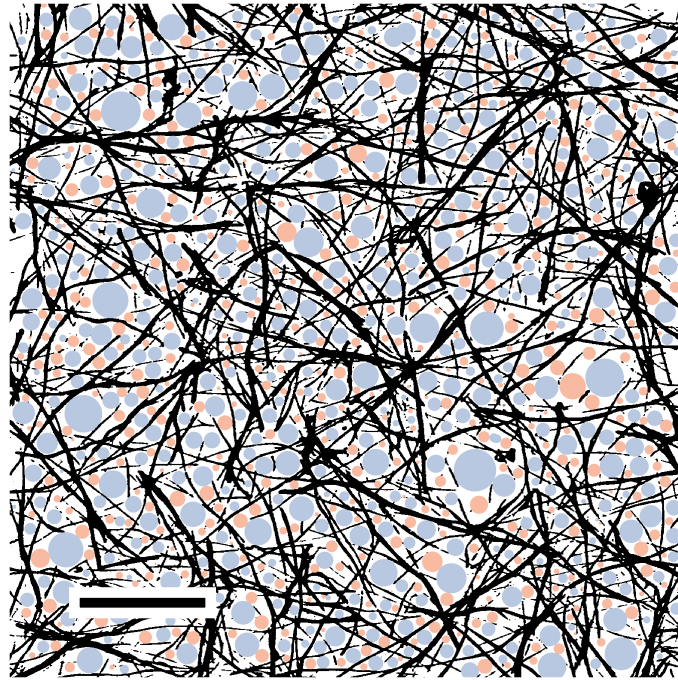


Figure 3.17: Visualization of detected pores inside the binary segmentation of the representative collagen seen in figure 3.15 on page 50. Black represents segmented collagen fibrils. The blue circles depict pores of the first detection step and red circles depict pores detected with the second, residual pore detection step. Scale bar is $20\ \mu\text{m}$.

Taking the median of the pore diameter distribution, we can calculate a median pore-size ζ for a single 3D collagen sample cube:

$$\zeta = \text{median } d_p \quad (3.6.5)$$

3.6.3.3 Fiber Thickness

Fiber thickness can be determined from the same binary segmentation calculated in section 3.6.3.1 on page 51. However, a minimally modified analysis as described in section 3.6.3.2 on the preceding page has to be used. Therefore, the logical inverse sgm_f of the segmentation sgm was calculated. This new segmentation sgm_f contains values of 1 for every pixel in the fluid phase and 0 otherwise. Here, only a single step EDM analysis was used to get pore sphere equivalents inside each collagen fibril. As collagen fibrils are much more defined structures in contrast to the highly inhomogeneous fluid phase, a single analysis step was sufficient. This revealed a set of fibril diameters d_f

distributed along every fibril, representing multiple measurement points. An illustration of the segmented collagen fibrils and fiber thickness measurement points can be seen in figure 3.18.

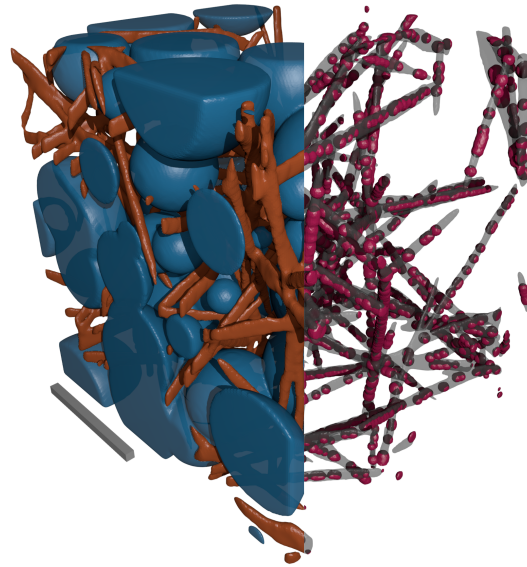


Figure 3.18: Illustration of 3D pore-size and fiber thickness analysis. Left half: collagen fibers in orange and fitted spheres in blue. Right half: collagen fibers in light black and fiber thickness in red. Scalebar is 10 μm .

3.7 Fiber Displacement

Cells anchor their cytoskeleton and stress fibers to the surrounding microenvironment through focal adhesions. When cells migrate, they generate forces to translocate, as described in section 2.4 on page 29. In doing so, cells actively deform their microenvironment depending on the amount of forces they generate during migration and also depending on the mechanical properties of the microenvironment itself. The ECM is a highly structured scaffold with defined protein content and mechanical and topological properties, as described in section 2.3 on page 24. Thus, it is possible to measure the deformation of the microenvironment and correlate this deformation to the amount of forces a cell generated during migration. In recent studies the displacement of reconstituted collagen matrices has been determined using fluorescent bead as fiducial markers (Steinwachs et al. 2016). However, it has been shown that phagocytosed beads

in cells drastically reducing their migration (Claudia T. Mierke 2013). In this work, a novel, minimally invasive approach to determine collagen fiber displacement of single cells has been developed, as described in this chapter.

3.7.1 Preparation

Collagen gels were prepared as described in section 3.2 on page 34. 150 μ l of the unpolymerized collagen-buffer solution were put in an IBIDI® 24 well μ -plate (Cat.No: 82406, ibidi GmbH, Gräfelfing, Germany). Subsequently, these samples were put in an incubator at 37 °C, 5 % CO₂, 95 % humidity to start collagen polymerization. This resulted in collagen gels inside each well of the μ -plate that were roughly 150 μ m in height at the center. The height is increased towards the edge of the well due to surface tensions.

Cells were prepared as described in section 3.1 on page 31. Depending on the proliferation rate of the specific cell line, 1000 to 3000 cells were seeded on top of the collagen gels, similar to the invasion assay described in figure 3.11 on page 43. However, in this assay, much less cells were used because only single cells were needed to be observed even after a certain proliferation time. The μ -plate with collagen gels and seeded cells were put in an incubator at 37 °C, 5 % CO₂, 95 % humidity for 1 days to 3 days to let the cells invade into the matrices. After the cells invaded the collagen matrix, the cell membrane was stained using DiO (Cat.No: V22886, ThermoFisher, Waltham, Massachusetts, USA) for at least 20 min.

3.7.2 Data Acquisition

Imaging of the prepared samples with invaded cells and stained cell membrane as described in section 3.7.1 was done using a confocal laser scanning microscope (Leica TCS SP8, Mannheim, Germany) with a 20x NA/0.75 dry objective. In this assay, two color channels were recorded simultaneously. In the fluorescence color channel, the membrane stain DiD was excited using a 633 nm laser and emission filters were set to 645 nm to 790 nm. The second channel was set to record transmitted light (TL) with a photo multiplier tube (PMT) called transmitted light detector (TLD). Thus, the collagen scaffold as well as the observed cell can be seen in bright field contrast. To optimize light

yield and thus contrast of the TL channel without interfering with optimal fluorescent channel settings, a second laser with 561 nm wavelength was used.

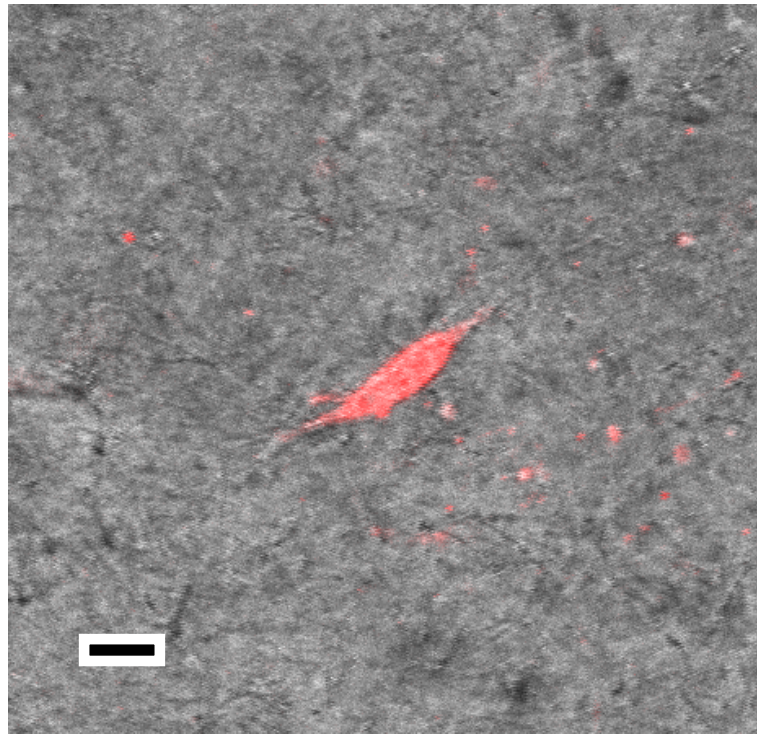


Figure 3.19: Representative MDA-MB-231 cell in 1.5 g/l collagen gel. Grey represents transmitted light image of the collagen gel, red depicts the fluorescently labeled cell membrane. Scale bar is 20 μm .

3D image cubes with a single cell in the center were recorded. The x-y resolution was set to 1024 pixel \times 1024 pixel with a z-distance of 1 μm . Multiple image stacks were recorded every 5 min. A single stack required 15 s to 30 s for recording, so that the simultaneous measurement of several cells was possible.

3.7.3 Data analysis

The whole analysis algorithm presented in this chapter has been implemented in a custom built PYTHON module called *ScaffoldTraction3D*. Raw image data and associated metadata was loaded using the custom built PYTHON module *LeicaBioFormats*, based on the *BIOFORMATS* library (Linkert et al. 2010). The source code can be provided on request. A simplified illustration of a full analysis process is outlined below:

```

1 import ScaffoldTraction3D as st
2 import LeicaBioFormats as lbf
3
4 # load image data
5 lif_file = lbf.LifFile('path/to/lif/file')
6 lif_image = lbf.LifImage(lif_file=lif_file, name='cell1')
7 data = lif_image.read_image()
8
9 # take two consecutive time frames
10 frame_1 = st.denoise(data[..., t])
11 frame_2 = st.denoise(data[..., t+1])
12
13 # calculate velocity matrix
14 Vx, Vy, Vz = st.normalized_flow_field_3d(frame_1, frame_2)
15 V = sqrt(Vx**2 + Vy**2 + Vz**2)
16
17 # segment cell
18 B = data[..., t] > threshold_otsu(data[..., t])
19 B = binary_closing(B, selem=ball(2)).astype('bool')
20
21 # fiber displacements in n shells from membrane
22 for i in range(n):
23     S = st.get_envelope_binary(B, i, size=shell_size)
24     V_cut = V * S
25     fiber_displacements[i] = mean(V_cut[V_cut > 0])

```

In this work, an algorithm based on the Lucas-Kanade method (Lucas et al. 1981) was used to calculate fiber displacements. The Lucas-Kanade method assumes an essentially constant optical flow in a local neighborhood of a considered pixel and solves the optical flow equations in that neighborhood by the least squares criterion. It is a highly efficient differential method for optical flow estimation and is also less sensitive to image noise compared to other methods.

The image data of a single color channel constitutes a 4D matrix with three spatial and one time dimensions. The TL channel contains a video of the cells migrating and deforming their microenvironment, or collagen matrix, and thus referred to as the fiber channel. The fluorescence channel is referred to as the cell channel accordingly.

3.7.3.1 Fiber Displacement

The first step was to calculate the optical flow of the fiber channel between two consecutive time points. Raw image data were preprocessed using total variation denoising (Chambolle 2004; van der Walt et al. 2014).

First, the partial derivatives of two consecutive time-frames I_t and I_{t+1} were calculated, with I being the image intensity value matrix and t time. This was done for a single voxel (x, y, z) in the 3D image matrix in a small neighborhood $m \times m \times k$ with $m, k > 1$ in each spatial dimension and time, called D_x, D_y, D_z, D_t , respectively. As the image x-y resolution differs from the z-resolution, this window needs an equivalent pixel size matching roughly μm size and was converted automatically. For each voxel $1 \dots n, n = m \cdot m \cdot k$ of the cut out neighborhood at (x, y, z) , an equation system can be set up:

$$\begin{aligned} D_{x_1} + D_{y_1} + D_{z_1} &= -D_{t_1} \\ D_{x_2} + D_{y_2} + D_{z_2} &= -D_{t_2} \\ &\vdots \\ D_{x_n} + D_{y_n} + D_{z_n} &= -D_{t_n} \end{aligned} \quad (3.7.1)$$

This system has more equations than variables und thus is over-determined. It can be written as the following matrix equation:

$$\begin{bmatrix} D_{x_1} & D_{y_1} & D_{z_1} \\ D_{x_2} & D_{y_2} & D_{z_2} \\ \vdots & \vdots & \vdots \\ D_{x_n} & D_{y_n} & D_{z_n} \end{bmatrix} \begin{bmatrix} V_x \\ V_y \\ V_z \end{bmatrix} = \begin{bmatrix} -D_{t_1} \\ -D_{t_2} \\ \vdots \\ -D_{t_n} \end{bmatrix} \quad (3.7.2)$$

The above matrix equation represents an over-determined system:

$$A\vec{v} = -b \quad (3.7.3)$$

This equation can be solved using the least squares principle:

$$\vec{v} = (A^T A)^{-1} A^T (-b) \quad (3.7.4)$$

The result can be written as a numerical problem:

$$\begin{bmatrix} V_x \\ V_y \\ V_z \end{bmatrix} = \begin{bmatrix} \sum D_{x_i}^2 & \sum D_{x_i} D_{y_i} & \sum D_{x_i} D_{z_i} \\ \sum D_{x_i} D_{y_i} & \sum D_{y_i}^2 & \sum D_{y_i} D_{z_i} \\ \sum D_{x_i} D_{z_i} & \sum D_{y_i} D_{z_i} & \sum D_{z_i}^2 \end{bmatrix}^{-1} \begin{bmatrix} -\sum D_{x_i} D_{t_i} \\ -\sum D_{y_i} D_{t_i} \\ -\sum D_{z_i} D_{t_i} \end{bmatrix} \quad (3.7.5)$$

with each sum ranging from $i = 1$ to n .

The numerical equation was solved for every voxel (x, y, z) between the two consecutive input images I_t and I_{t+1} . This gave velocity matrices $V_{x,t}$, $V_{y,t}$, $V_{z,t}$ for each image dimension at a specific time-point t the same size as the 3D input images with displacement values between the two time frames for each image voxel. These velocity matrices were drift-corrected using a three-dimensional Fast-Fourier-Transformation (FFT). Therefore, the zero-frequency in frequency-space after FFT represents a global drift. After an inverse FFT (iFFT) of the zero-frequency, the global drift velocity in time-space was calculated. This drift was subtracted from the velocity matrix for each dimension separately.

The main focus in this work were absolute fiber displacements. Therefore, the norm of the velocity vector in every voxel (x, y, z) was calculated, resulting in the absolute velocity matrix V_t in the following equation:

$$V_t = \left(V_{x,t}^{\circ 2} + V_{y,t}^{\circ 2} + V_{z,t}^{\circ 2} \right)^{\circ \frac{1}{2}} \quad (3.7.6)$$

with time-point t and Hadamard power $^{\circ}$ as element-wise power.

3.7.3.2 Cell Segmentation

The second step in the fiber displacement analysis was to segment the cell from the matrix environment. Therefore, we analyzed the cell channel, which contains image intensity data of the fluorescent cell membrane. Segmentation was done using the well established Otsu's method (Otsu 1979).

Subsequently, morphological closing was applied to further refine the obtained segmentation. This gave a binary matrix B_t for a specific time-point t containing 0 if the image pixel belongs to the cell body and 1 otherwise. B_t was used as a mask to diminish entries in V_t that originate from cell motion and not from fiber displacements. Finally,

the fiber displacement matrix F_t is calculated:

$$F_t = V_t \circ B_t \quad (3.7.7)$$

with time-point t and Hadamard product \circ as element-wise product.

3.7.3.3 Shell Analysis

In the third analysis step, only specific elements of the fiber displacement matrix F_t dependent on the cell surface were considered. The precise cell surface segmentation as boundary of B_t was already calculated. Based on this, F_t values in a shell around the cell surface were taken. Therefore, the binary B_t was dilated by an amount d in pixel, which was calculated to be approximately a certain distance in μm depending on the pixel to μm conversion factor, giving the dilated binary $B_t^{(d)}$. The shell binary mask S_t at a time-point t was calculated by subtracting the original binary from the dilated binary:

$$S_t = B_t^{(d)} - B_t \quad (3.7.8)$$

This process was repeated successively to get multiple shells around the cell going outwards from the membrane:

$$S_{t,i+1} = S_{t,i}^{(d)} - S_{t,i} \quad (3.7.9)$$

This method enabled us to precisely analyze long-range displacements and also cell polarization.

Finally, the obtained data was further reduced by calculating the mean fiber displacement in each shell. Therefore, fiber displacements in dependence of the distance from the cell surface and over time were analyzed, as seen in figure 3.20 on the following page.

On the one hand, these data was further reduced by taking the mean of all shells for each time point to calculate the time dependent development of the mean fiber displacements. On the other hand, the mean over a certain time-period was calculated to analyze a mean fiber displacement for that time-period in dependence on distance from the cell surface.

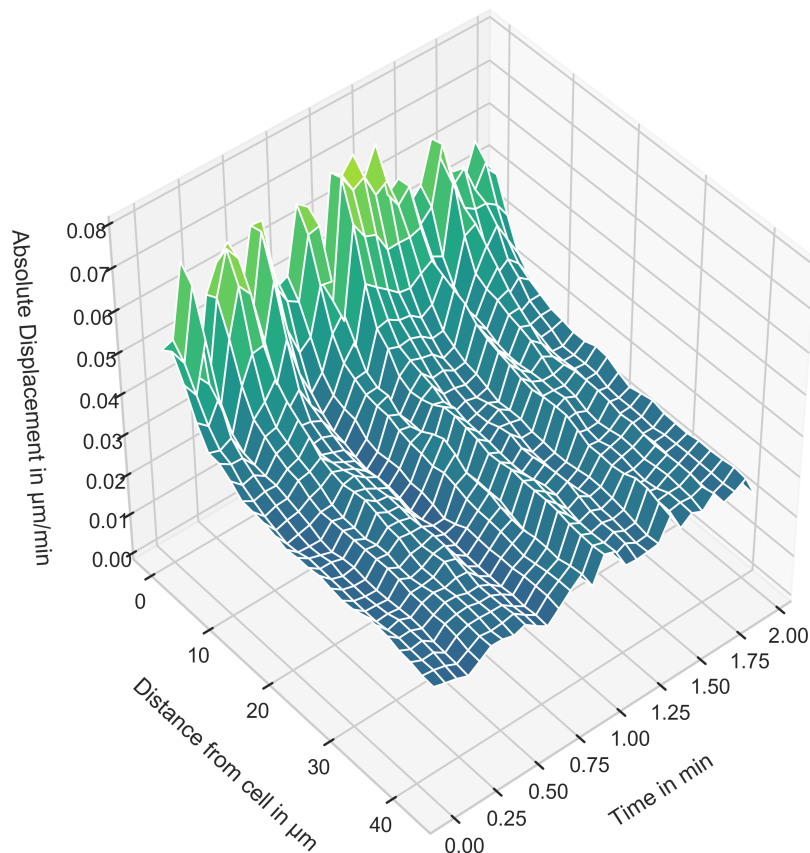


Figure 3.20: Representative multi-dimensional fiber displacement surface plot of a FAK^{+/+} cell. Shown are the fiber displacements in $\mu\text{m}/\text{min}$ in dependence of distance from cell and elapsed experiment time.

3.8 A toolset to understand Single Cell Migration and what influences it

As described in section 2.4 on page 29, cells are an active biophysical machine (Claudia Tanja Mierke 2018a). They are able to progressively generate forces and migrate in a 3D extracellular microenvironment and tissue (F. Huber et al. 2013; Alberts 2015; Claudia Tanja Mierke 2018b). This migration is influenced by cell mechanical properties and topological as well as mechanical properties of the microenvironment, such as artificial collagen gels (Fischer, Wilharm, et al. 2017).

In this work, several methods were developed and advanced, as seen in chapter 3 on

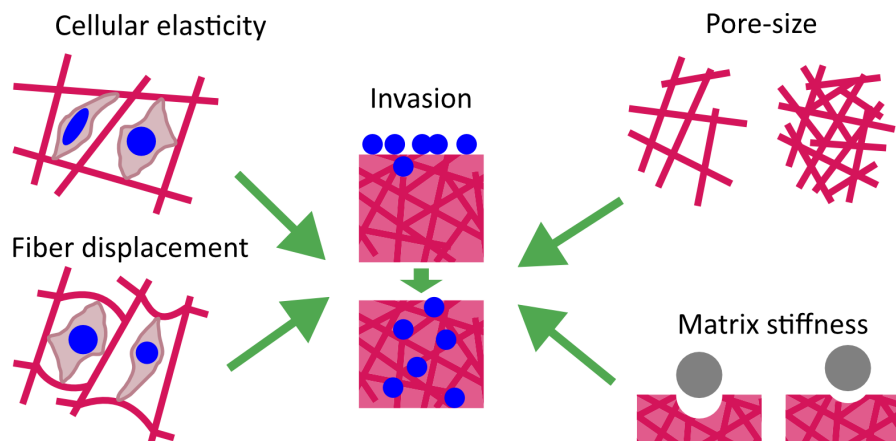


Figure 3.21: Illustration of the toolset concept to describe single cell migration in artificial 3D collagen networks. Mechanical properties of the cell (left) and mechanical and topological properties of the microenvironment (right) both influence single cell migration (middle).

page 31 and their applicability and results are shown in chapter 4 on page 65. Figure 3.21 shows an illustration of the toolset concept. The visualized methods were considered to be major aspects to describe and quantify single cell migration.

Chapter 4

Results

Contents

4.1 Cell Elasticity	65
4.2 Matrix Stiffness	69
4.3 Invasion	71
4.4 Matrix Topology	75
4.5 Influence of Cell Nucleus on Cell Migration	79
4.6 Fiber Displacement	89
4.7 Effect of FAK on Cell Invasion and Fiber Displacement	93

4.1 Cell Elasticity

Mechanical properties of single, adherent cancer cells were determined as described in section 3.3 on page 36. To consider the major contribution of the nucleus to cell mechanical properties, the cell cytoskeleton and nucleus were determined separately for each individual cell. In the following section, exemplary force-distance curves and cellular elasticity results are shown.

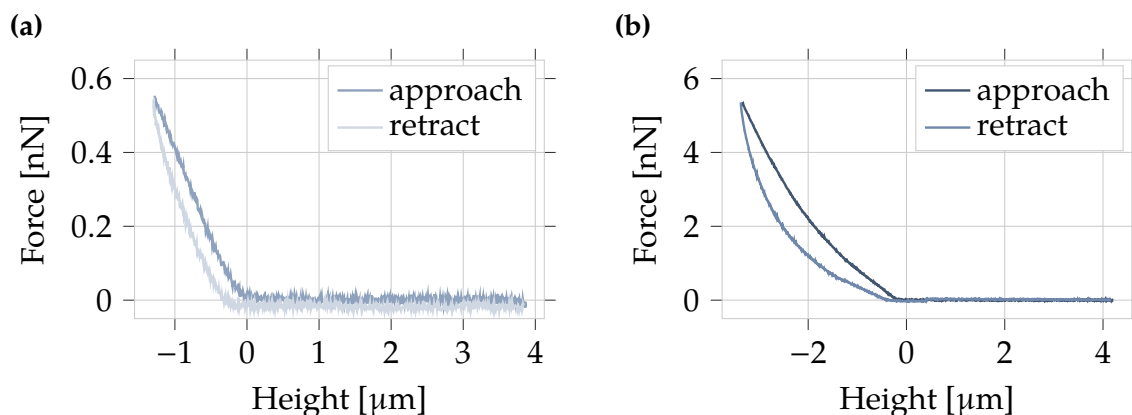


Figure 4.1: Exemplary AFM force-distance curves of a MDA-MB-231 cell. (a) Cytoskeletal and (b) nuclear curves are shown.

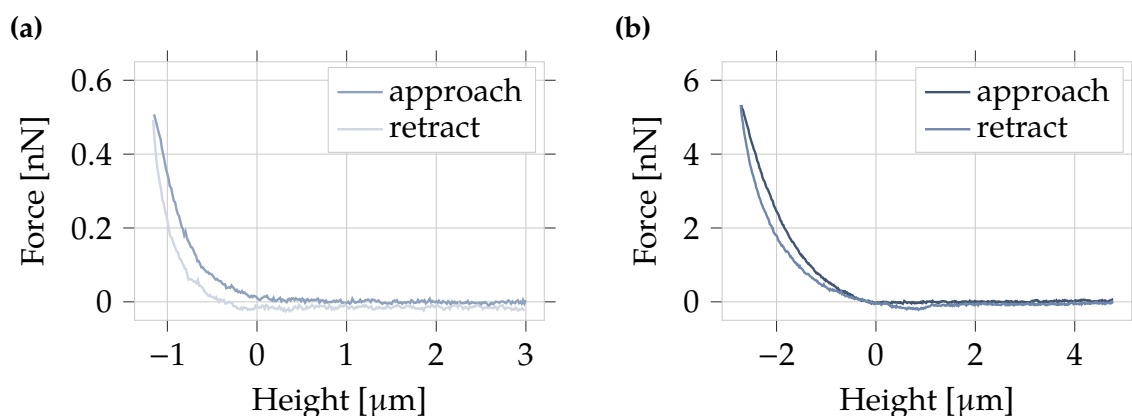


Figure 4.2: Exemplary AFM force-distance curves of a MCF-7 cell. (a) Cytoskeletal and (b) nuclear curves are shown.

4.1.1 Example Force-Distance Curves

Force-distance curves were recorded as described in section 3.3.3 on page 38. Exemplary force-distance curves for MDA-MB-231 cells are shown in figure 4.1.

The cytoskeletal curves in figure 4.1a show a clear approach and retract phase of this exemplary AFM measurement. Here, the maximal indentation force was 0.5 nN. The maximal retract length was 5 μm and restricted by the z-piezo of the AFM device. A similar curve for the nucleus can be seen in figure 4.1b. However, for the nucleus the maximal indentation force was 5 nN.

Exemplary force-distance curves for MCF-7 cells are shown in figure 4.2.

In all exemplary force-distance curves shown in this section, the much steeper

indentation part of a representative MCF-7 cell can be clearly seen indicating a much stiffer mechanical resistance to indentation compared to a representative MDA-MB-231 cell.

4.1.2 Single Cell Elasticity

Results are shown in figure 4.3. Clearly, the highly invasive cancer cell line MDA-MB-231 was softer than the less invasive cancer cell line MCF-7, as described in previous studies (Claudia Tanja Mierke 2014; Fischer, Wilharm, et al. 2017). The distinction between cytoskeletal and nuclear mechanical properties reveals that the cell nucleus for these two cell lines was significantly stiffer than the cytoskeleton. However, both cellular compartments of MDA-MB-231 cells were still softer than for MCF-7 cells.

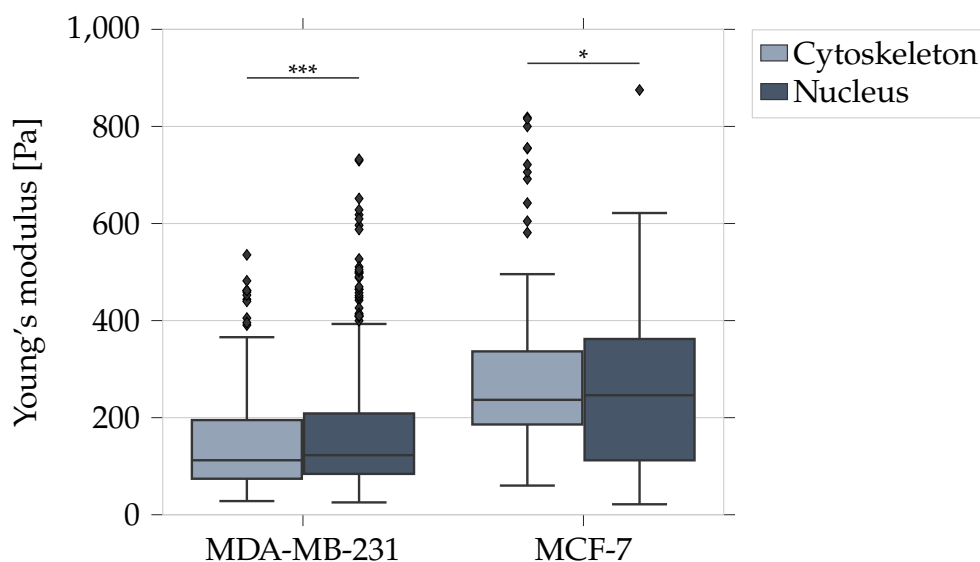


Figure 4.3: Young's modulus of single, adherent invasive cancer cell line MDA-MB-231 and less invasive cancer cell line MCF-7. Cell cytoskeletal and nuclear elasticity were determined separately.

Table 4.1 on the following page lists statistical values for each cell line and compartment. Denoted are the 25 %, 50 % and 75 % percentiles of the Young's modulus as an elastic modulus as well as the total number of measured single cells. The 50 % percentile denotes the median value of each distribution, while 25 % and 75 % describe upper and lower quartiles.

Cell line	Compartment	Count	Young's modulus [nN]		
			25%	50%	75%
MDA-MB-231	Cytoskeleton	68	54.48	80.33	113.89
	Nucleus	69	106.43	145.25	194.26
MCF-7	Cytoskeleton	34	209.83	251.63	495.33
	Nucleus	55	330.02	375.25	439.44

Table 4.1: Young's modulus of single, adherent invasive cancer cell line MDA-MB-231 and less invasive cancer cell line MCF-7. Listed are number of measured cells (Count) and 25 %, 50 % and 75 % percentiles.

4.2 Matrix Stiffness

Collagen matrix stiffness has been determined using AFM as described in section 3.4 on page 40. Figure 4.4 shows the resulting Young's modulus.

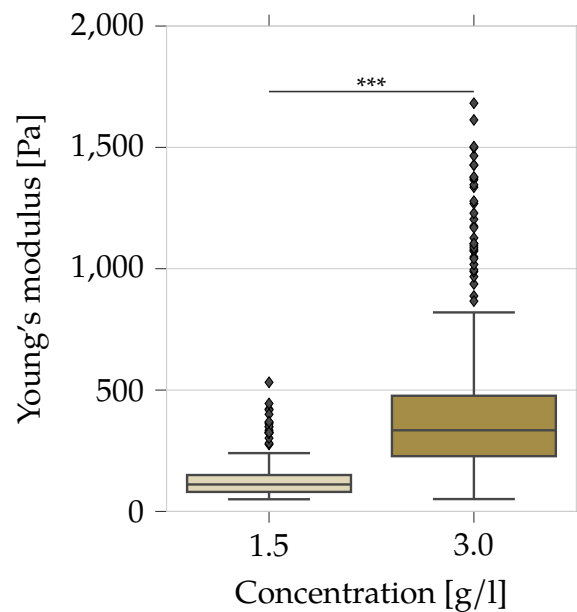


Figure 4.4: Young's modulus as measure of matrix stiffness for 1.5 g/l and 3.0 g/l collagen gels.

The data shows a significantly stiffer 3.0 g/l matrix compared to 1.5 g/l. Table 4.2 lists statistical values for the matrix stiffness. Denoted are the 25 %, 50 % and 75 % percentiles of the Young's modulus as a measure of matrix stiffness as well as the total number of measured data points. The 50 % percentile denotes the median value of each distribution, while 25 % and 75 % describe upper and lower quartiles.

Concentration [g/l]	Count	Young's modulus [nN]		
		25%	50%	75%
1.5	279	80.36	111.06	149.96
3	605	227.63	334.26	476.54

Table 4.2: Young's modulus as measure of matrix stiffness for 1.5 g/l and 3.0 g/l collagen gels. Listed are number of measured cells (Count) and 25 %, 50 % and 75 % percentiles.

4.3 Invasion

The invasion assays have been performed as described in section 3.5 on page 42. Figure 4.5 shows the invasiveness (percentage of invasive cells) of both MDA-MB-231 and MCF-7 cancer cell lines. Invasiveness is the percentage of cells that invaded into the collagen gel compared to cells that adhered and stayed at the gel surface after seeding, as described in section 3.5.3 on page 44.

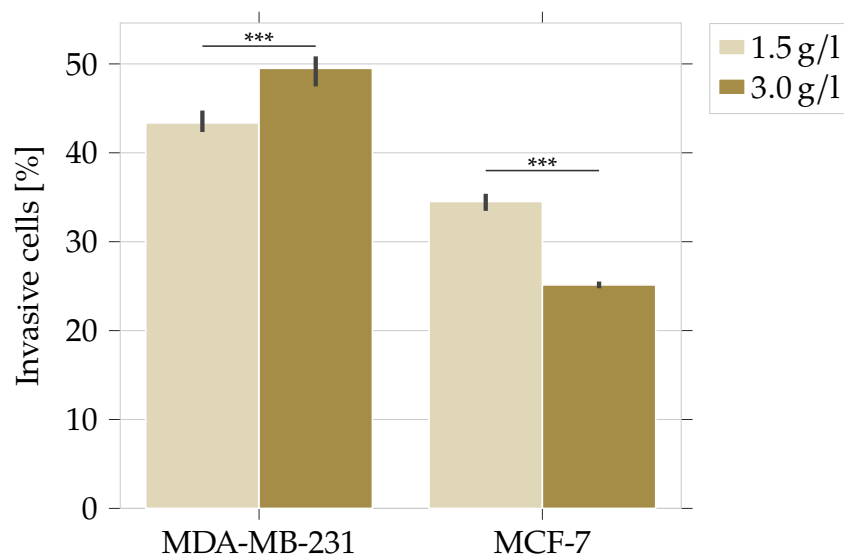


Figure 4.5: Invasiveness after three days of MDA-MB-231 and MCF-7 cells on 1.5 g/l and 3.0 g/l collagen gels with indicated error bars in black.

As seen in figure 4.5, the breast cancer cell line MDA-MB-231 was more invasive than the breast cancer cell line MCF-7. Moreover, the concentration of the collagen matrix has a major effect on invasiveness of both cancer cell lines. Increasing the collagen concentration from 1.5 g/l to 3.0 g/l has a promoting effect on MDA-MB-231 cells as significantly more cells invaded into the denser gels. However, the collagen concentration increase has an impaired effect on MCF-7 cells, where the invasiveness was significantly decreased.

Additionally, the invasion depth has been determined as described in section 3.5.3 on page 44. While MDA-MB-231 cells show an invasion depth of 145.60 μm in 1.5 g/l and 178.40 μm in 3.0 g/l collagen gels, MCF-7 cells invaded less deep to 52.00 μm in 1.5 g/l and 40.80 μm in 3.0 g/l collagen gels.

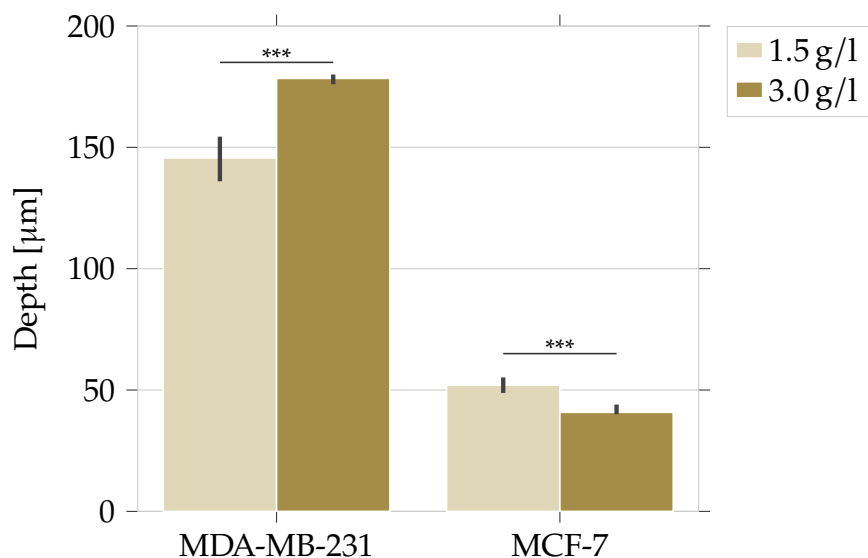


Figure 4.6: Invasion depth in μm of MDA-MB-231 and MCF-7 cells on 1.5 g/l and 3.0 g/l collagen gels with indicated error bars in black.

These data showed, that although MCF-7 cells show a less invasive behaviour than MDA-MB-231 cancer cells, the difference was more pronounced in the invasion depth.

Table 4.3 lists specific values as mean and standard deviation calculated through a bootstrap error estimation, as described in section 3.5.3 on page 44. First, the number of counted cells from all experiments are shown. Second, the invasiveness and invasion depth for each cell line and collagen gel concentration are listed.

Cell line	Conc.	Number of cells		Invasiveness [%]		Depth [μm]	
		mean	std	mean	std	mean	std
MCF-7	1.5 g/l	28074	663	34.52	0.84	52.00	2.83
	3.0 g/l	29473	798	25.14	0.37	40.80	1.79
MDA-MB-231	1.5 g/l	31987	655	43.37	1.11	145.60	7.80
	3.0 g/l	39507	1357	49.50	1.39	178.40	2.19

Table 4.3: Key values of the invasion assay for each cell line and collagen concentration (Conc.). The total number of counted cells as well as the invasiveness and invasion depth are listed. Values are denoted as mean with standard deviation calculated from a bootstrap error estimation.

The cumulative probability gives a more in depth view on the distribution of invasive

single cells. As described in section 3.5.3 on page 44, the cumulative probability represents the probability at a certain depth to find cells below this specific depth. Figure 4.7 shows the cumulative probability for invasive MDA-MB-231 and MCF-7 cancer cells on 1.5 g/l and 3.0 g/l collagen gels.

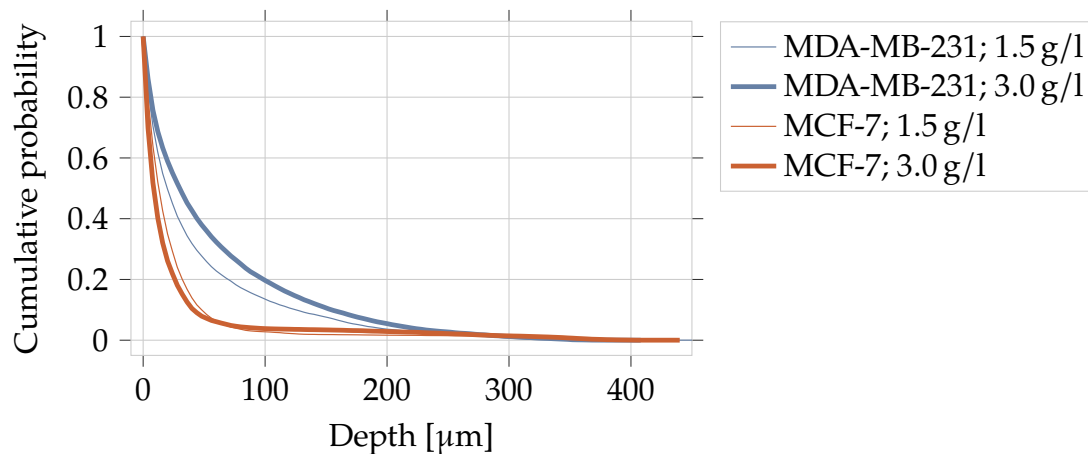


Figure 4.7: Cumulative probability for invasive MDA-MB-231 (blue) and MCF-7 (red) cancer cells on 1.5 g/l and 3.0 g/l collagen gels. 1.5 g/l plotted as thin line and 3.0 g/l as thicker line.

These data show a clear distribution of invasive MCF-7 and MDA-MB-231 cancer cells. The cumulative probability of invasive MCF-7 cells rapidly decreases to below 0.1 % at roughly 50 μm for both 1.5 g/l and 3.0 g/l collagen gels. In contrast, MDA-MB-231 cells show a much weaker decrease with high cumulative probability up to 200 μm . This indicates that MCF-7 cells penetrate into both collagen concentrations but do not invade deeply into them. Furthermore, the cumulative probability decrease for MCF-7 cells was almost identical for both collagen concentrations, whereas MDA-MB-231 cells show a higher cumulative probability for 3.0 g/l compared to 1.5 g/l. The aforementioned interpretations are in line with figure 4.5 on page 71 and figure 4.6 on the facing page.

4.4 Matrix Topology

Collagen pore diameter and pore-size have been determined as described in section 3.6.3.2 on page 53. Figure 4.8 shows a kernel density estimation (KDE) distribution for both 1.5 g/l and 3.0 g/l collagen gels. These pore diameter distributions reveal that the 1.5 g/l collagen gel has larger pores compared to the 3.0 g/l gels. Additionally, 3.0 g/l matrices show a much narrower pore diameter distribution than 1.5 g/l gels.

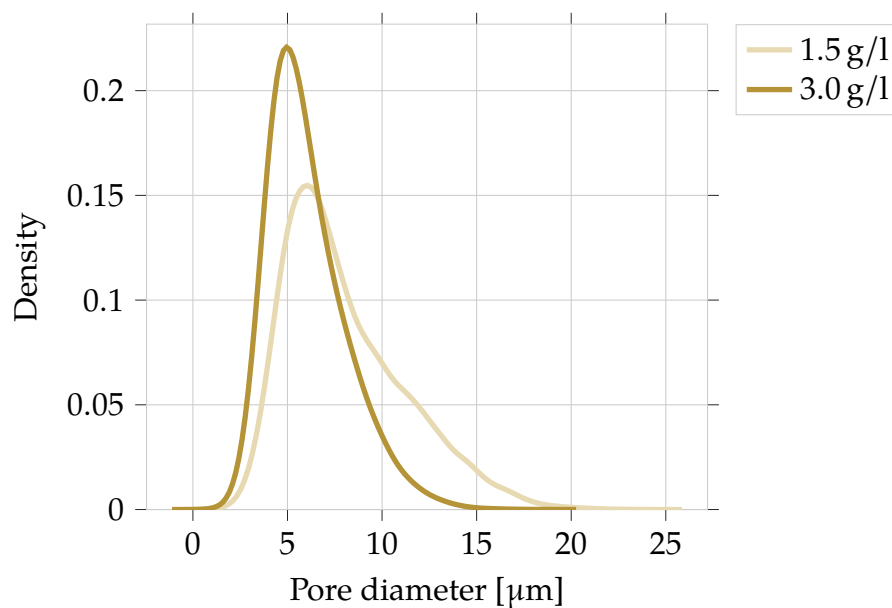


Figure 4.8: Pore diameter distribution as kernel density estimate (KDE). 1.5 g/l matrices shows a broader distribution with much larger pores than 3.0 g/l collagen gels.

As described in section 3.6.3.2 on page 53, the pore-size is a major collagen matrix topology parameter. Figure 4.8 shows the pore-size distributions for 1.5 g/l and 3.0 g/l collagen gels. For each collagen concentration, 30 individual collagen samples have been analyzed.

Figure 4.9 on the next page shows the pore-size distribution for each of these samples. Pore-size is a single value for each collagen sample and thus the mean and standard deviation can be calculated, as seen in table 4.4 on the following page.

These data clearly show that 1.5 g/l collagen gels have a significantly larger pore-size in comparison to 3.0 g/l matrices.

As already described in section 3.6.3.3 on page 54, the pore-size analysis in a slightly varied form can be utilized to determine the collagen fiber thickness. For each collagen

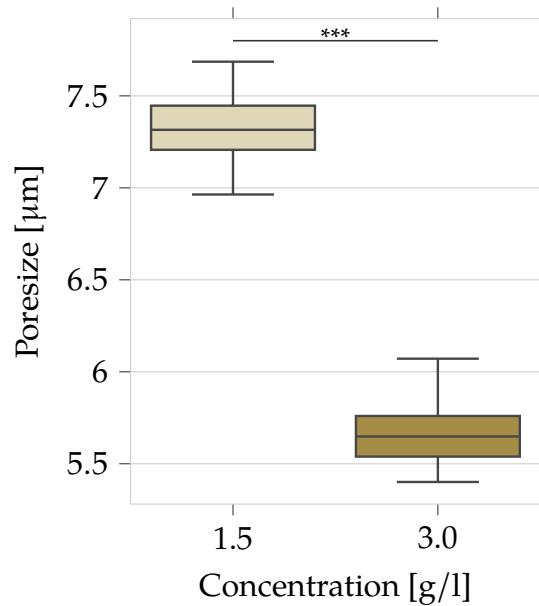


Figure 4.9: Pore-sizes of 1.5 g/l and 3.0 g/l collagen gels.

Concentration	Count	Pore-size [μm]	
		mean	std
1.5 g/l	30	7.34	0.22
3.0 g/l	30	5.63	0.21

Table 4.4: Pore-sizes of 1.5 g/l and 3.0 g/l collagen gels with number of samples (Count), mean and standard deviation (std) listed.

concentration, three individual experiments were performed. The kernel density estimation (KDE) distribution for 1.5 g/l and 3.0 g/l collagen matrices is shown in figure 4.10 on the facing page.

These distributions were almost identical. Figure 4.11 on the next page shows that the fiber thickness of both 1.5 g/l and 3.0 g/l collagen gels were not significantly different. Table 4.5 on page 78 confirms these findings. As explained in section 3.6.3.1 on page 51, the post-deconvolution and multiple post-processing steps allowed a pixel-wise analysis with a possible resolution considered to be below the optical diffraction limit.

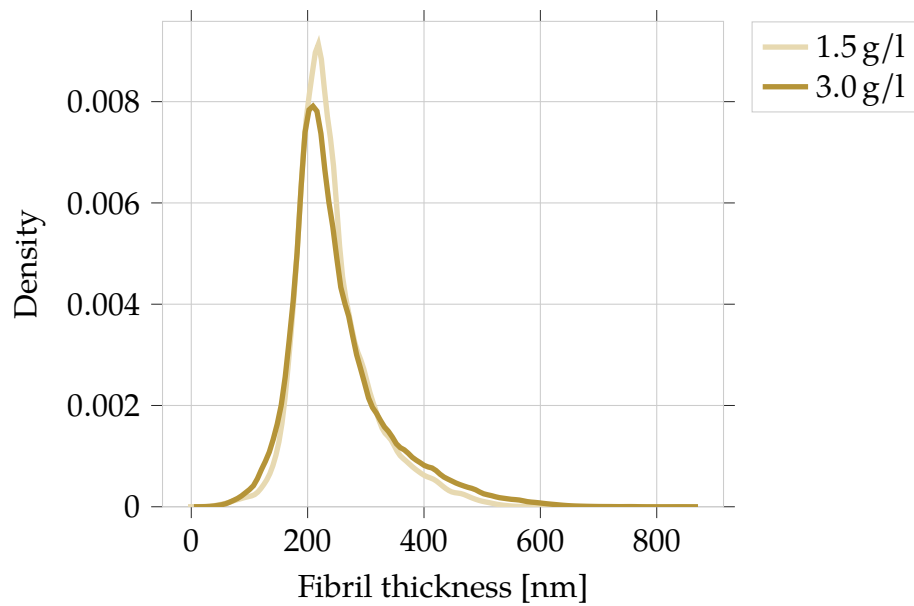


Figure 4.10: Fiber thickness distribution as kernel density estimate (KDE). 1.5 g/l and 3.0 g/l collagen matrices show an almost identical distribution.

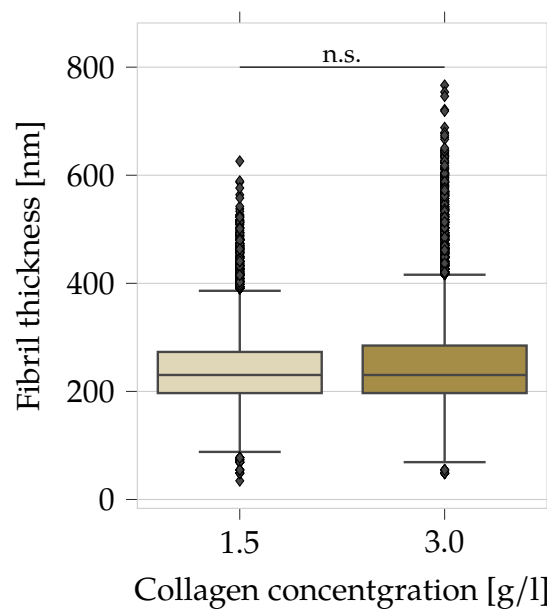


Figure 4.11: Fiber thickness of 1.5 g/l and 3.0 g/l collagen gels.

Concentration	Count	Fiber thickness [nm]	
		mean	std
1.5 g/l	29201	243.59	66.90
3.0 g/l	59715	251.26	85.37

Table 4.5: Fiber thickness of 1.5 g/l and 3.0 g/l collagen gels with number of measurement points as described in section 3.6.3.3 on page 54 (Count), mean and standard deviation (std) listed.

4.5 Influence of Cell Nucleus on Cell Migration

4.5.1 Cellular Elasticity

Both MDA-MB-231 and MCF-7 breast cancer cell lines were treated with TrichostatinA (TSA) to investigate the influence of nuclear mechanics on cell migration, see section 3.1.3 on page 34 for further information. As described in section 3.3 on page 36 and already shown in section 4.1 on page 65, a distinction between cytoskeletal and nuclear stiffness has been investigated in this work. The same technique can be used to investigate the effect of altered nuclear stiffness.

Figure 4.12 and Figure 4.13 on the following page show the results of TSA treatment on MDA-MB-231 and MCF-7 cancer cell lines.

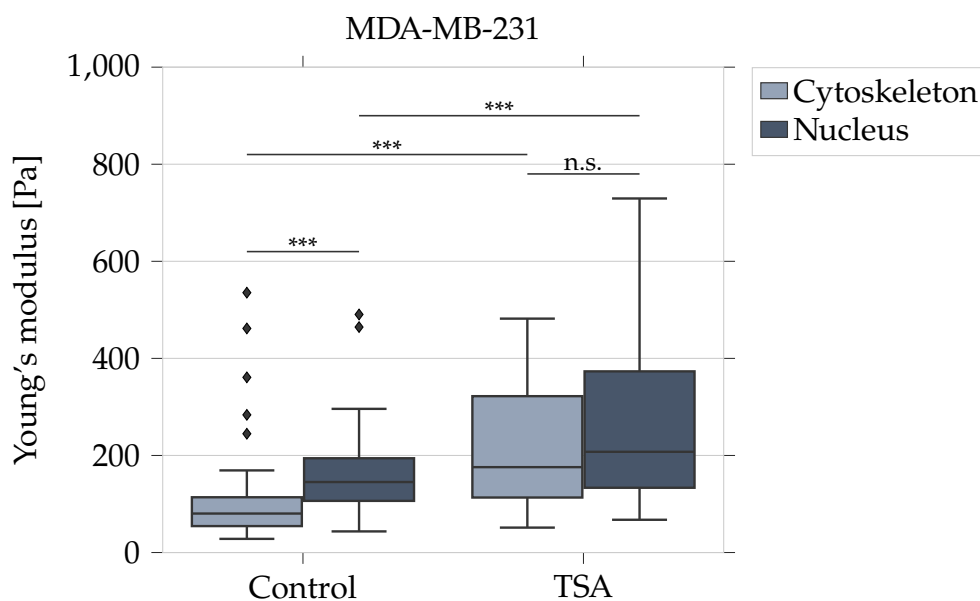


Figure 4.12: Cytoskeletal and nuclear elasticity determined using AFM of MDA-MB-231 cancer cells under DMSO control and TSA treatment.

These results show, that for MCF-7 cells, TSA has the expected effect of a softer nucleus due to the de-condensed chromatin (Krause et al. 2013). However, MDA-MB-231 cancer cells showed a contrary behavior. After TSA treatment, these cells show both a stiffer nucleus as well as cytoskeleton.

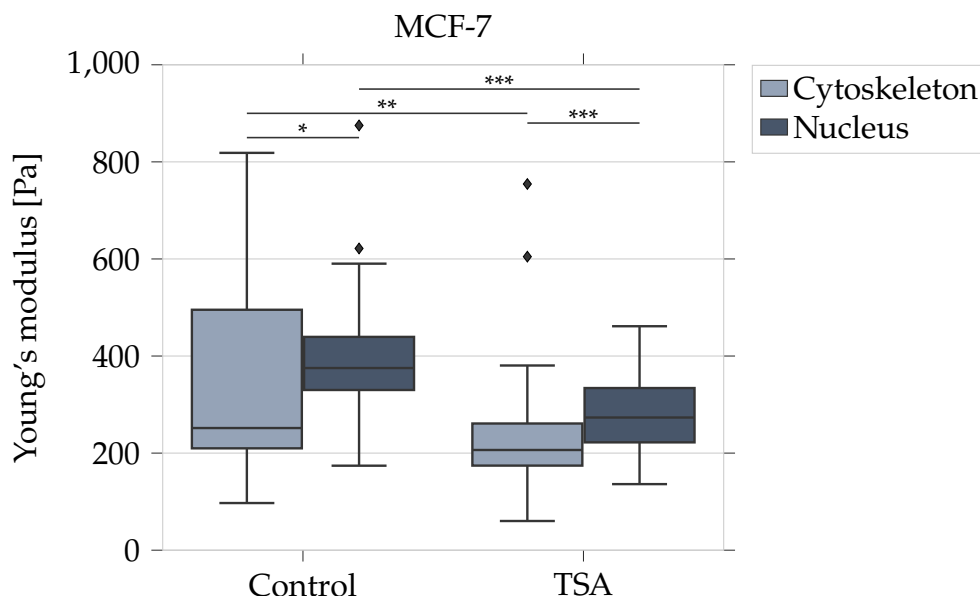


Figure 4.13: Cytoskeletal and nuclear elasticity determined using AFM of MCF-7 cancer cells under DMSO control and TSA treatment.

In a first step, a control experiment was carried out. Here, the cell nucleus was probed as explained in section 3.3 on page 36. Both cell lines were treated with 900 ng/ml TSA and as a control both 4.5 g/L DMEM and the pharmacological drug buffer (DMSO). Indeed, TSA has a significant effect on nuclear stiffness, but not the drug buffer control, as shown in figure 4.14 on the facing page.

To explain the discrepancy of MDA-MB-231 nuclear stiffness, additional pharmacological treatments have been carried out. As explained in section 3.1.3 on page 34, both MDA-MB-231 and MCF-7 cells were treated with 25 μ M BLEBBISTATIN, to reduce the affinity of myosin II motor proteins to the filamentous actin network by blocking it in the actin-detached state (Kovács et al. 2004). 0.2 μ M LATRUNCULINA was used to inhibit actin polymerization, which effectively eliminates actin filaments (Fischer, Wilharm, et al. 2017; Kunschmann, Puder, Fischer, Steffen, et al. 2019). Combinations of the two aforementioned drugs with TSA are used to explain the influence of the nuclear stiffness. Figure 4.15 on page 82 reveals a mechanistic insight into the nuclear stiffness discrepancy after TSA treatment of MDA-MB-231 cells.

First, BLEBBISTATIN had no significant effect on MDA-MB-231 cell nuclear stiffness. Additional treatment with TSA had no significant effect on MDA-MB-231 cells. However, the actin cytoskeleton depolymerizing drug LATRUNCULINA reduced nuclear stiffness

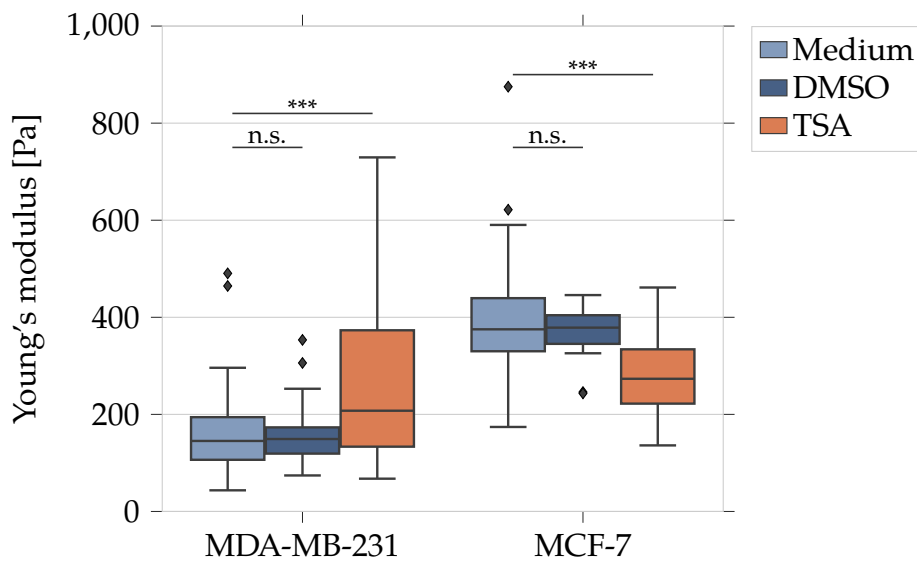


Figure 4.14: TSA buffer control effect on nuclear elasticity determined using AFM of MDA-MB-231 and MCF-7 cells. Medium control (light blue) and DMSO buffer control (dark blue) as well as TSA (orange) values are shown.

and additional treatment with TSA even further softened the cell nucleus as expected.

For MCF-7 cells, the expected behavior of TSA treatment was observed. BLEBBISTATIN reduced nuclear stiffness of MCF-7 and further TSA treatment drastically reduced nuclear stiffness. LATRUNCULINA and combined LATRUNCULINA and TSA treatment likewise reduced nuclear stiffness.

These data suggest that in fact a softening of the cell nucleus happens for both MDA-MB-231 and MCF-7 cells. However, the invasive cancer cell line MDA-MB-231 compensates the softer nucleus by increasing the actin cytoskeletal stiffness. Table 4.6 on the next page shows detailed values of cytoskeletal and table 4.7 on page 83 nuclear elasticity.

4.5.2 Invasion

Figure 4.16 on page 83 shows the effect of TSA treatment on the invasiveness in loose and figure 4.17 on page 84 in dense collagen gels. MDA-MB-231 are more invasive than MCF-7 cells with a more pronounced difference for 3.0 g/l matrices compared to 1.5 g/l. TSA treatment increased the invasiveness of MDA-MB-231 cells in 1.5 g/l collagen gels

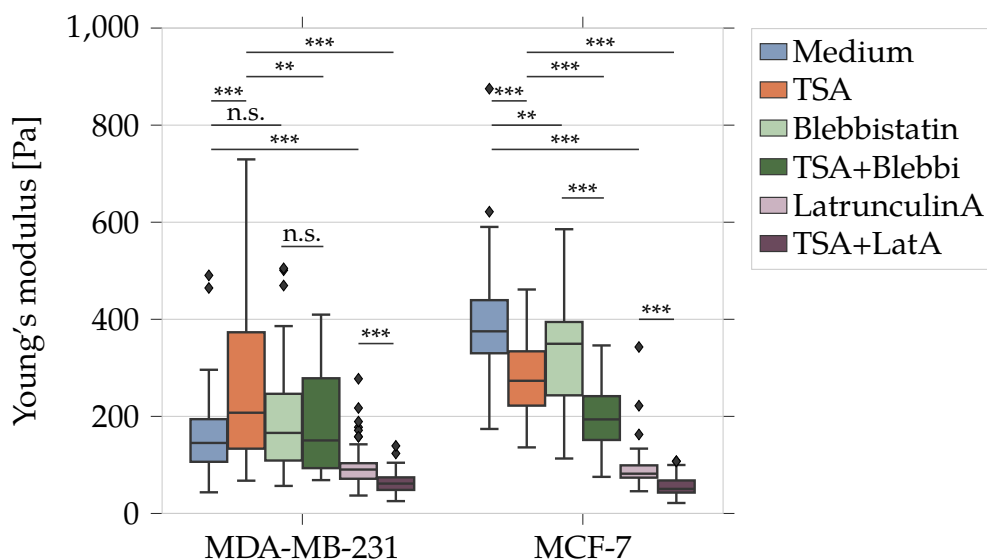


Figure 4.15: Pharmacological drug treatment reveals mechanistic insight into nuclear elasticity discrepancy of MDA-MB-231 cancer cells. Young's modulus determined using AFM. Shown are medium control (blue), TSA (orange), as well as BLEBBISTATIN (light green) and LATRUNCULINA (light purple) elasticities and their combined treatment TSA+BLEBBISTATIN (dark green) and TSA+LATRUNCULINA (dark purple).

Cell line	Drug	Count	Young's modulus [nN]		
			25%	50%	75%
MDA-MB-231	Medium	68	54.48	80.33	113.89
	TSA	54	113.33	175.90	322.14
MCF-7	Medium	34	209.83	251.63	495.33
	TSA	40	174.24	206.42	260.99

Table 4.6: Cytoskeletal Young's modulus of single, adherent invasive cancer cell line MDA-MB-231 and less invasive cancer cell line MCF-7 under TSA treatment. Listed are number of measured cells (Count) and 25 %, 50 % and 75 % percentiles.

but not for 3.0 g/l. For MCF-7 cells, the invasiveness was not altered for 1.5 g/l but for 3.0 g/l matrices.

However, TSA had a drastic effect on invasion depth. As seen in figure 4.18 on page 84 and figure 4.19 on page 85, TSA treatment decreased the invasion depth for both MDA-MB-231 and MCF-7 cells. In 3.0 g/l collagen gels, a softening of the cell nucleus did drastically increase invasion depth both for MDA-MB-231 and MCF-7 cells.

The cumulative probability reveals another interesting behavior. Figure 4.20 on the

Cell line	Drug	count	Young's modulus [nN]		
			25%	50%	75%
MDA-MB-231	Medium	69	106.43	145.25	194.26
	DMSO	30	119.14	149.25	173.23
	TSA	91	133.45	207.53	373.26
	BLEBBISTATIN	59	109.03	165.94	246.49
	LATRUNCULINA	72	71.45	90.46	103.54
	TSA+BLEBBISTATIN	59	93.35	150.43	278.50
	TSA+LATRUNCULINA	54	48.46	61.51	74.36
MCF-7	Medium	55	330.02	375.25	439.44
	DMSO	32	345.27	378.69	404.29
	TSA	54	222.13	273.32	334.04
	BLEBBISTATIN	44	243.36	349.56	394.53
	LATRUNCULINA	34	73.77	81.90	99.10
	TSA+BLEBBISTATIN	44	151.39	193.78	241.66
	TSA+LATRUNCULINA	45	42.99	50.59	68.02

Table 4.7: Young's modulus of single, adherent invasive cancer cell line MDA-MB-231 and less invasive cancer cell line MCF-7 under treatment of pharmacological drugs. Listed are number of measured cells (Count) and 25%, 50% and 75% percentiles.

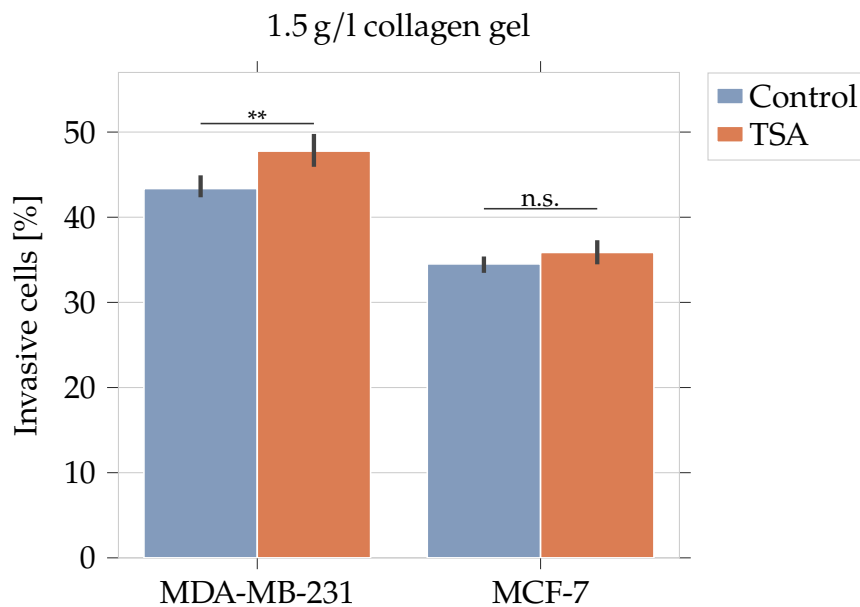


Figure 4.16: Effect of 900 ng/ml TSA treatment on the invasiveness of MDA-MB-231 and MCF-7 cells on 1.5 g/l collagen gels.

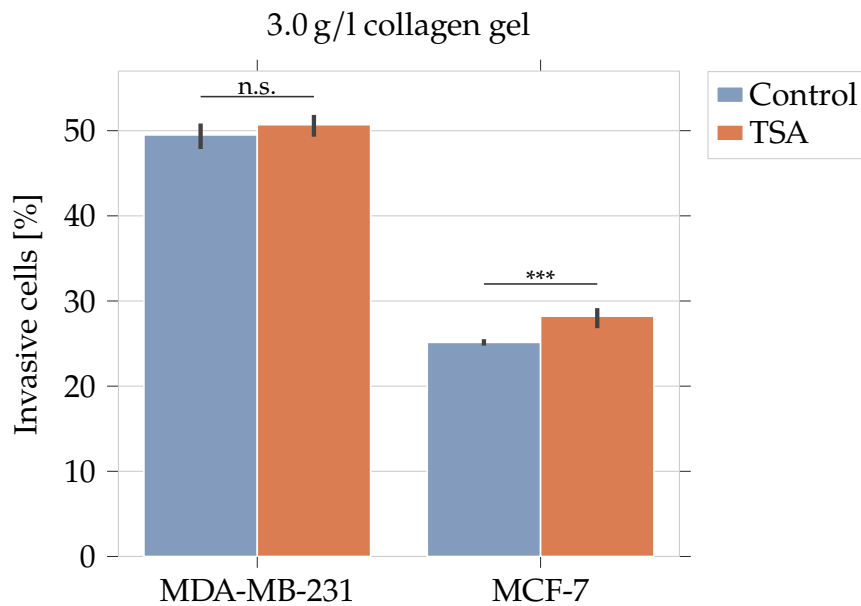


Figure 4.17: Effect of 900 ng/ml TSA treatment on the invasiveness of MDA-MB-231 and MCF-7 cells on 3.0 g/l collagen gels.

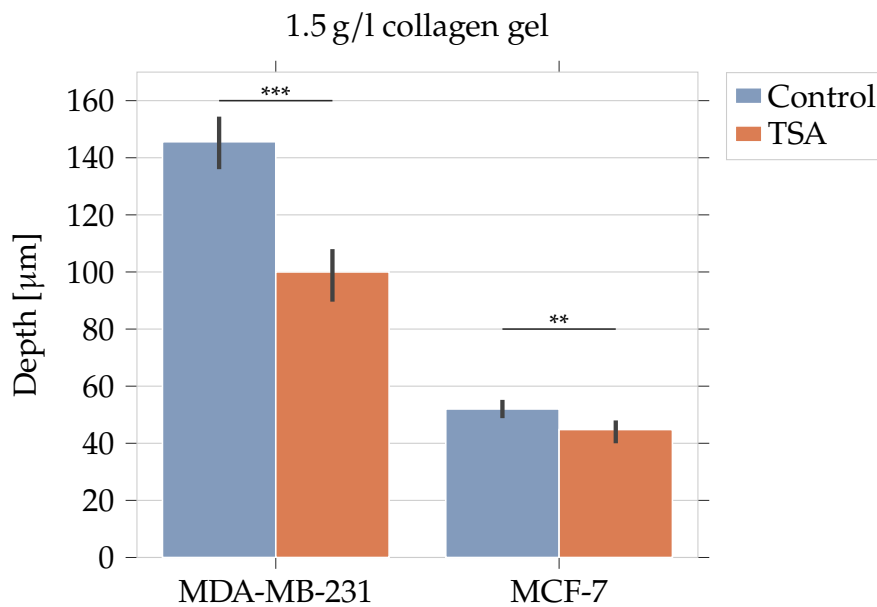


Figure 4.18: Effect of 900 ng/ml TSA treatment on the invasion depth of MDA-MB-231 and MCF-7 cells on 1.5 g/l collagen gels.

next page and figure 4.21 on page 86 show a pronounced plateau for higher invasion depths of MDA-MB-231 cells. This indicates that more MDA-MB-231 cells invaded

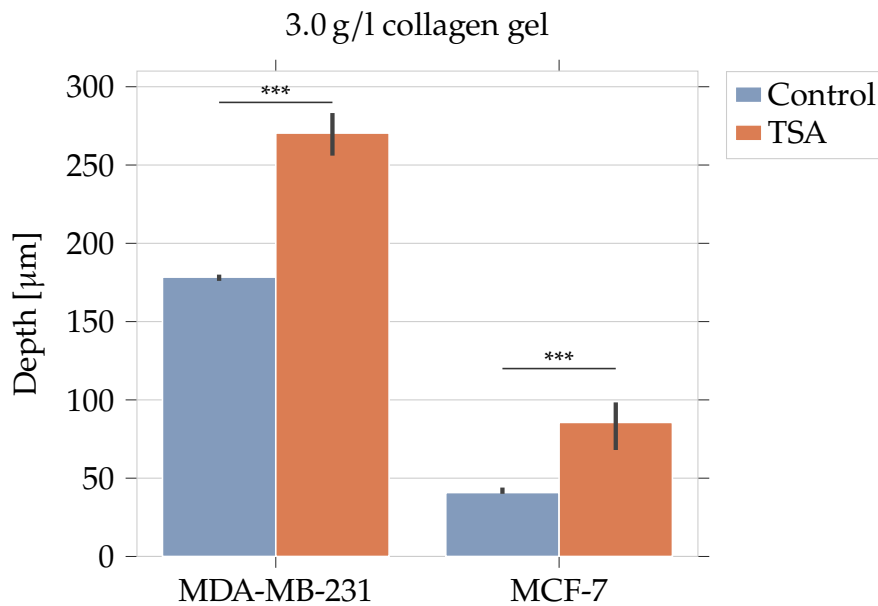


Figure 4.19: Effect of 900 ng/ml TSA treatment on the invasion depth of MDA-MB-231 and MCF-7 cells on 3.0 g/l collagen gels.

deeper into the bot 1.5 g/l and 3.0 g/l collagen gels.

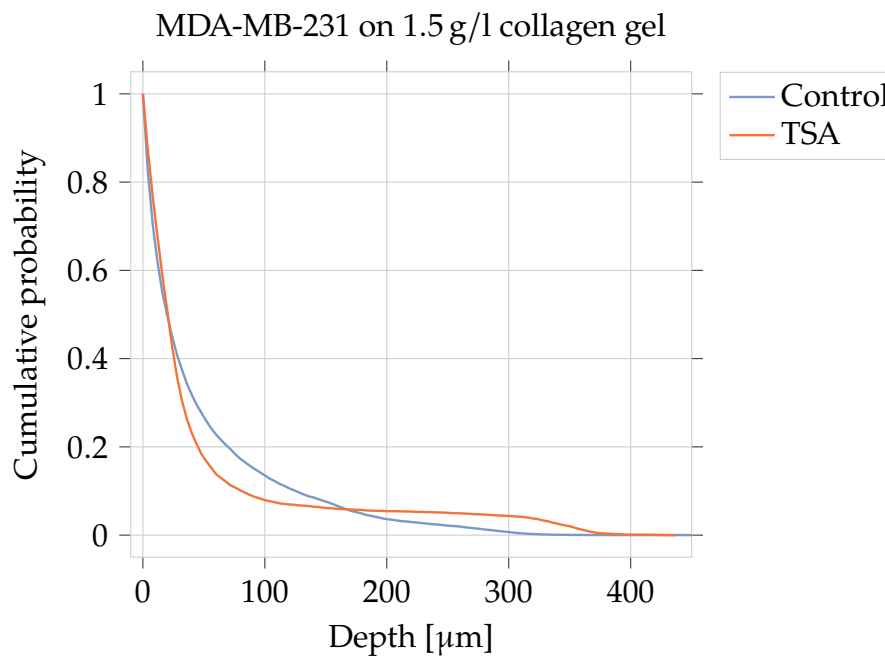


Figure 4.20: Effect of 900 ng/ml TSA treatment on the cumulative probability of MDA-MB-231 cells on 1.5 g/l collagen gels.

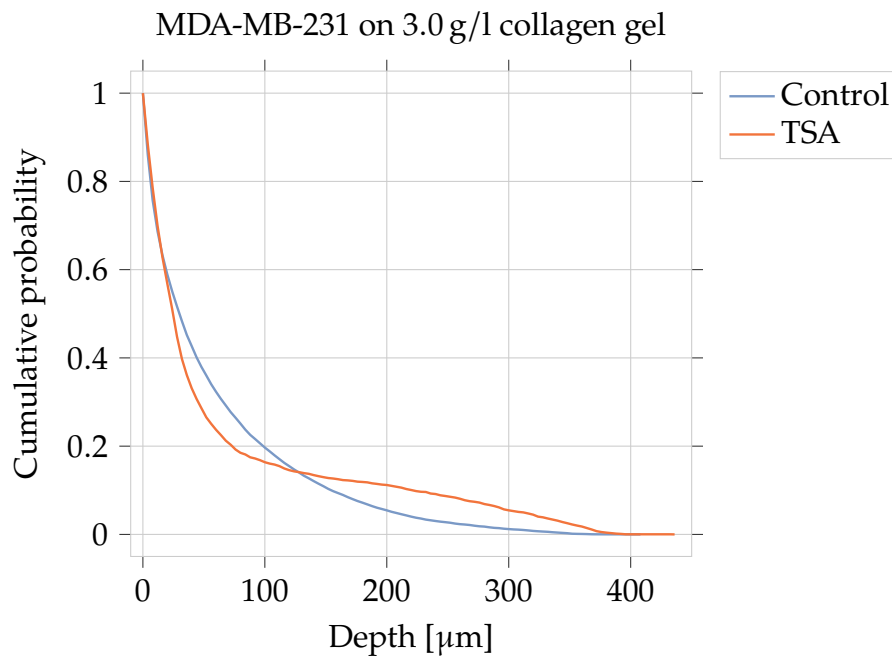


Figure 4.21: Effect of 900 ng/ml TSA treatment on the cumulative probability of MDA-MB-231 cells on 3.0 g/l collagen gels.

However, figure 4.22 on the next page shows almost identical distributions and figure 4.23 on the facing page a more pronounced invasion without deep plateau.

Table 4.8 on page 88 and Table 4.9 on page 88 lists specific values as mean and standard deviation calculated through a bootstrap error estimation, as described in section 3.5.3 on page 44. First, the number of counted cells from all five experiments are shown. Second, the invasiveness and invasion depth for each cell line and collagen gel concentration are listed.

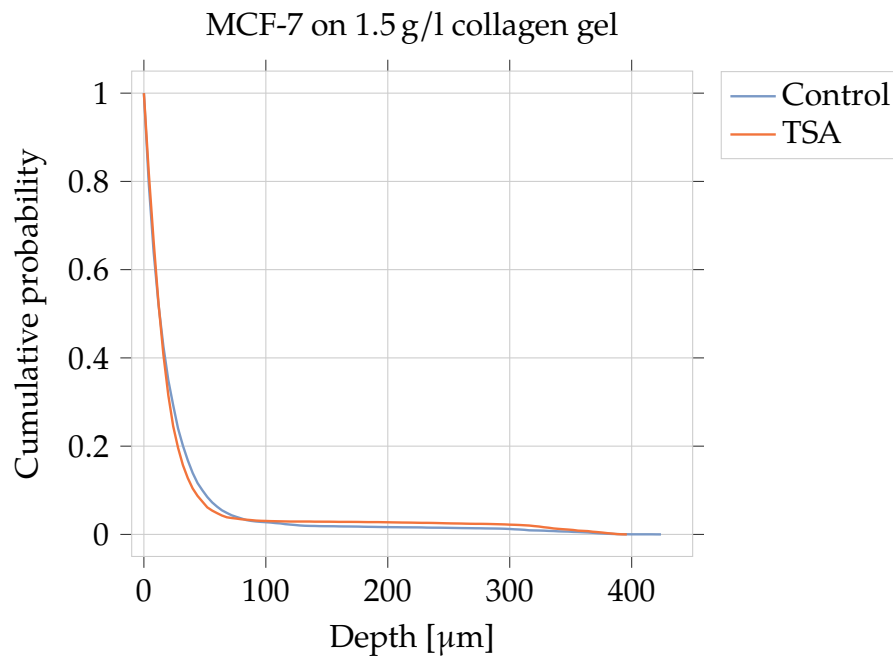


Figure 4.22: Effect of 900 ng/ml TSA treatment on the cumulative probability of MCF-7 cells on 1.5 g/l collagen gels.

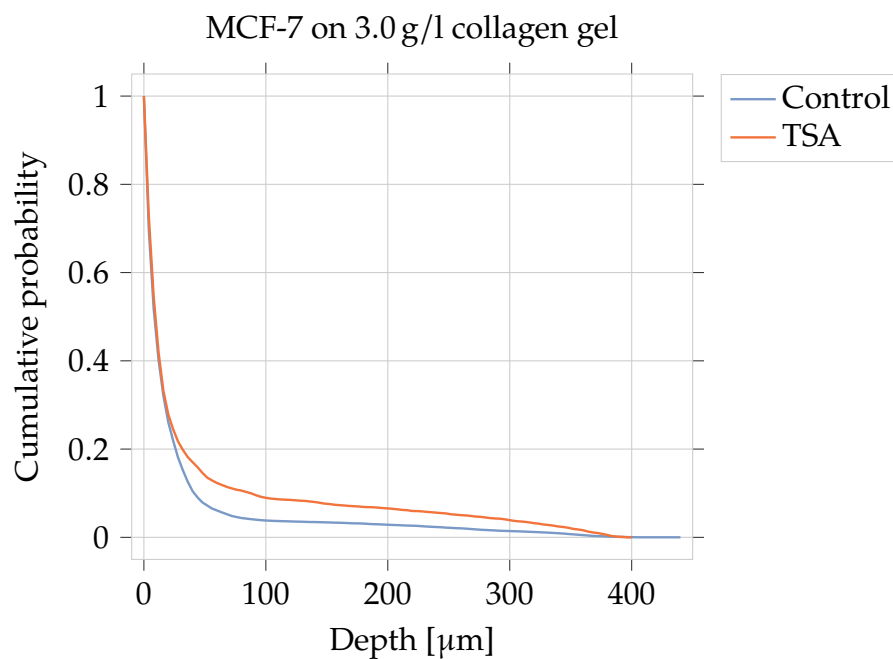


Figure 4.23: Effect of 900 ng/ml TSA treatment on the cumulative probability of MCF-7 cells on 3.0 g/l collagen gels.

Cell line	Drug	Number of cells		Invasiveness [%]		Depth [μm]	
		mean	std	mean	std	mean	std
MDA-MB-231	Control	31987	655	43.37	1.11	145.60	7.80
	TSA	12913	277	47.76	1.82	100.00	8.49
MCF-7	Control	28074	663	34.52	0.84	52.00	2.83
	TSA	24166	92	35.86	1.02	44.80	3.35

Table 4.8: Key values of the invasion assay and effect of 900 ng/ml TSA treatment for each cell line on 1.5 g/l collagen gel and pharmacological drug. The total number of counted cells as well as the invasiveness and invasion depth are listed. Values are denoted as mean with standard deviation calculated from a bootstrap error estimation.

Cell line	Drug	Number of cells		Invasiveness [%]		Depth [μm]	
		mean	std	mean	std	mean	std
MDA-MB-231	Control	39507	1357	49.50	1.39	178.40	2.19
	TSA	6997	161	50.70	1.07	270.40	13.45
MCF-7	Control	29473	798	25.14	0.37	40.80	1.79
	TSA	17190	426	28.22	1.18	85.60	13.45

Table 4.9: Key values of the invasion assay and effect of 900 ng/ml TSA treatment for each cell line on 3.0 g/l collagen gel and pharmacological drug. The total number of counted cells as well as the invasiveness and invasion depth are listed. Values are denoted as mean with standard deviation calculated from a bootstrap error estimation.

4.6 Fiber Displacement

In this work, a novel, minimally invasive approach to measure collagen fiber displacements of single, migrating cells in a 3D microenvironment was developed as described in section 3.7 on page 55. For each single cell, three-dimensional images of the collagen matrix and fluorescently stained cell membrane were recorded and the fiber displacement in dependence of distance from cell and time as well as the median fiber displacement was calculated, as explained in section 3.7.3 on page 57.

In this work, 1.5 g/l collagen gels were chosen, because these gels were significantly softer than 3.0 g/l matrices as shown in figure 4.4 on page 69. Thus, we hypothesized that 1.5 g/l collagen gels will get more deformed under the same amount of deformation force generated by migrating cells than 3.0 g/l collagen gels.

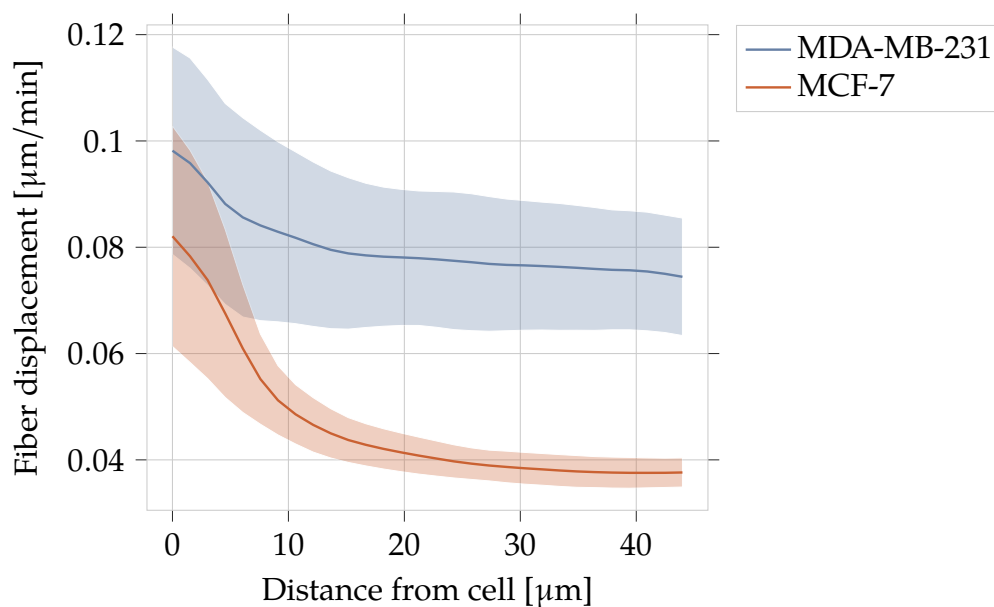


Figure 4.24: Fiber displacement in dependence of distance from cell surface in μm for MDA-MB-231 and MCF-7 cancer cell lines. Colored line represents median, shaded area 95 % confidence interval of all analyzed cells.

Figure 4.24 shows the fiber displacement in dependence of distance from cell for both MDA-MB-231 and MCF-7 cells in 1.5 g/l collagen gels. 16 MDA-MB-231 and 17 MCF-7 cells had been analyzed. The colored line represents the median of all analyzed cells, the shaded area represents the 95 % confidence interval.

Clearly, the invasive MDA-MB-231 cancer cell line deformed their 3D surrounding more than less invasive MCF-7. The higher deformations that MDA-MB-231 cells exerted on their surrounding continued at high distances from the cell surface. For MCF-7 cells, the generated fiber displacements decreased much closer to the cell surface.

The timely development of fiber displacements is shown in figure 4.25. Here, the mean over a time period of two hours was calculated.

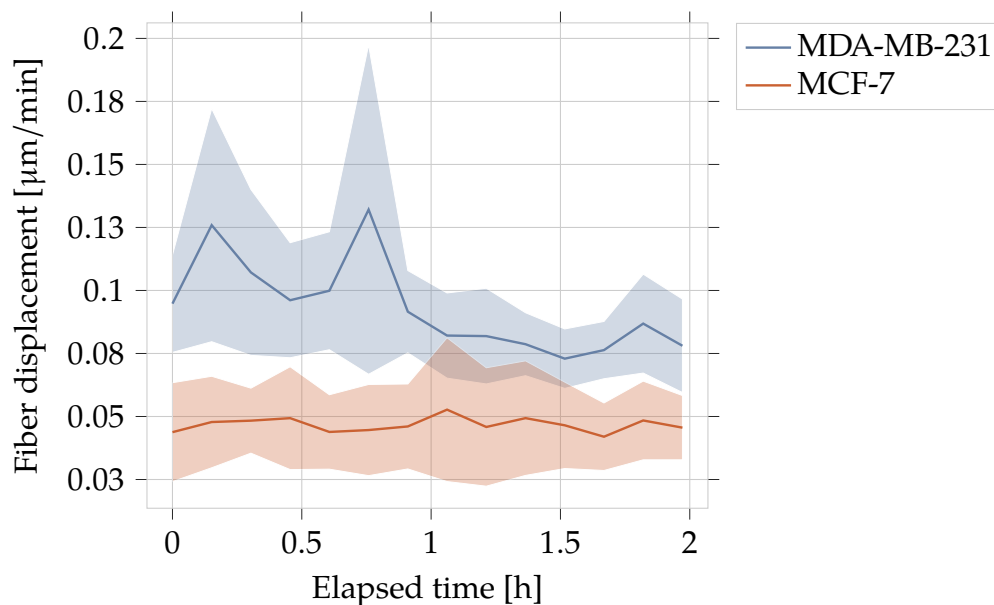


Figure 4.25: Fiber displacement in dependence of elapsed time for MDA-MB-231 and MCF-7 cancer cell lines. Colored line represents median, shaded area 95 % confidence interval of all analyzed cells.

In general, the higher matrix deformations of MDA-MB-231 cancer cells retained over the whole analyzed time period and for all time points. This indicates that the observed behaviour was indeed an active process conducted by each individual cell.

As explained in section 3.7.3 on page 57, the multi-dimensional data shown above can be condensed to the so called median fiber displacement, as shown in figure 4.26 on the facing page.

This reveals that the 3D microenvironment deformation was doubled for the invasive cancer cell line MDA-MB-231 compared to the less invasive MCF-7 cells. In table 4.10 on the next page are listed explicit values of median fiber displacements.

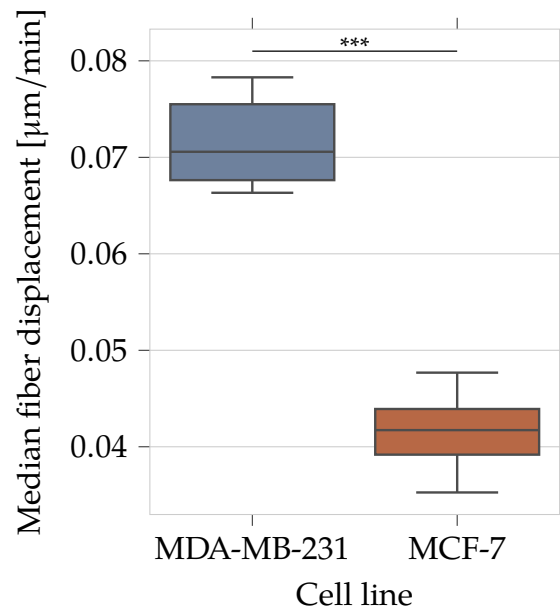


Figure 4.26: Median fiber displacement for MDA-MB-231 and MCF-7 with statistical significance indicated.

Cell Line	Count	Median fiber displacement [$\mu\text{m}/\text{min}$]		
		25%	50%	75%
MDA-MB-231	16	0.0676	0.0706	0.0755
MCF-7	17	0.0392	0.0417	0.0439

Table 4.10: Median fiber displacement in $\mu\text{m}/\text{min}$ of invasive cancer cell line MDA-MB-231 and less invasive cancer cell line MCF-7. Listed are number of measured cells (Count) and 25 %, 50 % and 75 % percentiles.

4.7 Effect of FAK on Cell Invasion and Fiber Displacement

FAK anchors actin stress fibers to the extracellular matrix and thus plays a crucial role during cell migration (Wolfenson et al. 2009). To study the role of FAK on cell migration and 3D fiber displacement, mouse embryonic fibroblast cell lines FAK^{+/+} and FAK^{-/-}. FAK^{-/-} is a FAK deficient knock-out cell line with FAK^{+/+} as a control. Additionally, a kinase-dead variant FAK^{WT/WT} and FAK^{R454/R454} wild-type cell lines were used, kindly provided by Dr. David D. Schlaepfer. In FAK^{R454/R454} cells, FAK was present at focal adhesions but was not phosphorylated, preserving cell proliferation (Lim et al. 2010). as described in section 3.1.2 on page 32 were used.

4.7.1 FAK Knock-Out

The invasion assay was performed as described in section 3.5 on page 42. Figure 4.27 on the following page shows the invasiveness of both FAK^{+/+} and FAK^{-/-} mouse embryonic fibroblasts. FAK^{+/+} cells were more invasive than FAK^{-/-} cells for both 1.5 g/l and 3.0 g/l collagen gels.

As seen in figure 4.28 on the next page, the invasion depth of FAK^{+/+} cells was significantly higher than for FAK^{-/-} cells for both 1.5 g/l and 3.0 g/l collagen gels.

Table 4.11 on page 95 lists specific values as mean and standard deviation calculated through a bootstrap error estimation, as described in section 3.5.3 on page 44. The number of counted cells from all experiments as well as invasiveness and invasion depth for each cell line and collagen gel concentration are listed.

Fiber displacements were determined as explained in section 3.7 on page 55. The dependence of distance from cell and time along with the median fiber displacement were calculated as described in section 3.7.3 on page 57.

In this work, 1.5 g/l collagen gels were chosen, as these gels were significantly softer compared to 3.0 g/l matrices as shown in figure 4.4 on page 69. Thus, we hypothesized that 1.5 g/l collagen gels will get more deformed by migrating cells generating deformation forces than in 3.0 g/l collagen gels.

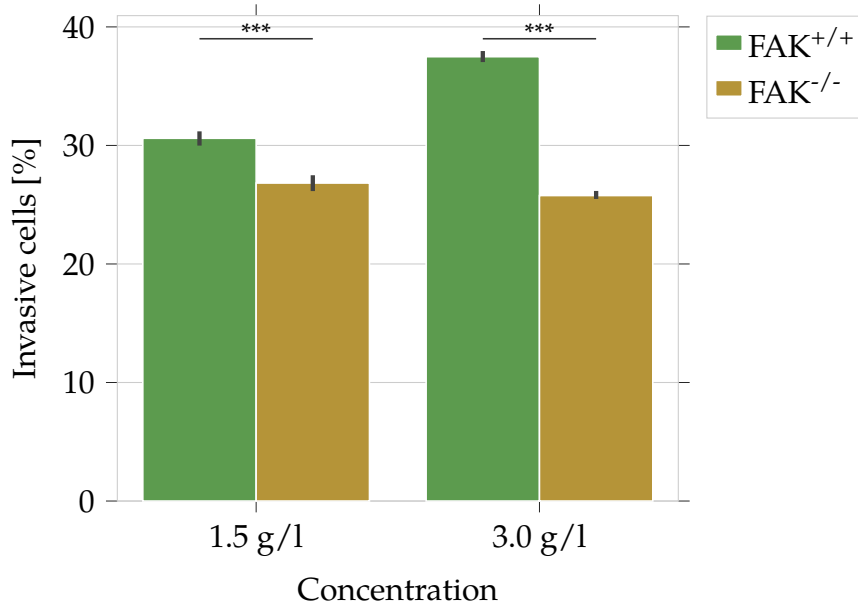


Figure 4.27: Invasiveness of FAK^{+/+} (green) and FAK^{-/-} (ochre) cells on 1.5 g/l and 3.0 g/l collagen gels with indicated error bars in black.

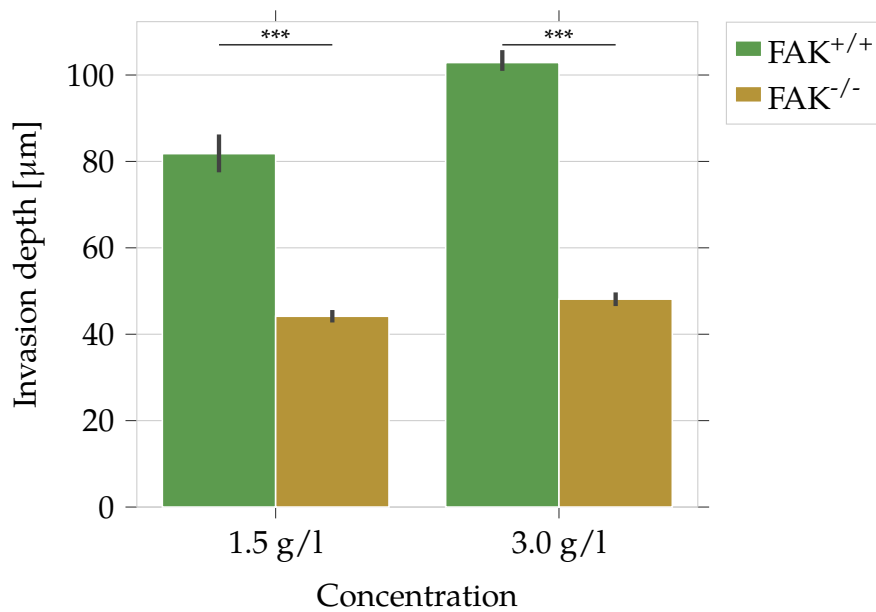


Figure 4.28: Invasion depth in µm of FAK^{+/+} and FAK^{-/-} cells on 1.5 g/l and 3.0 g/l collagen gels with indicated error bars in black.

Figure 4.29 on the next page shows the fiber displacement for both FAK^{+/+} and FAK^{-/-} mouse embryonic fibroblasts in 3.0 g/l collagen gels. The colored line represents the

Cell line	Conc.	Number of cells		Invasiveness [%]		Depth [μm]	
		mean	std	mean	std	mean	std
FAK ^{+/+}	1.5 g/l	11156	498	30.60	2.88	81.80	21.93
	3.0 g/l	10551	352	37.48	1.39	102.88	4.73
FAK ^{-/-}	1.5 g/l	23867	1153	26.83	2.38	44.16	7.45
	3.0 g/l	13059	345	25.77	0.93	48.12	3.03

Table 4.11: Key values of the invasion assay for FAK^{+/+} and FAK^{-/-} and each collagen concentration (Conc.). The total number of counted cells as well as the invasiveness and invasion depth are listed. Values are denoted as mean with standard deviation calculated from a bootstrap error estimation.

median of all analyzed cells, the shaded area represents the 95 % confidence interval.

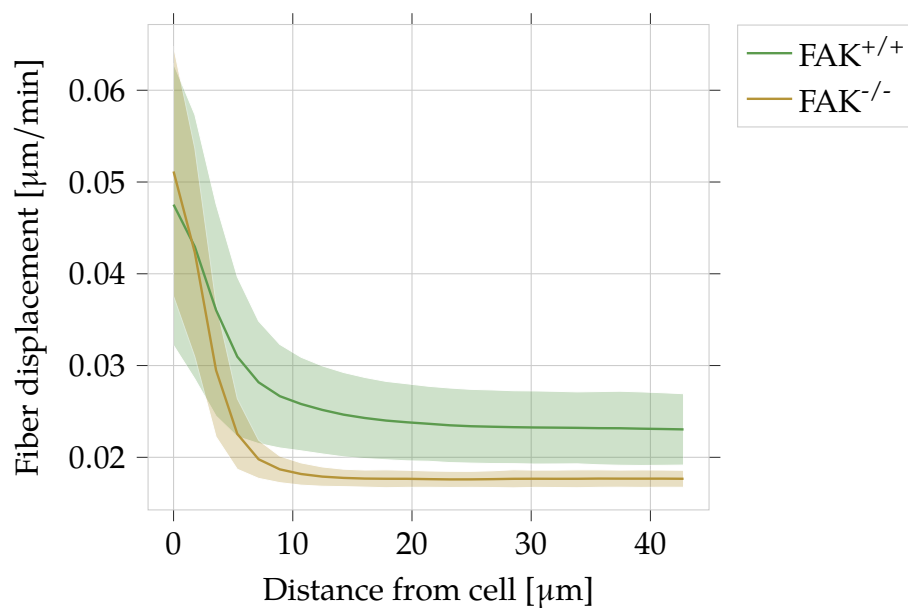


Figure 4.29: Fiber displacement in dependence of distance from cell surface in μm for FAK^{+/+} and FAK^{-/-} mouse embryonic fibroblasts. Colored line represents median, shaded area 95 % confidence interval of all analyzed cells.

FAK^{+/+} cells generated higher fiber displacements than FAK^{-/-} cells. Moreover, these higher deformations continue to larger distances from the cell surface.

Figure 4.30 on the following page shows the timely development of fiber displacements. Here, the mean over a time period of two hours was calculated.

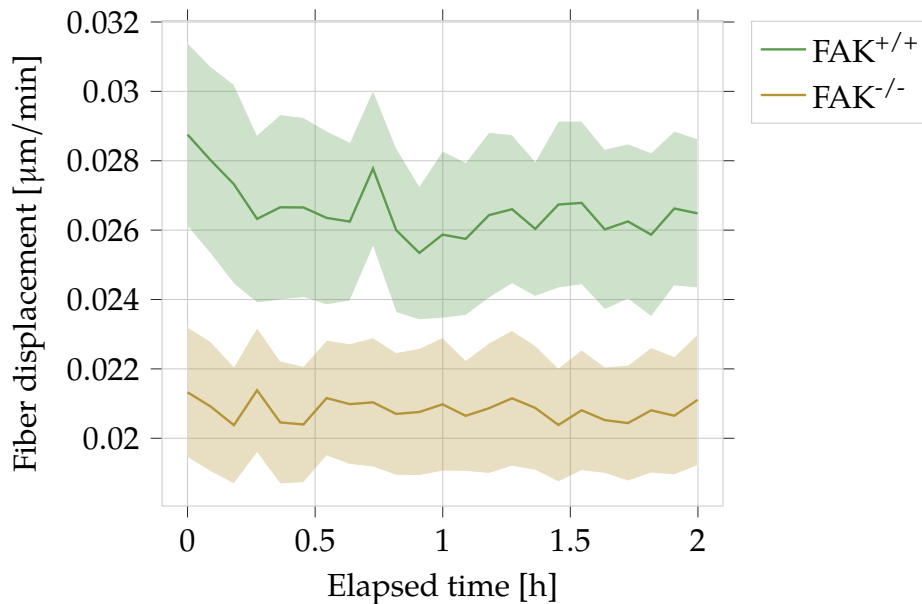


Figure 4.30: Fiber displacement in dependence of elapsed time for FAK^{+/+} and FAK^{-/-} mouse embryonic fibroblasts. Colored line represents median, shaded area 95% confidence interval of all analyzed cells.

The higher matrix deformations of FAK^{+/+} mouse embryonic fibroblasts were preserved over the whole analyzed time period and for all time points. This indicates that the observed behaviour was indeed an active process conducted by each individual cell, similar to the analyzed cancer cell lines in figure 4.25 on page 90.

As explained in section 3.7.3 on page 57, the multi-dimensional data shown above can be condensed to the so called median fiber displacement, as shown in figure 4.31 on the next page.

Indeed, FAK^{+/+} cells deformed their 3D microenvironment significantly more than FAK^{-/-} cells. Thus suggests a major contribution of FAK to force generation during cell invasion and migration.

Table 4.12 on the facing page lists explicit values of median fiber displacements for FAK^{+/+} and FAK^{-/-} mouse embryonic fibroblasts.

4.7.2 Kinase-dead FAK Mutant

The invasion assay has been performed as described in section 3.5 on page 42. Figure 4.32 on page 98 shows the invasiveness of both FAK^{WT/WT} and FAK^{R454/R454} mouse

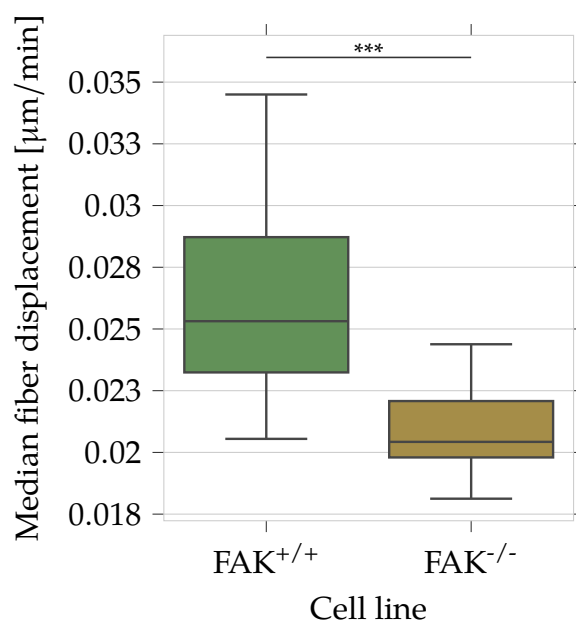


Figure 4.31: Median fiber displacement for FAK^{+/+} and FAK^{-/-} with statistical significance indicated.

Cell Line	Count	Median fiber displacement [$\mu\text{m}/\text{min}$]		
		25%	50%	75%
FAK ^{+/+}	17	0.0232	0.0253	0.0287
FAK ^{-/-}	26	0.0198	0.0204	0.0221

Table 4.12: Median fiber displacement in $\mu\text{m}/\text{min}$ of FAK^{+/+} and FAK^{-/-} mouse embryonic fibroblasts. Listed are number of measured cells (Count) and 25 %, 50 % and 75 % percentiles.

embryonic fibroblasts. FAK^{WT/WT} cells were more invasive than FAK^{R454/R454} cells for both 1.5 g/l and 3.0 g/l collagen gels.

As seen in figure 4.33 on the next page, the invasion depth of FAK^{WT/WT} cells was significantly higher than for FAK^{R454/R454} cells for both 1.5 g/l and 3.0 g/l collagen gels.

Table 4.13 on page 99 lists specific values as mean and standard deviation calculated through a bootstrap error estimation, as described in section 3.5.3 on page 44. The number of counted cells from all five experiments as well as invasiveness and invasion depth for each cell line and collagen gel concentration are listed.

In section 4.7.1 on page 93, the FAK knock-out mouse embryonic fibroblast cell lines FAK^{-/-} and wild-type control FAK^{+/+} were studied. As FAK fulfills multiple roles during

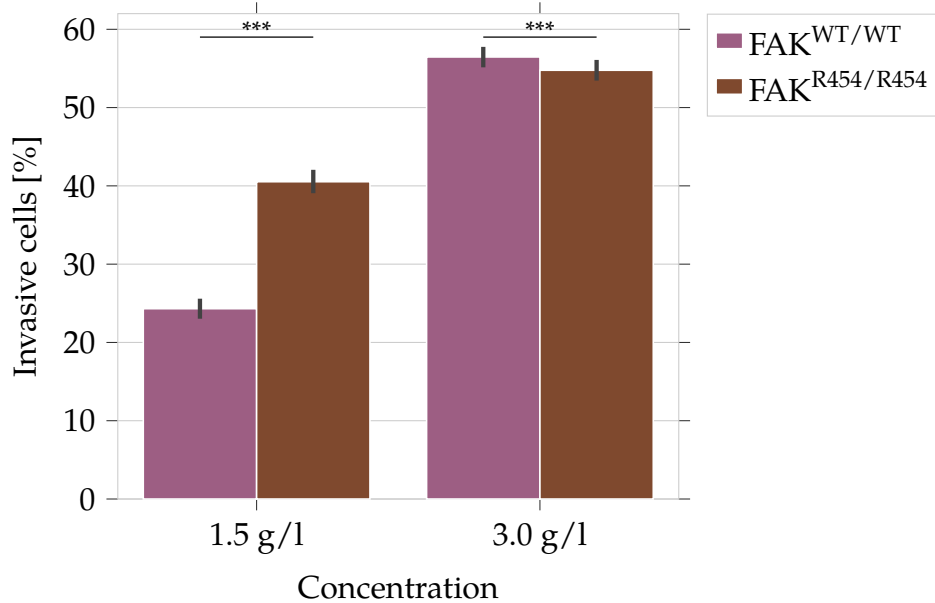


Figure 4.32: Invasiveness of FAK^{WT/WT} and FAK^{R454/R454} cells on 1.5 g/l and 3.0 g/l collagen gels with indicated error bars in black.

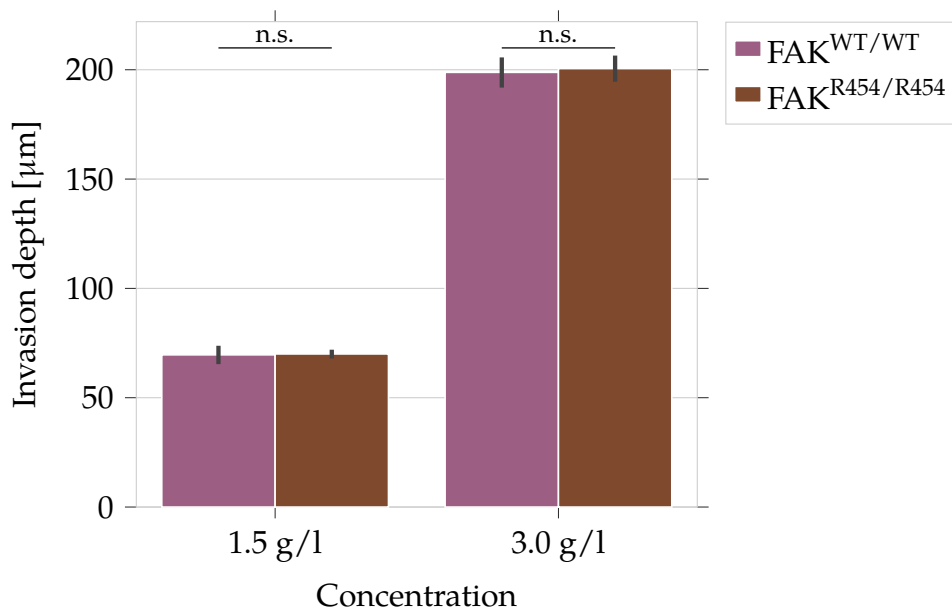


Figure 4.33: Invasion depth in μm of FAK^{WT/WT} and FAK^{R454/R454} cells on 1.5 g/l and 3.0 g/l collagen gels with indicated error bars in black.

cell migration (Lim et al. 2010), a kinase-dead mutation FAK^{R454/R454} and wild-type control FAK^{WT/WT} were used, as described in section 3.1.2 on page 32.

Cell line	Conc.	Number of cells		Invasiveness [%]		Depth [μm]	
		mean	std	mean	std	mean	std
FAK ^{WT/WT}	1.5 g/l	3570	179	24.31	1.43	69.60	11.51
	3.0 g/l	2101	75	56.46	1.64	198.80	9.62
FAK ^{R454/R454}	1.5 g/l	2779	128	40.53	2.48	70.00	5.32
	3.0 g/l	2092	77	54.77	1.68	200.52	5.01

Table 4.13: Key values of the invasion assay for FAK^{WT/WT} and FAK^{R454/R454} and each collagen concentration (Conc.). The total number of counted cells as well as the invasiveness and invasion depth are listed. Values are denoted as mean with standard deviation calculated from a bootstrap error estimation.

Fiber displacements were determined as explained in section 3.7 on page 55. The dependence of distance from cell and time along with the median fiber displacement were calculated as described in section 3.7.3 on page 57.

As shown in figure 4.4 on page 69, 1.5 g/l were significantly softer than 3.0 g/l matrices and thus 1.5 g/l collagen gels were chosen in this work. We hypothesized that 1.5 g/l collagen gels will get more deformed by migrating cells generating deformation forces than 3.0 g/l collagen gels.

Figure 4.34 on the next page shows the fiber displacement for both FAK^{WT/WT} and FAK^{R454/R454} mouse embryonic fibroblasts in 3.0 g/l collagen gels. The colored line represents the median of all analyzed cells, the shaded area represents the 95 % confidence interval.

FAK^{WT/WT} showed almost identical behaviour to FAK^{R454/R454}, in contrast to FAK^{+/+} and FAK^{-/-} cell lines, as shown in section 4.7.1 on page 93. The fiber displacements in dependence to distance from cell surface behaved similarly for both FAK^{WT/WT} and FAK^{R454/R454} fibroblasts.

A similar result for the time dependency of fiber displacements can be seen in figure 4.35 on the next page.

Over the whole analyzed time period of two hours, no or small differences were observed. Again, this indicates that the observed behaviour was indeed an active process conducted by each individual cell.

Figure 4.36 on page 101 shows the median fiber displacement, explained in section 3.7.3 on page 57.

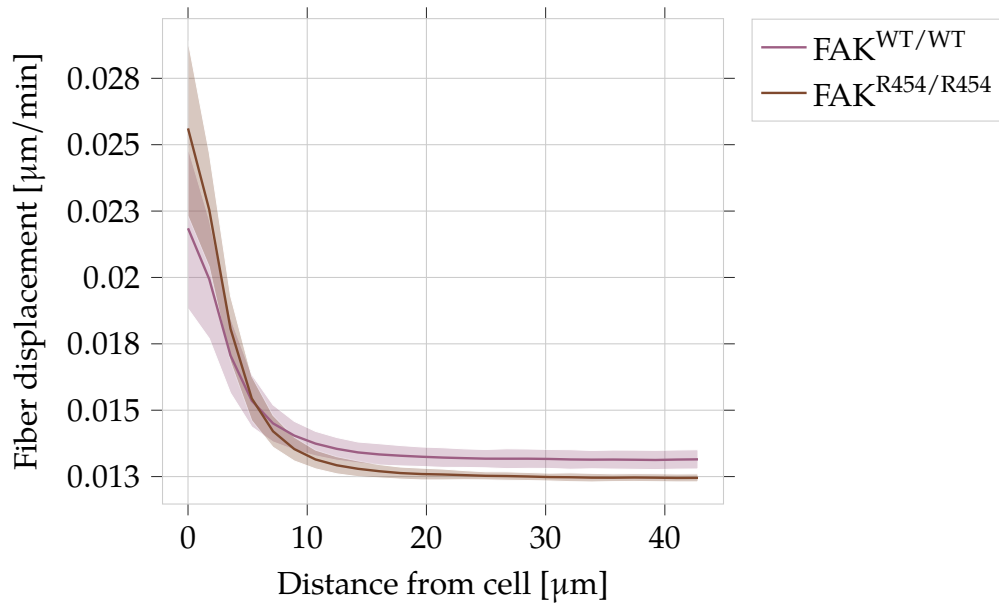


Figure 4.34: Fiber displacement in dependence of distance from cell surface in μm for FAK^{WT/WT} and FAK^{R454/R454} mouse embryonic fibroblasts. Colored line represents median, shaded area 95% confidence interval of all analyzed cells.

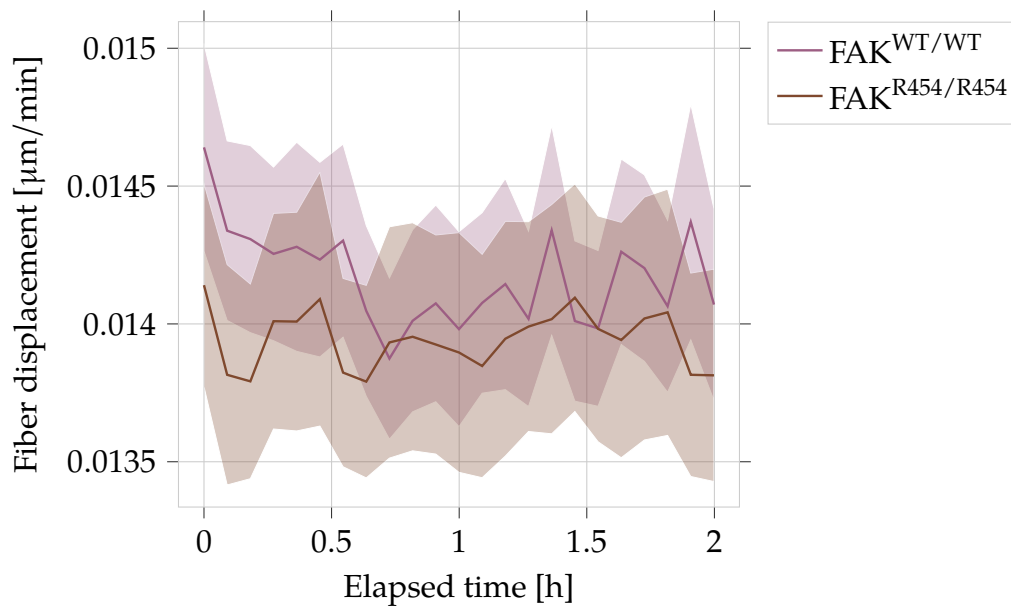


Figure 4.35: Fiber displacement in dependence of elapsed time for FAK^{+/+} and FAK^{-/-} mouse embryonic fibroblasts. Colored line represents median, shaded area 95% confidence interval of all analyzed cells.

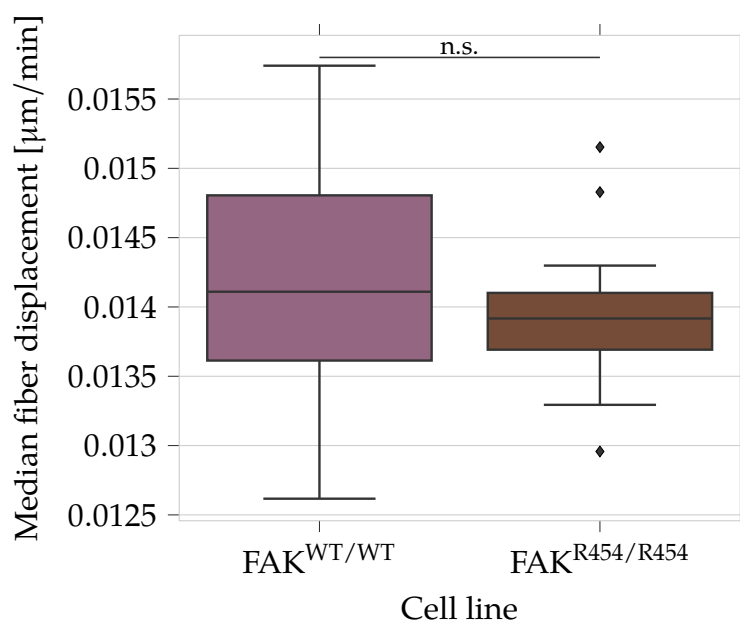


Figure 4.36: Median fiber displacement for FAK^{WT/WT} and FAK^{R454/R454} with statistical significance indicated.

Clearly, the median fiber displacements for both FAK^{WT/WT} and FAK^{R454/R454} were not significantly different.

Table 4.14 lists explicit values of median fiber displacements for FAK^{WT/WT} and FAK^{R454/R454} mouse embryonic fibroblasts.

Cell Line	Count	Median fiber displacement [$\mu\text{m}/\text{min}$]		
		25%	50%	75%
FAK ^{WT/WT}	21	0.0136	0.0141	0.0148
FAK ^{R454/R454}	28	0.0137	0.0139	0.0141

Table 4.14: Median fiber displacement in $\mu\text{m}/\text{min}$ of FAK^{WT/WT} and FAK^{R454/R454} mouse embryonic fibroblasts. Listed are number of measured cells (Count) and 25 %, 50 % and 75 % percentiles.

Chapter 5

Discussion

In this work, a toolset of biophysical methods has been introduced and used to study single cell migration in artificial collagen I networks as an ECM model system. These methods were advancements of established assays or completely novel methods. Cell and matrix mechanical and topological properties were determined and the deformation of the microenvironment during single cell migration was measured. Additionally, the influence of the cell nucleus on cell migration and mechanical properties as well as the influence of focal adhesion kinase (FAK) on fiber displacement was analyzed. The results indicate, that these methods are well suited to study the biophysical aspects of and major influences on single cell migration.

Cell mechanical properties are directly linked to structural cell components such as the actin cytoskeleton and cell nucleus and have impact on cell migration (Okeyo et al. 2009; F. Huber et al. 2013). Thus, measuring the elastic properties of these major cellular structures leads to insights into properties of these components. The results are in line with current research that single, invasive cancer cells appear softer than less invasive cells (Alibert et al. 2017; Fischer, Wilharm, et al. 2017).

Cell migration is a complex process during which a cell exerts forces to translocate and deform their microenvironment (F. Huber et al. 2013). However, current methods utilize fluorescent beads as fiducial markers (Steinwachs et al. 2016). Recent studies have shown that these beads inhibit cell migration when phagocytosed (Claudia T. Mierke 2013). The novel method presented in this work uses a minimally invasive approach to measure fiber displacements of single cells in 3D artificial collagen scaffolds. Additionally, a completely automated analysis procedure is introduced. The results show clear trends in fiber displacements of cancer cells as well as mouse embryonic fibroblasts. The

invasive cancer cell line MDA-MB-231 exhibited almost double the amount of median fiber displacements and long range deformation than the less invasive MCF-7 cancer cell line.

As these single cells reside in a 3D collagen scaffold, the mechanical and topological properties of this microenvironment can not be ignored. In this work, a reliable method to determine matrix stiffness is described and the results confirm recent studies (Sapudom et al. 2015; Fischer, Wilharm, et al. 2017). Additionally, a completely novel approach to determine a major structural parameter, the so called pore-size, is described. The results indicate that this method is superior to previous approaches (Molteni et al. 2013a; Molteni et al. 2013b; Münster et al. 2013). This method has been studied in detail in (Fischer, Hayn, et al. 2019). However, in this thesis, the analysis has been extended to determine the collagen fiber thickness as well. Although the pore-size of 1.5 g/l was significantly larger than of 3.0 g/l, the fiber thickness showed no difference. This indicates that the difference in mechanical properties might arise solely from topological differences and not from thicker and thus stiffer collagen fibers.

Understanding single cell migration is the subject of current research, especially in cancer research (Claudia Tanja Mierke 2018a; Claudia Tanja Mierke 2018b). Cell invasion into 3D artificial collagen gels has developed as a powerful tool to quantify and describe cell migration in 3D extracellular matrices and tissue (Claudia Tanja Mierke, Frey, et al. 2011; Claudia Tanja Mierke 2013a; Fischer, Wilharm, et al. 2017; Claudia T. Mierke et al. 2017; Kunschmann, Puder, Fischer, Steffen, et al. 2019). This 3D cell invasion is correlated with the metastatic potential of cancer cells (Claudia Tanja Mierke 2018a; Claudia Tanja Mierke 2018b). The assay and analysis method presented in this work provide a reliable method and sophisticated analysis to this cell invasion assay. Additionally, a user friendly software was developed, enabling high throughput analysis.

Using pharmacological drugs targeting specific cellular structures and processes, the methods developed in this work enable to precisely measure the effects on the discussed biophysical properties such as cell elasticity and invasion. The results lead to a mechanistic insight on the role of nuclear elasticity for the two studied cancer cell lines MDA-MB-231 and MCF-7. These data suggest, that MDA-MB-231 cancer cells seem to compensate a softer nucleus by stiffening their cytoskeleton.

Finally, cell invasion and fiber displacement analysis is used to study the influence of focal adhesion kinase (FAK) using a FAK deficient knock-out cell line FAK^{-/-} and control FAK^{+/+} as well as a kinase-dead cell line FAK^{R454/R454} and control FAK^{WT/WT}.

The results indicate that FAK^{-/-} are less invasive and invade less deep into 1.5 g/l and 3.0 g/l 3D collagen gels. These findings correlate with the results showing that FAK^{-/-} cells are not able to deform their microenvironment as much as FAK^{+/+} cells, indicating that FAK^{-/-} cells are less able to generate forces needed for cell invasion. However, the results for the kinase-dead cell line FAK^{R454/R454} and control FAK^{WT/WT} show another interesting trend. FAK^{R454/R454} were significantly more invasive than FAK^{WT/WT} on 1.5 g/l, but slightly less invasive on 3.0 g/l. Conversely, the invasion depth was almost identical for both cell lines on both collagen gels. However, invasiveness and invasion depth were higher on 3.0 g/l than on 1.5 g/l for both cell lines. In line with these findings, both cell lines showed no significant difference in fiber displacements. This suggests a major role of FAK on cell migration and amount of forces generated during cell migration, in line with current research (Gilmore et al. 1996; Claudia T. Mierke et al. 2017). Although recent studies showed significant differences in fiber displacements for FAK^{WT/WT} and FAK^{R454/R454} mouse embryonic fibroblasts (Claudia T. Mierke et al. 2017), this study used 3.0 g/l collagen gels for the fiber displacement experiments. In this work, based on the finding that the invasiveness of FAK^{R454/R454} was significantly increased on 1.5 g/l collagen gels, these 1.5 g/l matrices were used for all fiber displacement measurements.

The results presented in this work provide new insights into major aspects of cell single cell migration in 3D artificial collagen gels, indicating that the presented methods are well suited as a toolset. These biophysical aspects include 3D invasion, cellular elasticity, matrix stiffness and pore-size as well as fiber displacements. However, no claim is made that these parameters are exhaustive. In fact, other biophysical and biochemical aspects exist to study different cellular and extracellular structures and processes.

The generalizability of the results is limited by the used cell lines, collagen concentration and composition. In more detail, the used collagen gels are composed of a specific mixture of monomers extracted from rat tail and bovine skin, as described in section 2.3.2 on page 26. Other compositions and concentrations as well as cell lines and primary cells need to be tested in future studies. Additional biopolymer components such as fibronectin or hyaluronan further broaden the possible applications. It is beyond the scope of this study to make general claims about cancer and metastasis or clinical therapies. The presented novel approach to determine collagen pore-size had been shown to be superior to previous approaches (Fischer, Hayn, et al. 2019).

However, collagen networks are a highly in-homogenous structure and spherical pores must be considered an approximation. The fiber displacements revealed in this work were absolute values of 3D vectors for each three dimensional image pixel, constituting another approximation.

Further advancement in fiber displacement studies might include complex vector field analysis of 3D fiber displacement vector fields, calculated by the algorithm presented in this work. These lead to further insights into cell polarities and force directionalities during cell migration. Based on the precise collagen network segmentation calculated by the pore-size algorithm introduced in this thesis, complex network structure analyses can be developed. The detailed network structure of biopolymer networks, such as number of nodes, fiber connections per node and fiber lengths, will enable complex analysis of specific structural properties of different biopolymer networks, such as artificial collagen I gels.

References

- Abedin, Monika et al. (Dec. 1, 2010). "Diverse Evolutionary Paths to Cell Adhesion". In: *Trends in Cell Biology*. Special Issue - CellBio-X 20.12, pp. 734–742. ISSN: 0962-8924. DOI: 10.1016/j.tcb.2010.08.002.
- Adams, Josephine C (Oct. 1, 2004a). "Roles of Fascin in Cell Adhesion and Motility". In: *Current Opinion in Cell Biology* 16.5, pp. 590–596. ISSN: 0955-0674. DOI: 10.1016/j.ceb.2004.07.009.
- (Aug. 1, 2004b). "Fascin Protrusions in Cell Interactions". In: *Trends in Cardiovascular Medicine* 14.6, pp. 221–226. ISSN: 1050-1738. DOI: 10.1016/j.tcm.2004.06.002.
- Alam, Samer et al. (2014). "Nuclear Forces and Cell Mechanosensing". In: *Progress in molecular biology and translational science* 126, pp. 205–215. ISSN: 1877-1173. DOI: 10.1016/B978-0-12-394624-9.00008-7.
- Alberts, Bruce, ed. (2004). *Essential Cell Biology*. 2nd ed. New York, NY: Garland Science Pub. 740 pp. ISBN: 978-0-8153-3480-4.
- (2015). *Molecular Biology of the Cell*. Sixth edition. New York, NY: Garland Science, Taylor and Francis Group. 1 p. ISBN: 978-0-8153-4432-2 978-0-8153-4464-3 978-0-8153-4524-4.
- Albiges-Rizo, Corinne et al. (Sept. 1, 2009). "Actin Machinery and Mechanosensitivity in Invadopodia, Podosomes and Focal Adhesions". In: *Journal of Cell Science* 122.17, pp. 3037–3049. ISSN: 0021-9533, 1477-9137. DOI: 10.1242/jcs.052704.
- Alblazi, Kamila Mohamed Om et al. (2015). "Cellular Protrusions–Lamellipodia, Filopodia, Invadopodia and Podosomes–and Their Roles in Progression of Orofacial Tumours: Current Understanding". In: *Asian Pacific journal of cancer prevention: APJCP* 16.6, pp. 2187–2191. ISSN: 2476-762X. DOI: 10.7314/apjcp.2015.16.6.2187.
- Alessandrini, Andrea et al. (Apr. 2005). "AFM: A Versatile Tool in Biophysics". In: *Measurement Science and Technology* 16.6, R65–R92. ISSN: 0957-0233. DOI: 10.1088/0957-0233/16/6/R01.
- Alibert, Charlotte et al. (2017). "Are Cancer Cells Really Softer than Normal Cells?" In: *Biology of the Cell* 109.5, pp. 167–189. ISSN: 1768-322X. DOI: 10.1111/boc.201600078.

- Antoine, Elizabeth E. et al. (Dec. 1, 2014). "Review of Collagen I Hydrogels for Bioengineered Tissue Microenvironments: Characterization of Mechanics, Structure, and Transport". In: *Tissue Engineering. Part B, Reviews* 20.6, pp. 683–696. ISSN: 1937-3368. DOI: 10.1089/ten.teb.2014.0086.
- Bartles, James R (Feb. 1, 2000). "Parallel Actin Bundles and Their Multiple Actin-Bundling Proteins". In: *Current Opinion in Cell Biology* 12.1, pp. 72–78. ISSN: 0955-0674. DOI: 10.1016/S0955-0674(99)00059-9.
- Berg, Jeremy M. et al. (2015). *Biochemistry*. Eighth edition. New York: W.H. Freeman & Company, a Macmillan Education Imprint. 1 p. ISBN: 978-1-4641-2610-9.
- Binnig, G. et al. (Mar. 3, 1986). "Atomic Force Microscope". In: *Physical Review Letters* 56.9, pp. 930–933. DOI: 10.1103/PhysRevLett.56.930.
- Birukova, Anna A. et al. (2004). "Microtubule Disassembly Induces Cytoskeletal Remodeling and Lung Vascular Barrier Dysfunction: Role of Rho-Dependent Mechanisms". In: *Journal of Cellular Physiology* 201.1, pp. 55–70. ISSN: 1097-4652. DOI: 10.1002/jcp.20055.
- Block, Jennifer et al. (June 5, 2012). "FMNL2 Drives Actin-Based Protrusion and Migration Downstream of Cdc42". In: *Current Biology* 22.11, pp. 1005–1012. ISSN: 0960-9822. DOI: 10.1016/j.cub.2012.03.064.
- Bonnans, Caroline et al. (Dec. 2014). "Remodelling the Extracellular Matrix in Development and Disease". In: *Nature Reviews Molecular Cell Biology* 15.12, pp. 786–801. ISSN: 1471-0080. DOI: 10.1038/nrm3904.
- Bosse, Tanja et al. (Oct. 1, 2007). "Cdc42 and Phosphoinositide 3-Kinase Drive Rac-Mediated Actin Polymerization Downstream of c-Met in Distinct and Common Pathways". In: *Molecular and Cellular Biology* 27.19, pp. 6615–6628. ISSN: 0270-7306, 1098-5549. DOI: 10.1128/MCB.00367-07.
- Brábek, Jan et al. (Sept. 7, 2010). "The Role of the Tissue Microenvironment in the Regulation of Cancer Cell Motility and Invasion". In: *Cell Communication and Signaling : CCS* 8, p. 22. ISSN: 1478-811X. DOI: 10.1186/1478-811X-8-22.
- Bravo-Cordero, Jose Javier et al. (May 7, 2014). "Spatial Regulation of Tumor Cell Protrusions by RhoC". In: *Cell Adhesion & Migration* 8.3, pp. 263–267. ISSN: 1933-6918. DOI: 10.4161/cam.28405.
- Breitsprecher, Dennis, Antje K. Kiesewetter, Joern Linkner, Claus Urbanke, et al. (Nov. 19, 2008). "Clustering of VASP Actively Drives Processive, WH2 Domain-mediated Actin Filament Elongation". In: *The EMBO Journal* 27.22, pp. 2943–2954. ISSN: 1460-2075. DOI: 10.1038/emboj.2008.211.

- Breitsprecher, Dennis, Antje K. Kieseewetter, Joern Linkner, Marlene Vinzenz, et al. (Feb. 2, 2011). "Molecular Mechanism of Ena/VASP-mediated Actin-filament Elongation". In: *The EMBO Journal* 30.3, pp. 456–467. ISSN: 1460-2075. DOI: 10.1038/emboj.2010.348.
- Brugués, Jan et al. (Aug. 31, 2010). "Dynamical Organization of the Cytoskeletal Cortex Probed by Micropipette Aspiration". In: *Proceedings of the National Academy of Sciences* 107.35, pp. 15415–15420. ISSN: 0027-8424, 1091-6490. DOI: 10.1073/pnas.0913669107.
- Cairns, Rob A. et al. (Feb. 2011). "Regulation of Cancer Cell Metabolism". In: *Nature Reviews Cancer* 11.2, pp. 85–95. ISSN: 1474-1768. DOI: 10.1038/nrc2981.
- Campellone, Kenneth G. et al. (Apr. 2010). "A Nucleator Arms Race: Cellular Control of Actin Assembly". In: *Nature Reviews Molecular Cell Biology* 11.4, pp. 237–251. ISSN: 1471-0080. DOI: 10.1038/nrm2867.
- Cappella, B. et al. (Jan. 1, 1999). "Force-Distance Curves by Atomic Force Microscopy". In: *Surface Science Reports* 34.1, pp. 1–104. ISSN: 0167-5729. DOI: 10.1016/S0167-5729(99)00003-5.
- Carrier, M. F. et al. (1994). "Actin Polymerization: Regulation by Divalent Metal Ion and Nucleotide Binding, ATP Hydrolysis and Binding of Myosin". In: *Advances in Experimental Medicine and Biology* 358, pp. 71–81. ISSN: 0065-2598. DOI: 10.1007/978-1-4615-2578-3_7.
- Caswell, Patrick T. et al. (Oct. 1, 2018). "Actin-Based Cell Protrusion in a 3D Matrix". In: *Trends in Cell Biology* 28.10, pp. 823–834. ISSN: 0962-8924, 1879-3088. DOI: 10.1016/j.tcb.2018.06.003.
- Chaffer, Christine L. et al. (Mar. 25, 2011). "A Perspective on Cancer Cell Metastasis". In: *Science* 331.6024, pp. 1559–1564. ISSN: 0036-8075, 1095-9203. DOI: 10.1126/science.1203543.
- Chambolle, Antonin (Jan. 1, 2004). "An Algorithm for Total Variation Minimization and Applications". In: *Journal of Mathematical Imaging and Vision* 20.1-2, pp. 89–97. ISSN: 0924-9907, 1573-7683. DOI: 10.1023/B:JMIV.0000011325.36760.1e.
- Chang, Wakam et al. (Jan. 5, 2015). "Accessorizing and Anchoring the LINC Complex for Multifunctionality". In: *The Journal of Cell Biology* 208.1, pp. 11–22. ISSN: 0021-9525, 1540-8140. DOI: 10.1083/jcb.201409047.
- Charras, Guillaume et al. (Sept. 2008). "Blebs Lead the Way: How to Migrate without Lamellipodia". In: *Nature Reviews. Molecular Cell Biology* 9.9, pp. 730–736. ISSN: 1471-0080. DOI: 10.1038/nrm2453.

- Chen, Yan et al. (Oct. 22, 2014). "Viral Carcinogenesis: Factors Inducing DNA Damage and Virus Integration". In: *Cancers* 6.4, pp. 2155–2186. ISSN: 2072-6694. DOI: 10.3390/cancers6042155.
- Christiansen, David L. et al. (Sept. 1, 2000). "Assembly of Type I Collagen: Fusion of Fibril Subunits and the Influence of Fibril Diameter on Mechanical Properties". In: *Matrix Biology* 19.5, pp. 409–420. ISSN: 0945-053X. DOI: 10.1016/S0945-053X(00)00089-5.
- Clark, Andrew G. et al. (Aug. 6, 2013). "Monitoring Actin Cortex Thickness in Live Cells". In: *Biophysical Journal* 105.3, pp. 570–580. ISSN: 0006-3495. DOI: 10.1016/j.bpj.2013.05.057.
- Colin-York, Huw et al. (Apr. 13, 2016). "Super-Resolved Traction Force Microscopy (STFM)". In: *Nano Letters* 16.4, pp. 2633–2638. ISSN: 1530-6984. DOI: 10.1021/acs.nanolett.6b00273.
- Cooper, Geoffrey M. (2000). "Structure and Organization of Actin Filaments". In: *The Cell: A Molecular Approach. 2nd Edition*.
- Cramer, Louise P. et al. (Mar. 24, 1997). "Identification of Novel Graded Polarity Actin Filament Bundles in Locomoting Heart Fibroblasts: Implications for the Generation of Motile Force". In: *The Journal of Cell Biology* 136.6, pp. 1287–1305. ISSN: 0021-9525, 1540-8140. DOI: 10.1083/jcb.136.6.1287.
- Critchley, David R (Feb. 1, 2000). "Focal Adhesions – the Cytoskeletal Connection". In: *Current Opinion in Cell Biology* 12.1, pp. 133–139. ISSN: 0955-0674. DOI: 10.1016/S0955-0674(99)00067-8.
- Davidson, Patricia M. et al. (Apr. 1, 2014). "Broken Nuclei – Lamins, Nuclear Mechanics, and Disease". In: *Trends in Cell Biology* 24.4, pp. 247–256. ISSN: 0962-8924. DOI: 10.1016/j.tcb.2013.11.004.
- De Wever, Olivier et al. (Nov. 15, 2008). "Stromal Myofibroblasts Are Drivers of Invasive Cancer Growth". In: *International Journal of Cancer* 123.10, pp. 2229–2238. ISSN: 1097-0215. DOI: 10.1002/ijc.23925.
- Desai, Arshad et al. (Nov. 1, 1997). "Microtubule Polymerization Dynamics". In: *Annual Review of Cell and Developmental Biology* 13.1, pp. 83–117. ISSN: 1081-0706. DOI: 10.1146/annurev.cellbio.13.1.83.
- Dimchev, Georgi et al. (Mar. 22, 2017). "Efficiency of Lamellipodia Protrusion Is Determined by the Extent of Cytosolic Actin Assembly". In: *Molecular Biology of the Cell* 28.10, pp. 1311–1325. ISSN: 1059-1524. DOI: 10.1091/mbc.e16-05-0334.

- Diz-Muñoz, Alba et al. (Nov. 30, 2010). "Control of Directed Cell Migration In Vivo by Membrane-to-Cortex Attachment". In: *PLOS Biology* 8.11, e1000544. ISSN: 1545-7885. DOI: 10.1371/journal.pbio.1000544.
- Dominguez, Roberto (Nov. 1, 2004). "Actin-Binding Proteins – a Unifying Hypothesis". In: *Trends in Biochemical Sciences* 29.11, pp. 572–578. ISSN: 0968-0004. DOI: 10.1016/j.tibs.2004.09.004.
- Dominguez, Roberto and Kenneth C. Holmes (2011). "Actin Structure and Function". In: *Annual Review of Biophysics* 40.1, pp. 169–186. DOI: 10.1146/annurev-biophys-042910-155359.
- Eales, K. L. et al. (Jan. 2016). "Hypoxia and Metabolic Adaptation of Cancer Cells". In: *Oncogenesis* 5.1, e190. ISSN: 2157-9024. DOI: 10.1038/oncsis.2015.50.
- Edlund, Magnus et al. (2001). "Dynamics of α -Actinin in Focal Adhesions and Stress Fibers Visualized with α -Actinin-Green Fluorescent Protein". In: *Cell Motility* 48.3, pp. 190–200. ISSN: 1097-0169. DOI: 10.1002/1097-0169(200103)48:3<190::AID-CM1008>3.0.CO;2-C.
- Etienne-Manneville, Sandrine (Oct. 6, 2013). "Microtubules in Cell Migration". In: *Annual Review of Cell and Developmental Biology* 29.1, pp. 471–499. ISSN: 1081-0706. DOI: 10.1146/annurev-cellbio-101011-155711.
- Ezratty, Ellen J. et al. (June 2005). "Microtubule-Induced Focal Adhesion Disassembly Is Mediated by Dynamin and Focal Adhesion Kinase". In: *Nature Cell Biology* 7.6, pp. 581–590. ISSN: 1476-4679. DOI: 10.1038/ncb1262.
- Fischer, Tony, Alexander Hayn, et al. (June 7, 2019). "Fast and Reliable Advanced Two-Step Pore-Size Analysis of Biomimetic 3D Extracellular Matrix Scaffolds". In: *Scientific Reports* 9.1, p. 8352. ISSN: 2045-2322. DOI: 10.1038/s41598-019-44764-5.
- Fischer, Tony, Nils Wilharm, et al. (Nov. 29, 2017). "Matrix and Cellular Mechanical Properties Are the Driving Factors for Facilitating Human Cancer Cell Motility into 3D Engineered Matrices". In: *Convergent Science Physical Oncology* 3.4, pp. 044003–044003. ISSN: 2057-1739. DOI: 10.1088/2057-1739/aa8bbb.
- Fletcher, Daniel A. et al. (Feb. 2004). "An Introduction to Cell Motility for the Physical Scientist". In: *Physical Biology* 1.1, T1–T10. ISSN: 1478-3975. DOI: 10.1088/1478-3967/1/1/T01.
- Frantz, Christian et al. (Dec. 15, 2010). "The Extracellular Matrix at a Glance". In: *Journal of Cell Science* 123.24, pp. 4195–4200. ISSN: 0021-9533. DOI: 10.1242/jcs.023820.

- Fratzl, Peter, ed. (2008). *Collagen: Structure and Mechanics*. OCLC: ocn172979453. New York: Springer. 506 pp. ISBN: 978-0-387-73905-2.
- Friedl, Peter and Katarina Wolf (Jan. 11, 2010). "Plasticity of Cell Migration: A Multiscale Tuning Model". In: *The Journal of Cell Biology* 188.1, pp. 11–19. ISSN: 0021-9525, 1540-8140. DOI: 10.1083/jcb.200909003.
- Friedl, Peter, Katarina Wolf, and Jan Lammerding (Feb. 1, 2011). "Nuclear Mechanics during Cell Migration". In: *Current Opinion in Cell Biology*. Cell Structure and Dynamics 23.1, pp. 55–64. ISSN: 0955-0674. DOI: 10.1016/j.ceb.2010.10.015.
- Fritzsche, Marco, Christoph Erlenkämper, et al. (Apr. 1, 2016). "Actin Kinetics Shapes Cortical Network Structure and Mechanics". In: *Science Advances* 2.4, e1501337. ISSN: 2375-2548. DOI: 10.1126/sciadv.1501337.
- Fritzsche, Marco, Richard Thorogate, et al. (Jan. 21, 2014). "Quantitative Analysis of Ezrin Turnover Dynamics in the Actin Cortex". In: *Biophysical Journal* 106.2, pp. 343–353. ISSN: 0006-3495. DOI: 10.1016/j.bpj.2013.11.4499.
- Fruleux, Antoine et al. (July 2016). "Physical Role for the Nucleus in Cell Migration". In: *Journal of Physics: Condensed Matter* 28.36, p. 363002. ISSN: 0953-8984. DOI: 10.1088/0953-8984/28/36/363002.
- Fuchs, Elaine et al. (June 1, 1994). "INTERMEDIATE FILAMENTS: Structure, Dynamics, Function and Disease". In: *Annual Review of Biochemistry* 63.1, pp. 345–382. ISSN: 0066-4154. DOI: 10.1146/annurev.bi.63.070194.002021.
- Fujii, Takashi et al. (Oct. 2010). "Direct Visualization of Secondary Structures of F-Actin by Electron Cryomicroscopy". In: *Nature* 467.7316, pp. 724–728. ISSN: 1476-4687. DOI: 10.1038/nature09372.
- Gau, David M. et al. (June 18, 2015). "BRCA1 Deficiency in Ovarian Cancer Is Associated with Alteration in Expression of Several Key Regulators of Cell Motility – A Proteomics Study". In: *Cell Cycle* 14.12, pp. 1884–1892. ISSN: 1538-4101. DOI: 10.1080/15384101.2015.1036203.
- Geiger, Benjamin et al. (Nov. 2001). "Transmembrane Crosstalk between the Extracellular Matrix and the Cytoskeleton". In: *Nature Reviews Molecular Cell Biology* 2.11, p. 793. ISSN: 1471-0080. DOI: 10.1038/35099066.
- Gelman, R. A. et al. (Nov. 25, 1979). "Collagen Fibril Formation in Vitro. The Role of the Nonhelical Terminal Regions". In: *The Journal of Biological Chemistry* 254.22, pp. 11741–11745. ISSN: 0021-9258.

- Gilmore, A P et al. (Aug. 1, 1996). "Inhibition of Focal Adhesion Kinase (FAK) Signaling in Focal Adhesions Decreases Cell Motility and Proliferation." In: *Molecular Biology of the Cell* 7.8, pp. 1209–1224. ISSN: 1059-1524. DOI: 10.1091/mbc.7.8.1209.
- Goldstein, Lawrence S. B. et al. (2000). "Microtubule-Based Transport Systems in Neurons: The Roles of Kinesins and Dyneins". In: *Annual Review of Neuroscience* 23.1, pp. 39–71. DOI: 10.1146/annurev.neuro.23.1.39.
- Gorlin, J. B. et al. (Sept. 1, 1990). "Human Endothelial Actin-Binding Protein (ABP-280, Nonmuscle Filamin): A Molecular Leaf Spring." In: *The Journal of Cell Biology* 111.3, pp. 1089–1105. ISSN: 0021-9525, 1540-8140. DOI: 10.1083/jcb.111.3.1089.
- Gruenbaum, Yosef et al. (June 2, 2015). "Lamins: Nuclear Intermediate Filament Proteins with Fundamental Functions in Nuclear Mechanics and Genome Regulation". In: *Annual Review of Biochemistry* 84.1, pp. 131–164. ISSN: 0066-4154. DOI: 10.1146/annurev-biochem-060614-034115.
- Guilluy, Christophe et al. (Apr. 2014). "Isolated Nuclei Adapt to Force and Reveal a Mechanotransduction Pathway in the Nucleus". In: *Nature Cell Biology* 16.4, pp. 376–381. ISSN: 1476-4679. DOI: 10.1038/ncb2927.
- Gundersen, Gregg G. et al. (Mar. 14, 2013). "Nuclear Positioning". In: *Cell* 152.6, pp. 1376–1389. ISSN: 0092-8674, 1097-4172. DOI: 10.1016/j.cell.2013.02.031.
- Guolla, Louise et al. (Feb. 1, 2012). "Force Transduction and Strain Dynamics in Actin Stress Fibres in Response to Nanonewton Forces". In: *Journal of Cell Science* 125.3, pp. 603–613. ISSN: 0021-9533, 1477-9137. DOI: 10.1242/jcs.088302.
- Hanahan, Douglas and Robert A Weinberg (Jan. 7, 2000). "The Hallmarks of Cancer". In: *Cell* 100.1, pp. 57–70. ISSN: 0092-8674. DOI: 10.1016/S0092-8674(00)81683-9.
- (Mar. 4, 2011). "Hallmarks of Cancer: The Next Generation". In: *Cell* 144.5, pp. 646–674. ISSN: 0092-8674, 1097-4172. DOI: 10.1016/j.cell.2011.02.013.
- Hartman, M. Amanda et al. (Apr. 1, 2012). "The Myosin Superfamily at a Glance". In: *Journal of Cell Science* 125.7, pp. 1627–1632. ISSN: 0021-9533, 1477-9137. DOI: 10.1242/jcs.094300.
- Harunaga, Jill S. et al. (Sept. 1, 2011). "Cell-Matrix Adhesions in 3D". In: *Matrix Biology* 30.7, pp. 363–368. ISSN: 0945-053X. DOI: 10.1016/j.matbio.2011.06.001.
- Hashimoto, Yosuke, Dae Joong Kim, et al. (2011). "The Roles of Fascins in Health and Disease". In: *The Journal of Pathology* 224.3, pp. 289–300. ISSN: 1096-9896. DOI: 10.1002/path.2894.

- Hashimoto, Yosuke, Maddy Parsons, et al. (Sept. 12, 2007). "Dual Actin-Bundling and Protein Kinase C-Binding Activities of Fascin Regulate Carcinoma Cell Migration Downstream of Rac and Contribute to Metastasis". In: *Molecular Biology of the Cell* 18.11, pp. 4591–4602. ISSN: 1059-1524. DOI: 10.1091/mbc.e07-02-0157.
- Hashimoto, Yosuke, Marek Skacel, et al. (Sept. 1, 2005). "Roles of Fascin in Human Carcinoma Motility and Signaling: Prospects for a Novel Biomarker?" In: *The International Journal of Biochemistry & Cell Biology* 37.9, pp. 1787–1804. ISSN: 1357-2725. DOI: 10.1016/j.biocel.2005.05.004.
- Heinemann, Fabian et al. (Apr. 2, 2013). "Lateral Membrane Diffusion Modulated by a Minimal Actin Cortex". In: *Biophysical Journal* 104.7, pp. 1465–1475. ISSN: 0006-3495. DOI: 10.1016/j.bpj.2013.02.042.
- Herman, Ira M. (Feb. 1, 1993). "Actin Isoforms". In: *Current Opinion in Cell Biology* 5.1, pp. 48–55. ISSN: 0955-0674. DOI: 10.1016/S0955-0674(05)80007-9.
- Hetzer, Martin W. (Mar. 2010). "The Nuclear Envelope". In: *Cold Spring Harbor Perspectives in Biology* 2.3. ISSN: 1943-0264. DOI: 10.1101/cshperspect.a000539.
- Hirokawa, Nobutaka (Jan. 23, 1998). "Kinesin and Dynein Superfamily Proteins and the Mechanism of Organelle Transport". In: *Science* 279.5350, pp. 519–526. ISSN: 0036-8075, 1095-9203. DOI: 10.1126/science.279.5350.519.
- Holmes, Roison et al. (Aug. 2017). "Influence of Telopeptides on the Structural and Physical Properties of Polymeric and Monomeric Acid-Soluble Type I Collagen". In: *Materials Science and Engineering: C* 77, pp. 823–827. ISSN: 09284931. DOI: 10.1016/j.msec.2017.03.267.
- Horton, Edward R. et al. (Dec. 2015). "Definition of a Consensus Integrin Adhesome and Its Dynamics during Adhesion Complex Assembly and Disassembly". In: *Nature Cell Biology* 17.12, pp. 1577–1587. ISSN: 1476-4679. DOI: 10.1038/ncb3257.
- Hosseini, Sayed-Rzgar et al. (July 2019). "Estimating the Predictability of Cancer Evolution". In: *Bioinformatics* 35.14, pp. i389–i397. ISSN: 1367-4803. DOI: 10.1093/bioinformatics/btz332.
- Huber, F. et al. (Feb. 1, 2013). "Emergent Complexity of the Cytoskeleton: From Single Filaments to Tissue". In: *Advances in Physics* 62.1, pp. 1–112. ISSN: 0001-8732. DOI: 10.1080/00018732.2013.771509.
- Huber, Veronica et al. (Apr. 1, 2017). "Cancer Acidity: An Ultimate Frontier of Tumor Immune Escape and a Novel Target of Immunomodulation". In: *Seminars in Cancer*

- Biology*. The New pH-Centric Anticancer Paradigm in Oncology and Medicine 43, pp. 74–89. ISSN: 1044-579X. DOI: 10.1016/j.semcancer.2017.03.001.
- Hynes, Richard O. (Sept. 20, 2002). “Integrins: Bidirectional, Allosteric Signaling Machines”. In: *Cell* 110.6, pp. 673–687. ISSN: 0092-8674. DOI: 10.1016/S0092-8674(02)00971-6.
- Innocenti, Metello et al. (Apr. 2004). “Abi1 Is Essential for the Formation and Activation of a WAVE2 Signalling Complex”. In: *Nature Cell Biology* 6.4, p. 319. ISSN: 1476-4679. DOI: 10.1038/ncb1105.
- Iorio, Valentina et al. (Apr. 1, 2015). “Laminins: Roles and Utility in Wound Repair”. In: *Advances in Wound Care* 4.4, pp. 250–263. ISSN: 2162-1918. DOI: 10.1089/wound.2014.0533.
- Iwasa, Janet H. et al. (Mar. 6, 2007). “Spatial and Temporal Relationships between Actin-Filament Nucleation, Capping, and Disassembly”. In: *Current Biology* 17.5, pp. 395–406. ISSN: 0960-9822. DOI: 10.1016/j.cub.2007.02.012.
- Izawa, Ichiro et al. (2006). “Regulatory Mechanisms and Functions of Intermediate Filaments: A Study Using Site- and Phosphorylation State-Specific Antibodies”. In: *Cancer Science* 97.3, pp. 167–174. ISSN: 1349-7006. DOI: 10.1111/j.1349-7006.2006.00161.x.
- Jacquemet, Guillaume et al. (Oct. 1, 2013). “Role of Adhesion Receptor Trafficking in 3D Cell Migration”. In: *Current Opinion in Cell Biology*. Cell Adhesion and Migration 25.5, pp. 627–632. ISSN: 0955-0674. DOI: 10.1016/j.ceb.2013.05.008.
- Janmey, Paul A. et al. (Aug. 2009). “The Hard Life of Soft Cells”. In: *Cell motility and the cytoskeleton* 66.8, pp. 597–605. ISSN: 0886-1544. DOI: 10.1002/cm.20382.
- Järveläinen, Hannu et al. (June 2009). “Extracellular Matrix Molecules: Potential Targets in Pharmacotherapy”. In: *Pharmacological Reviews* 61.2, pp. 198–223. ISSN: 0031-6997. DOI: 10.1124/pr.109.001289.
- Jones, Eric et al. (Jan. 2001). “SciPy: Open Source Scientific Tools for Python”. In:
- Kadler, K E et al. (May 15, 1996). “Collagen Fibril Formation.” In: *Biochemical Journal* 316 (Pt 1), pp. 1–11. ISSN: 0264-6021.
- Kage, Frieda et al. (Mar. 22, 2017). “FMNL Formins Boost Lamellipodial Force Generation”. In: *Nature Communications* 8, p. 14832. ISSN: 2041-1723. DOI: 10.1038/ncomms14832.

- Kasza, Karen E. et al. (Feb. 2011). "Dynamics and Regulation of Contractile Actin-Myosin Networks in Morphogenesis". In: *Current Opinion in Cell Biology* 23.1, pp. 30–38. ISSN: 0955-0674. DOI: 10.1016/j.ceb.2010.10.014.
- Kato, Yasumasa et al. (Sept. 3, 2013). "Acidic Extracellular Microenvironment and Cancer". In: *Cancer Cell International* 13, p. 89. ISSN: 1475-2867. DOI: 10.1186/1475-2867-13-89.
- Kennedy, Kelly M et al. (Dec. 18, 2009). "Tumor Metabolism of Lactate: The Influence and Therapeutic Potential for MCT and CD147 Regulation". In: *Future Oncology* 6.1, pp. 127–148. ISSN: 1479-6694. DOI: 10.2217/fon.09.145.
- Khatau, Shyam B., Ryan J. Bloom, et al. (July 3, 2012). "The Distinct Roles of the Nucleus and Nucleus-Cytoskeleton Connections in Three-Dimensional Cell Migration". In: *Scientific Reports* 2, p. 488. ISSN: 2045-2322. DOI: 10.1038/srep00488.
- Khatau, Shyam B., Christopher M. Hale, et al. (Nov. 10, 2009). "A Perinuclear Actin Cap Regulates Nuclear Shape". In: *Proceedings of the National Academy of Sciences* 106.45, pp. 19017–19022. ISSN: 0027-8424, 1091-6490. DOI: 10.1073/pnas.0908686106.
- Klein, Christoph A. (Sept. 26, 2008). "The Metastasis Cascade". In: *Science* 321.5897, pp. 1785–1787. ISSN: 0036-8075, 1095-9203. DOI: 10.1126/science.1164853.
- Koestler, Stefan A. et al. (July 24, 2013). "Arp2/3 Complex Is Essential for Actin Network Treadmilling as Well as for Targeting of Capping Protein and Cofilin". In: *Molecular Biology of the Cell* 24.18, pp. 2861–2875. ISSN: 1059-1524. DOI: 10.1091/mbc.e12-12-0857.
- Kollmannsberger, Philip et al. (2011). "Linear and Nonlinear Rheology of Living Cells". In: *Annual Review of Materials Research* 41.1, pp. 75–97. DOI: 10.1146/annurev-matsci-062910-100351.
- Kovács, Mihály et al. (Aug. 20, 2004). "Mechanism of Blebbistatin Inhibition of Myosin II". In: *The Journal of Biological Chemistry* 279.34, pp. 35557–35563. ISSN: 0021-9258. DOI: 10.1074/jbc.M405319200.
- Krause, Marina et al. (Dec. 4, 2013). "Probing the Compressibility of Tumor Cell Nuclei by Combined Atomic Force–Confocal Microscopy". In: *Physical Biology* 10.6, pp. 065002–065002. ISSN: 1478-3967, 1478-3975. DOI: 10.1088/1478-3975/10/6/065002.
- Kreger, S. T. et al. (Aug. 2010). "Polymerization and Matrix Physical Properties as Important Design Considerations for Soluble Collagen Formulations". In: *Biopolymers* 93.8, pp. 690–707. ISSN: 0006-3525. DOI: 10.1002/bip.21431.

- Kumar, Sanjay et al. (June 1, 2009). "Mechanics, Malignancy, and Metastasis: The Force Journey of a Tumor Cell". In: *Cancer and Metastasis Reviews* 28.1, pp. 113–127. ISSN: 1573-7233. DOI: 10.1007/s10555-008-9173-4.
- Kunschmann, Tom, Stefanie Puder, Tony Fischer, Jeremy Perez, et al. (Dec. 19, 2017). "Integrin-Linked Kinase Regulates Cellular Mechanics Facilitating the Motility in 3D Extracellular Matrices". In: *Biochimica et Biophysica Acta (BBA) - Molecular Cell Research* 1864.3, pp. 580–593. ISSN: 01674889. DOI: 10.1016/j.bbamcr.2016.12.019.
- Kunschmann, Tom, Stefanie Puder, Tony Fischer, Anika Steffen, et al. (May 22, 2019). "The Small GTPase Rac1 Increases Cell Surface Stiffness and Enhances 3D Migration Into Extracellular Matrices". In: *Scientific Reports* 9.1, p. 7675. ISSN: 2045-2322. DOI: 10.1038/s41598-019-43975-0.
- Kuznetsova, Tatyana G. et al. (Dec. 1, 2007). "Atomic Force Microscopy Probing of Cell Elasticity". In: *Micron. Microscopy in Nanobiotechnology* 38.8, pp. 824–833. ISSN: 0968-4328. DOI: 10.1016/j.micron.2007.06.011.
- Lai, Frank PL et al. (Apr. 9, 2008). "Arp2/3 Complex Interactions and Actin Network Turnover in Lamellipodia". In: *The EMBO Journal* 27.7, pp. 982–992. ISSN: 1460-2075. DOI: 10.1038/emboj.2008.34.
- Lambert, Arthur W. et al. (Feb. 9, 2017). "Emerging Biological Principles of Metastasis". In: *Cell* 168.4, pp. 670–691. ISSN: 0092-8674. DOI: 10.1016/j.cell.2016.11.037.
- Lammerding, Jan et al. (Jan. 9, 2006). "Lamins A and C but Not Lamin B1 Regulate Nuclear Mechanics". In: *Journal of Biological Chemistry* 281.35, pp. 25768–25780. ISSN: 0021-9258, 1083-351X. DOI: 10.1074/jbc.M513511200.
- Lang, Nadine R. et al. (Feb. 1, 2015). "Biphasic Response of Cell Invasion to Matrix Stiffness in Three-Dimensional Biopolymer Networks". In: *Acta Biomaterialia* 13, pp. 61–67. ISSN: 1742-7061. DOI: 10.1016/j.actbio.2014.11.003.
- Lanzicher, Thomas et al. (Aug. 26, 2015). "AFM Single-Cell Force Spectroscopy Links Altered Nuclear and Cytoskeletal Mechanics to Defective Cell Adhesion in Cardiac Myocytes with a Nuclear Lamin Mutation". In: *Nucleus* 6.5, pp. 394–407. ISSN: 1949-1034. DOI: 10.1080/19491034.2015.1084453.
- Lee, Chang-Hun et al. (June 17, 2012). "Structural Basis for Heteromeric Assembly and Perinuclear Organization of Keratin Filaments". In: *Nature structural & molecular biology* 19.7. ISSN: 1545-9993. DOI: 10.1038/nsmb.2330.

- Li, Ang et al. (Feb. 23, 2010). "The Actin-Bundling Protein Fascin Stabilizes Actin in Invadopodia and Potentiates Protrusive Invasion". In: *Current Biology* 20.4, pp. 339–345. ISSN: 0960-9822. DOI: 10.1016/j.cub.2009.12.035.
- Li, Chaoyang et al. (Sept. 24, 2010). "Pro-Prion Binds Filamin A, Facilitating Its Interaction with Integrin B1, and Contributes to Melanomagenesis". In: *Journal of Biological Chemistry* 285.39, pp. 30328–30339. ISSN: 0021-9258, 1083-351X. DOI: 10.1074/jbc.M110.147413.
- Lim, Ssang-Taek et al. (Sept. 7, 2010). "Knock-in Mutation Reveals an Essential Role for Focal Adhesion Kinase Activity in Blood Vessel Morphogenesis and Cell Motility-Polarity but Not Cell Proliferation". In: *Journal of Biological Chemistry* 285.28, pp. 21526–21536. ISSN: 0021-9258, 1083-351X. DOI: 10.1074/jbc.M110.129999.
- Linkert, Melissa et al. (May 31, 2010). "Metadata Matters: Access to Image Data in the Real World". In: *The Journal of Cell Biology* 189.5, pp. 777–782. ISSN: 0021-9525, 1540-8140. DOI: 10.1083/jcb.201004104.
- Lipinski, Kamil A. et al. (Jan. 2016). "Cancer Evolution and the Limits of Predictability in Precision Cancer Medicine". In: *Trends in Cancer* 2.1, pp. 49–63. ISSN: 2405-8033. DOI: 10.1016/j.trecan.2015.11.003.
- Liu, Mine-Yine et al. (2005). "In Vitro Regulation of Single Collagen Fibril Length by Buffer Compositions and Temperature". In: *Bio-Medical Materials and Engineering* 15.6, pp. 413–420. ISSN: 0959-2989.
- Liu, Shu Ming et al. (1993). "Microtubules Are Involved in Transport of Macromolecules by Vesicles in Cultured Bovine Aortic Endothelial Cells". In: *Journal of Cellular Physiology* 156.2, pp. 311–316. ISSN: 1097-4652. DOI: 10.1002/jcp.1041560213.
- Lodish, Harvey F. (2016). *Molecular Cell Biology*. Eighth edition. OCLC: ocn949909675. New York: W.H. Freeman-Macmillan Learning. 1170 pp. ISBN: 978-1-4641-8339-3.
- Lucas, Bruce D. et al. (1981). "An Iterative Image Registration Technique with an Application to Stereo Vision". In: *Proceedings of the 7th International Joint Conference on Artificial Intelligence - Volume 2* (Vancouver, BC, Canada). IJCAI'81. San Francisco, CA, USA: Morgan Kaufmann Publishers Inc., pp. 674–679.
- Madsen, Chris D. et al. (Jan. 2015). "STRIPAK Components Determine Mode of Cancer Cell Migration and Metastasis". In: *Nature Cell Biology* 17.1, pp. 68–80. ISSN: 1476-4679. DOI: 10.1038/ncb3083.

- Martin, Sarah K et al. (Apr. 5, 2014). "Cytoskeleton Targeting Value in Prostate Cancer Treatment". In: *American Journal of Clinical and Experimental Urology* 2.1, pp. 15–26. ISSN: 2330-1910.
- Mattila, Pieta K. et al. (June 2008). "Filopodia: Molecular Architecture and Cellular Functions". In: *Nature Reviews Molecular Cell Biology* 9.6, pp. 446–454. ISSN: 1471-0080. DOI: 10.1038/nrm2406.
- McGinty, Robert K. et al. (Mar. 25, 2015). "Nucleosome Structure and Function". In: *Chemical Reviews* 115.6, pp. 2255–2273. ISSN: 0009-2665. DOI: 10.1021/cr500373h.
- McKeown, S R (Mar. 2014). "Defining Normoxia, Physoxia and Hypoxia in Tumours - Implications for Treatment Response". In: *The British Journal of Radiology* 87.1035. ISSN: 0007-1285. DOI: 10.1259/bjr.20130676.
- Mecham, Robert P., ed. (2011). *The Extracellular Matrix: An Overview*. Biology of Extracellular Matrix. OCLC: ocn690089447. Berlin ; New York: Springer Verlag. 425 pp. ISBN: 978-3-642-16554-2 978-3-642-16555-9.
- Mierke, Claudia T. (July 1, 2013). "Phagocytized Beads Reduce the A5 β 1 Integrin Facilitated Invasiveness of Cancer Cells by Regulating Cellular Stiffness". In: *Cell Biochemistry and Biophysics* 66.3, pp. 599–622. ISSN: 1559-0283. DOI: 10.1007/s12013-012-9506-3.
- Mierke, Claudia T. et al. (Feb. 16, 2017). "Focal Adhesion Kinase Activity Is Required for Actomyosin Contractility-Based Invasion of Cells into Dense 3D Matrices". In: *Scientific Reports* 7.42780, p. 42780. ISSN: 2045-2322. DOI: 10.1038/srep42780.
- Mierke, Claudia Tanja (Jan. 2013a). "The Integrin Alpha ν Beta3 Increases Cellular Stiffness and Cytoskeletal Remodeling Dynamics to Facilitate Cancer Cell Invasion". In: *New Journal of Physics* 15.1, p. 015003. ISSN: 1367-2630. DOI: 10.1088/1367-2630/15/1/015003.
- (Dec. 2013b). "The Role of Focal Adhesion Kinase in the Regulation of Cellular Mechanical Properties". In: *Physical Biology* 10.6, p. 065005. ISSN: 1478-3975. DOI: 10.1088/1478-3975/10/6/065005.
- (2014). "The Fundamental Role of Mechanical Properties in the Progression of Cancer Disease and Inflammation". In: *Reports on Progress in Physics* 77.7, p. 076602. ISSN: 0034-4885. DOI: 10.1088/0034-4885/77/7/076602.
- (2018a). *Physics of Cancer, Volume 1: Interplay between Tumor Biology, Inflammation and Cell Mechanics*. IOP Publishing. ISBN: 978-0-7503-1753-5. DOI: 10.1088/978-0-7503-1753-5.

- Mierke, Claudia Tanja (2018b). *Physics of Cancer, Volume 2: Cellular and Microenvironmental Effects*. IOP Publishing. ISBN: 978-0-7503-2117-4. DOI: 10.1088/978-0-7503-2117-4.
- Mierke, Claudia Tanja, Benjamin Frey, et al. (Feb. 1, 2011). "Integrin A5 β 1 Facilitates Cancer Cell Invasion through Enhanced Contractile Forces". In: *Journal of Cell Science* 124.3, pp. 369–383. ISSN: 0021-9533, 1477-9137. DOI: 10.1242/jcs.071985.
- Mierke, Claudia Tanja, Daniel Rösler, et al. (Sept. 4, 2008). "Contractile Forces in Tumor Cell Migration". In: *European Journal of Cell Biology*. FEBS Workshop: Invadopodia, Podosomes and Focal Adhesions in Tissue Invasion 87.8, pp. 669–676. ISSN: 0171-9335. DOI: 10.1016/j.ejcb.2008.01.002.
- Mierke, Claudia Tanja, Frank Sauer, et al. (Dec. 7, 2017). "The Two Faces of Enhanced Stroma: Stroma Acts as a Tumor Promoter and a Steric Obstacle". In: *NMR in Biomedicine*, e3831–e3831. ISSN: 09523480. DOI: 10.1002/nbm.3831.
- Mierke, Claudia Tanja, Daniel Paranhos Zitterbart, et al. (Apr. 1, 2008). "Breakdown of the Endothelial Barrier Function in Tumor Cell Transmigration". In: *Biophysical Journal* 94.7, pp. 2832–2846. ISSN: 0006-3495. DOI: 10.1529/biophysj.107.113613.
- Mitra, Satyajit K. et al. (Jan. 2005). "Focal Adhesion Kinase: In Command and Control of Cell Motility". In: *Nature Reviews Molecular Cell Biology* 6.1, p. 56. ISSN: 1471-0080. DOI: 10.1038/nrm1549.
- Mohan, Renu et al. (2015). "Microtubule-Associated Proteins as Direct Crosslinkers of Actin Filaments and Microtubules". In: *IUBMB Life* 67.6, pp. 395–403. ISSN: 1521-6551. DOI: 10.1002/iub.1384.
- Molteni, Matteo et al. (Mar. 2013a). "Fast Two-Dimensional Bubble Analysis of Biopolymer Filamentous Networks Pore Size from Confocal Microscopy Thin Data Stacks". In: *Biophysical Journal* 104.5, pp. 1160–1169. ISSN: 00063495. DOI: 10.1016/j.bpj.2013.01.016.
- (June 2013b). "Response to "a Simplified Implementation of the Bubble Analysis of Biopolymer Networks Pores"." In: *Biophysical journal* 104.12, pp. 2776–7. DOI: 10.1016/j.bpj.2013.05.015.
- Mornet, D. et al. (June 1, 1984). "Proteolysis and Structure of Skeletal Muscle Actin". In: *Proceedings of the National Academy of Sciences* 81.12, pp. 3680–3684. ISSN: 0027-8424, 1091-6490. DOI: 10.1073/pnas.81.12.3680.
- Münster, Stefan et al. (June 2013). "A Simplified Implementation of the Bubble Analysis of Biopolymer Network Pores". In: *Biophysical Journal* 104.12, pp. 2774–2775. ISSN: 00063495. DOI: 10.1016/j.bpj.2013.05.016.

- Murphy, Danielle A. et al. (July 2011). "The 'ins' and 'Outs' of Podosomes and Invadopodia: Characteristics, Formation and Function". In: *Nature Reviews Molecular Cell Biology* 12.7, pp. 413–426. ISSN: 1471-0080. DOI: 10.1038/nrm3141.
- Narumiya, Shuh et al. (June 1, 2009). "Rho Signaling, ROCK and mDia1, in Transformation, Metastasis and Invasion". In: *Cancer and Metastasis Reviews* 28.1, pp. 65–76. ISSN: 1573-7233. DOI: 10.1007/s10555-008-9170-7.
- Naumanen, P. et al. (2008). "Mechanisms of Actin Stress Fibre Assembly". In: *Journal of Microscopy* 231.3, pp. 446–454. ISSN: 1365-2818. DOI: 10.1111/j.1365-2818.2008.02057.x.
- Neelam, Srujana et al. (May 5, 2015). "Direct Force Probe Reveals the Mechanics of Nuclear Homeostasis in the Mammalian Cell". In: *Proceedings of the National Academy of Sciences* 112.18, pp. 5720–5725. ISSN: 0027-8424, 1091-6490. DOI: 10.1073/pnas.1502111112.
- Nogales, Eva et al. (Apr. 1, 2006). "Structural Intermediates in Microtubule Assembly and Disassembly: How and Why?" In: *Current Opinion in Cell Biology*. Cell Regulation 18.2, pp. 179–184. ISSN: 0955-0674. DOI: 10.1016/j.ceb.2006.02.009.
- Nürnberg, Alexander et al. (Mar. 2011). "Nucleating Actin for Invasion". In: *Nature Reviews Cancer* 11.3, pp. 177–187. ISSN: 1474-1768. DOI: 10.1038/nrc3003.
- Okeyo, Kennedy Omondi et al. (Nov. 13, 2009). "Actomyosin Contractility Spatiotemporally Regulates Actin Network Dynamics in Migrating Cells". In: *Journal of Biomechanics* 42.15, pp. 2540–2548. ISSN: 1873-2380. DOI: 10.1016/j.jbiomech.2009.07.002.
- Otsu, Nobuyuki (Jan. 1979). "A Threshold Selection Method from Gray-Level Histograms". In: *IEEE Transactions on Systems, Man, and Cybernetics* 9.1, pp. 62–66. ISSN: 0018-9472, 2168-2909. DOI: 10.1109/TSMC.1979.4310076.
- Otterbein, Ludovic R. et al. (July 27, 2001). "The Crystal Structure of Uncomplexed Actin in the ADP State". In: *Science* 293.5530, pp. 708–711. ISSN: 0036-8075, 1095-9203. DOI: 10.1126/science.1059700.
- Pantel, Klaus et al. (June 2004). "Dissecting the Metastatic Cascade". In: *Nature Reviews Cancer* 4.6, p. 448. ISSN: 1474-1768. DOI: 10.1038/nrc1370.
- Parenteau-Bareil, Rémi et al. (Oct. 2011). "Comparative Study of Bovine, Porcine and Avian Collagens for the Production of a Tissue Engineered Dermis". In: *Acta Biomaterialia* 7.10, pp. 3757–3765. ISSN: 1878-7568. DOI: 10.1016/j.actbio.2011.06.020.
- Parsons, J. Thomas (Apr. 15, 2003). "Focal Adhesion Kinase: The First Ten Years". In: *Journal of Cell Science* 116.8, pp. 1409–1416. ISSN: 0021-9533, 1477-9137. DOI: 10.1242/jcs.00373.

- Parsons, J. Thomas et al. (Sept. 2010). "Cell Adhesion: Integrating Cytoskeletal Dynamics and Cellular Tension". In: *Nature Reviews Molecular Cell Biology* 11.9, pp. 633–643. ISSN: 1471-0080. DOI: 10.1038/nrm2957.
- Paszek, Matthew J. et al. (Sept. 1, 2005). "Tensional Homeostasis and the Malignant Phenotype". In: *Cancer Cell* 8.3, pp. 241–254. ISSN: 1535-6108. DOI: 10.1016/j.ccr.2005.08.010.
- Paterson, Elyse K. et al. (2017). "Invadosomes Are Coming: New Insights into Function and Disease Relevance". In: *The FEBS Journal*, pp. 8–27. ISSN: 1742-4658. DOI: 10.1111/febs.14123@10.1002/(ISSN)1742-4658(CAT)StateoftheArtReviews(VI)SoAReviews.
- Pellegrin, Stéphanie et al. (Oct. 15, 2007). "Actin Stress Fibres". In: *Journal of Cell Science* 120.20, pp. 3491–3499. ISSN: 0021-9533, 1477-9137. DOI: 10.1242/jcs.018473.
- Persi, Erez et al. (July 31, 2018). "Systems Analysis of Intracellular pH Vulnerabilities for Cancer Therapy". In: *Nature Communications* 9.1, p. 2997. ISSN: 2041-1723. DOI: 10.1038/s41467-018-05261-x.
- Petrie, Ryan J., Heather M. Harlin, et al. (Jan. 2, 2017). "Activating the Nuclear Piston Mechanism of 3D Migration in Tumor Cells". In: *The Journal of Cell Biology* 216.1, pp. 93–100. ISSN: 0021-9525, 1540-8140. DOI: 10.1083/jcb.201605097.
- Petrie, Ryan J. and Kenneth M. Yamada (Nov. 2015). "Fibroblasts Lead the Way: A Unified View of 3D Cell Motility". In: *Trends in Cell Biology* 25.11, pp. 666–674. ISSN: 1879-3088. DOI: 10.1016/j.tcb.2015.07.013.
- Pollard, Thomas D. (Aug. 2016). "Actin and Actin-Binding Proteins". In: *Cold Spring Harbor Perspectives in Biology* 8.8. ISSN: 1943-0264. DOI: 10.1101/cshperspect.a018226.
- Pollard, Thomas D. and John A. Cooper (Nov. 27, 2009). "Actin, a Central Player in Cell Shape and Movement". In: *Science* 326.5957, pp. 1208–1212. ISSN: 0036-8075, 1095-9203. DOI: 10.1126/science.1175862.
- Popowicz, Grzegorz M. et al. (July 1, 2006). "Filamins: Promiscuous Organizers of the Cytoskeleton". In: *Trends in Biochemical Sciences* 31.7, pp. 411–419. ISSN: 0968-0004. DOI: 10.1016/j.tibs.2006.05.006.
- Pula, G. et al. (2008). "Role of Ena/VASP Proteins in Homeostasis and Disease". In: *Protein-Protein Interactions as New Drug Targets*. Ed. by Enno Klussmann et al. Handbook of Experimental Pharmacology. Berlin, Heidelberg: Springer Berlin Heidelberg, pp. 39–65. ISBN: 978-3-540-72843-6. DOI: 10.1007/978-3-540-72843-6_3.

- Radmacher, M. et al. (Sept. 25, 1992). "From Molecules to Cells: Imaging Soft Samples with the Atomic Force Microscope". In: *Science* 257.5078, pp. 1900–1905. ISSN: 0036-8075, 1095-9203. DOI: 10.1126/science.1411505.
- Ridley, Anne J. (June 24, 2011). "Life at the Leading Edge". In: *Cell* 145.7, pp. 1012–1022. ISSN: 0092-8674, 1097-4172. DOI: 10.1016/j.cell.2011.06.010.
- Rothbaler, Andrea et al. (Oct. 1, 2013). "The Diverse Functional LINC's of the Nuclear Envelope to the Cytoskeleton and Chromatin". In: *Chromosoma* 122.5, pp. 415–429. ISSN: 1432-0886. DOI: 10.1007/s00412-013-0417-x.
- Rottner, Klemens, Barbara Behrendt, et al. (Sept. 1999). "VASP Dynamics during Lamellipodia Protrusion". In: *Nature Cell Biology* 1.5, p. 321. ISSN: 1476-4679. DOI: 10.1038/13040.
- Rottner, Klemens and Theresia EB Stradal (Oct. 1, 2011). "Actin Dynamics and Turnover in Cell Motility". In: *Current Opinion in Cell Biology*. Cell-to-Cell Contact and Extracellular Matrix 23.5, pp. 569–578. ISSN: 0955-0674. DOI: 10.1016/j.ceb.2011.07.003.
- Roussos, Evanthia T. et al. (Aug. 2011). "Chemotaxis in Cancer". In: *Nature Reviews Cancer* 11.8, pp. 573–587. ISSN: 1474-1768. DOI: 10.1038/nrc3078.
- Rozario, Tania et al. (May 1, 2010). "The Extracellular Matrix In Development and Morphogenesis: A Dynamic View". In: *Developmental biology* 341.1, pp. 126–140. ISSN: 0012-1606. DOI: 10.1016/j.ydbio.2009.10.026.
- Saka, Sinem K. et al. (July 25, 2014). "Multi-Protein Assemblies Underlie the Mesoscale Organization of the Plasma Membrane". In: *Nature Communications* 5, p. 4509. ISSN: 2041-1723. DOI: 10.1038/ncomms5509.
- San-Millán, Iñigo et al. (Feb. 2017). "Reexamining Cancer Metabolism: Lactate Production for Carcinogenesis Could Be the Purpose and Explanation of the Warburg Effect". In: *Carcinogenesis* 38.2, pp. 119–133. ISSN: 0143-3334. DOI: 10.1093/carcin/bgw127.
- Sapudom, Jiranuwat et al. (Feb. 2, 2015). "The Phenotype of Cancer Cell Invasion Controlled by Fibril Diameter and Pore Size of 3D Collagen Networks". In: *Biomaterials* 52, pp. 367–375. ISSN: 01429612. DOI: 10.1016/j.biomaterials.2015.02.022.
- Schaefer, Liliana et al. (Jan. 2010). "Proteoglycans: From Structural Compounds to Signaling Molecules". In: *Cell and Tissue Research* 339.1, pp. 237–246. ISSN: 1432-0878. DOI: 10.1007/s00441-009-0821-y.
- Schek, Henry T. et al. (Sept. 4, 2007). "Microtubule Assembly Dynamics at the Nanoscale". In: *Current Biology* 17.17, pp. 1445–1455. ISSN: 0960-9822. DOI: 10.1016/j.cub.2007.07.011.

- Schoumacher, Marie et al. (May 3, 2010). "Actin, Microtubules, and Vimentin Intermediate Filaments Cooperate for Elongation of Invadopodia". In: *The Journal of Cell Biology* 189.3, pp. 541–556. ISSN: 0021-9525, 1540-8140. DOI: 10.1083/jcb.200909113.
- Schreiner, Sarah M. et al. (June 15, 2015). "The Tethering of Chromatin to the Nuclear Envelope Supports Nuclear Mechanics". In: *Nature Communications* 6, p. 7159. ISSN: 2041-1723. DOI: 10.1038/ncomms8159.
- Schultz, Gregory S. et al. (2009). "Interactions between Extracellular Matrix and Growth Factors in Wound Healing". In: *Wound Repair and Regeneration* 17.2, pp. 153–162. ISSN: 1524-475X. DOI: 10.1111/j.1524-475X.2009.00466.x.
- Scott, Jeanie A. et al. (Dec. 21, 2005). "Ena/VASP Proteins Can Regulate Distinct Modes of Actin Organization at Cadherin-Adhesive Contacts". In: *Molecular Biology of the Cell* 17.3, pp. 1085–1095. ISSN: 1059-1524. DOI: 10.1091/mbc.e05-07-0644.
- Seyfried, Thomas N. et al. (2013). "On the Origin of Cancer Metastasis". In: *Critical reviews in oncogenesis* 18.1-2, pp. 43–73. ISSN: 0893-9675.
- Siddiqui, Imtiaz A. et al. (Aug. 2015). "Resveratrol Nanoformulation for Cancer Prevention and Therapy". In: *Annals of the New York Academy of Sciences* 1348.1, pp. 20–31. ISSN: 1749-6632. DOI: 10.1111/nyas.12811.
- Small, J. Victor et al. (Mar. 1, 2002). "The Lamellipodium: Where Motility Begins". In: *Trends in Cell Biology* 12.3, pp. 112–120. ISSN: 0962-8924, 1879-3088. DOI: 10.1016/S0962-8924(01)02237-1.
- Smith, Michael L et al. (Oct. 2007). "Force-Induced Unfolding of Fibronectin in the Extracellular Matrix of Living Cells". In: *PLoS Biology* 5.10. ISSN: 1544-9173. DOI: 10.1371/journal.pbio.0050268.
- Starr, Daniel A. (Sept. 2007). "Communication between the Cytoskeleton and the Nuclear Envelope to Position the Nucleus". In: *Molecular bioSystems* 3.9, pp. 583–589. ISSN: 1742-206X. DOI: 10.1039/b703878j.
- Steffen, Anika, Stefan A. Koestler, et al. (May 1, 2014). "Requirements for and Consequences of Rac-Dependent Protrusion". In: *European Journal of Cell Biology*. Special Issue: SPP 1464: Actin Dynamics - Part II 93.5, pp. 184–193. ISSN: 0171-9335. DOI: 10.1016/j.ejcb.2014.01.008.
- Steffen, Anika, Klemens Rottner, et al. (Feb. 25, 2004). "Sra-1 and Nap1 Link Rac to Actin Assembly Driving Lamellipodia Formation". In: *The EMBO Journal* 23.4, pp. 749–759. ISSN: 0261-4189. DOI: 10.1038/sj.emboj.7600084.

- Stehbens, Samantha et al. (Aug. 20, 2012). "Targeting and Transport: How Microtubules Control Focal Adhesion Dynamics". In: *The Journal of Cell Biology* 198.4, pp. 481–489. ISSN: 0021-9525, 1540-8140. DOI: 10.1083/jcb.201206050.
- Steinwachs, Julian et al. (Feb. 2016). "Three-Dimensional Force Microscopy of Cells in Biopolymer Networks". In: *Nature Methods* 13.2, pp. 171–176. ISSN: 1548-7105. DOI: 10.1038/nmeth.3685.
- Stradal, Theresia E. B. et al. (June 1, 2004). "Regulation of Actin Dynamics by WASP and WAVE Family Proteins". In: *Trends in Cell Biology* 14.6, pp. 303–311. ISSN: 0962-8924. DOI: 10.1016/j.tcb.2004.04.007.
- Strelkov, Sergei V. et al. (2003). "Molecular Architecture of Intermediate Filaments". In: *BioEssays* 25.3, pp. 243–251. ISSN: 1521-1878. DOI: 10.1002/bies.10246.
- Suraneni, Praveen et al. (Apr. 16, 2012). "The Arp2/3 Complex Is Required for Lamellipodia Extension and Directional Fibroblast Cell Migration". In: *The Journal of Cell Biology* 197.2, pp. 239–251. ISSN: 0021-9525, 1540-8140. DOI: 10.1083/jcb.201112113.
- Svitkina, Tatyana M. et al. (Feb. 3, 2003). "Mechanism of Filopodia Initiation by Reorganization of a Dendritic Network". In: *The Journal of Cell Biology* 160.3, pp. 409–421. ISSN: 0021-9525, 1540-8140. DOI: 10.1083/jcb.200210174.
- Swift, Joe et al. (July 15, 2014). "The Nuclear Lamina Is Mechano-Responsive to ECM Elasticity in Mature Tissue". In: *Journal of Cell Science* 127.14, pp. 3005–3015. ISSN: 0021-9533. DOI: 10.1242/jcs.149203.
- Tapley, Erin C. et al. (Feb. 2013). "Connecting the Nucleus to the Cytoskeleton by SUN-KASH Bridges across the Nuclear Envelope". In: *Current opinion in cell biology* 25.1, pp. 57–62. ISSN: 0955-0674. DOI: 10.1016/j.ceb.2012.10.014.
- Teitelbaum, Steven L. (Sept. 1, 2000). "Bone Resorption by Osteoclasts". In: *Science* 289.5484, pp. 1504–1508. ISSN: 0036-8075, 1095-9203. DOI: 10.1126/science.289.5484.1504.
- Theocharis, Achilleas D., Spyridon S. Skandalis, et al. (Oct. 2010). "Proteoglycans in Health and Disease: Novel Roles for Proteoglycans in Malignancy and Their Pharmacological Targeting". In: *The FEBS journal* 277.19, pp. 3904–3923. ISSN: 1742-4658. DOI: 10.1111/j.1742-4658.2010.07800.x.
- Theocharis, Achilleas D., Spyros S. Skandalis, et al. (Feb. 1, 2016). "Extracellular Matrix Structure". In: *Advanced Drug Delivery Reviews*. Extracellular Matrix (ECM) and ECM-like Materials: Therapeutic Tools and Targets in Cancer Treatment 97, pp. 4–27. ISSN: 0169-409X. DOI: 10.1016/j.addr.2015.11.001.

- Tojkander, Sari et al. (Apr. 15, 2012). "Actin Stress Fibers – Assembly, Dynamics and Biological Roles". In: *Journal of Cell Science* 125.8, pp. 1855–1864. ISSN: 0021-9533, 1477-9137. DOI: 10.1242/jcs.098087.
- Van der Walt, Stéfan et al. (June 19, 2014). "Scikit-Image: Image Processing in Python". In: *PeerJ* 2, e453. ISSN: 2167-8359. DOI: 10.7717/peerj.453.
- Wagenseil, Jessica E. et al. (2007). "New Insights into Elastic Fiber Assembly". In: *Birth Defects Research Part C: Embryo Today: Reviews* 81.4, pp. 229–240. ISSN: 1542-9768. DOI: 10.1002/bdrc.20111.
- Wang, Xian et al. (July 1, 2018). "Mechanical Stability of the Cell Nucleus – Roles Played by the Cytoskeleton in Nuclear Deformation and Strain Recovery". In: *Journal of Cell Science* 131.13, jcs209627. ISSN: 0021-9533, 1477-9137. DOI: 10.1242/jcs.209627.
- Wang, Y. L. (Aug. 1, 1985). "Exchange of Actin Subunits at the Leading Edge of Living Fibroblasts: Possible Role of Treadmilling." In: *The Journal of Cell Biology* 101.2, pp. 597–602. ISSN: 0021-9525, 1540-8140. DOI: 10.1083/jcb.101.2.597.
- Wanger, M. et al. (June 1985). "The Actin Treadmill". In: *Canadian Journal of Biochemistry and Cell Biology = Revue Canadienne De Biochimie Et Biologie Cellulaire* 63.6, pp. 414–421. ISSN: 0714-7511. DOI: 10.1139/o85-060.
- Watanabe, Takashi et al. (Feb. 1, 2005). "Regulation of Microtubules in Cell Migration". In: *Trends in Cell Biology* 15.2, pp. 76–83. ISSN: 0962-8924. DOI: 10.1016/j.tcb.2004.12.006.
- Weaver, Alissa M. (Apr. 1, 2006). "Invadopodia: Specialized Cell Structures for Cancer Invasion". In: *Clinical & Experimental Metastasis* 23.2, pp. 97–105. ISSN: 1573-7276. DOI: 10.1007/s10585-006-9014-1.
- (July 8, 2008). "Cortactin in Tumor Invasiveness". In: *Cancer Letters* 265.2, pp. 157–166. ISSN: 0304-3835. DOI: 10.1016/j.canlet.2008.02.066.
- Webb, Donna J. et al. (Feb. 2004). "FAK–Src Signalling through Paxillin, ERK and MLCK Regulates Adhesion Disassembly". In: *Nature Cell Biology* 6.2, pp. 154–161. ISSN: 1476-4679. DOI: 10.1038/ncb1094.
- Weinstein, I. Bernard et al. (Aug. 2006). "Mechanisms of Disease: Oncogene Addiction—a Rationale for Molecular Targeting in Cancer Therapy". In: *Nature Clinical Practice Oncology* 3.8, p. 448. ISSN: 1743-4262. DOI: 10.1038/ncponc0558.
- Welte, Michael A (July 13, 2004). "Bidirectional Transport along Microtubules". In: *Current Biology* 14.13, R525–R537. ISSN: 0960-9822. DOI: 10.1016/j.cub.2004.06.045.

- Winograd-Katz, Sabina E. et al. (Apr. 2014). "The Integrin Adhesome: From Genes and Proteins to Human Disease". In: *Nature Reviews Molecular Cell Biology* 15.4, pp. 273–288. ISSN: 1471-0080. DOI: 10.1038/nrm3769.
- Wise, Steven G. et al. (Mar. 2009). "Tropoelastin". In: *The International Journal of Biochemistry & Cell Biology* 41.3, pp. 494–497. ISSN: 1878-5875. DOI: 10.1016/j.biocel.2008.03.017.
- Wolf, Katarina et al. (Oct. 1, 2009). "Collagen-Based Cell Migration Models in Vitro and in Vivo". In: *Seminars in Cell & Developmental Biology*. Imaging in Cell and Developmental Biology 20.8, pp. 931–941. ISSN: 1084-9521. DOI: 10.1016/j.semcdb.2009.08.005.
- Wolfenson, Haguy et al. (2009). "The Heel and Toe of the Cell's Foot: A Multifaceted Approach for Understanding the Structure and Dynamics of Focal Adhesions". In: *Cell Motility* 66.11, pp. 1017–1029. ISSN: 1097-0169. DOI: 10.1002/cm.20410.
- Woodley, D. T. et al. (Sept. 1991). "Collagen Telopeptides (Cross-Linking Sites) Play a Role in Collagen Gel Lattice Contraction". In: *The Journal of Investigative Dermatology* 97.3, pp. 580–585. ISSN: 0022-202X.
- Woolley, Thomas E. et al. (July 18, 2017). "Random Blebbing Motion: A Simple Model Linking Cell Structural Properties to Migration Characteristics". In: *Physical Review E* 96.1, p. 012409. DOI: 10.1103/PhysRevE.96.012409.
- Wu, Congying et al. (Mar. 2, 2012). "Arp2/3 Is Critical for Lamellipodia and Response to Extracellular Matrix Cues but Is Dispensable for Chemotaxis". In: *Cell* 148.5, pp. 973–987. ISSN: 0092-8674, 1097-4172. DOI: 10.1016/j.cell.2011.12.034.
- Yue, Jiping et al. (Dec. 8, 2014). "Microtubules Regulate Focal Adhesion Dynamics through MAP4K4". In: *Developmental cell* 31.5, pp. 572–585. ISSN: 1534-5807. DOI: 10.1016/j.devcel.2014.10.025.
- Zhou, Jing et al. (Nov. 6, 2015). "Mechanism of Focal Adhesion Kinase Mechanosensing". In: *PLOS Computational Biology* 11.11, e1004593. ISSN: 1553-7358. DOI: 10.1371/journal.pcbi.1004593.
- Zimmerman, Baruch et al. (2004). "Early Molecular Events in the Assembly of the Focal Adhesion-Stress Fiber Complex during Fibroblast Spreading". In: *Cell Motility* 58.3, pp. 143–159. ISSN: 1097-0169. DOI: 10.1002/cm.20005.

Eidesstattliche Erklärung

Ich, Tony Fischer, versichere hiermit, dass die vorliegende Arbeit mit dem Titel „Biophysical techniques to study cell and matrix properties in the context of single cell migration“ ohne unzulässige Hilfe und ohne Benutzung anderer als der angegebenen Hilfsmittel angefertigt und dass die aus fremden Quellen direkt oder indirekt übernommenen Gedanken in der Arbeit als solche kenntlich gemacht wurden.

Bei der Auswahl und Auswertung des Materials sowie bei der Herstellung des Manuskripts habe ich außer von den in der Danksagung genannten keine Unterstützungsleistungen erhalten.

Ich versichere, dass außer der oben genannten Person keine weiteren Personen bei der geistigen Herstellung der vorliegenden Arbeit beteiligt waren, insbesondere nicht die Hilfe eines Promotionsberaters in Anspruch genommen wurde und weitere Personen von mir oder in meinem Auftrag weder unmittelbar noch mittelbar geldwerte Leistungen für Arbeiten erhalten haben, die im Zusammenhang mit dem Inhalt der vorgelegten Dissertation stehen.

Ich versichere außerdem, dass die vorgelegte Arbeit oder Teile daraus weder im Inland noch im Ausland in gleicher oder in ähnlicher Form einer anderen Prüfungsbehörde zum Zwecke einer Promotion oder eines anderen Prüfungsverfahrens vorgelegt wurde und keine früheren erfolglosen Promotionsversuche stattgefunden haben.

Unterschrift:

Ort, Datum:
